

**NONLINEAR STRUCTURAL BEHAVIOR OF
ELECTRICALLY ACTUATED MEMS ACTUATOR**

BY
ABDULRAHMAN ALOFI

A Thesis Presented to the
DEANSHIP OF GRADUATE STUDIES

KING FAHD UNIVERSITY OF PETROLEUM & MINERALS
DHAHRAN, SAUDI ARABIA

In Partial Fulfillment of the
Requirements for the Degree of

MASTER OF SCIENCE

In
MECHANICAL ENGINEERING

November 2015

KING FAHD UNIVERSITY OF PETROLEUM & MINERALS

DHAHRAN- 31261, SAUDI ARABIA

DEANSHIP OF GRADUATE STUDIES

This thesis, written by **ABDULRAHMAN MOHAMMED ALOFI** under the direction his thesis advisor and approved by his thesis committee, has been presented and accepted by the Dean of Graduate Studies, in partial fulfillment of the requirements for the degree of **MASTER OF SCIENCE IN MECHANICAL ENGINEERING**.



THESIS COMMITTEE



Dr. Zuhair Gasem
Department Chairman



Dr. Hassen Ouakad
(Advisor)



Dr. Salam A. Zummo
Dean of Graduate Studies



Dr. Hussain Al-Qahtani
(Member)

24/12/15

Date



Dr. Muhammad Hawwa
(Member)

© Abdulrahman Alofi

2015

To my parents, my beloved wife and all of my brothers and sisters

Acknowledgments

First of all, I would like to thank almighty Allah for this achievement. He covered me in his blessings throughout my life and gave me the patience and strength to reach to this level in knowledge and accomplish this work.

I would like to thank my parents for all of the unconditional support provided over the years. They made me recognize my own potential and to always have the ambition to be the best. Also, a special thanks to my beloved wife for her patience and love. She always understands my circumstances and provides me the support I need. Thanks also to the rest of my family, who encouraged me and gave me their affection.

I would like to thank my advisor Dr. Hassen Ouakad for his continuous guidance and efforts throughout my master graduate program. He introduced me to the exciting MEMS world and I learned a lot from him in both science and morals. Also, I would like to thank Dr. Hussain Al-Qahtani and Dr. Mohammad Hawwa for accepting to be part of my evaluation committee and for their kind guidance in my graduate program. I would like also to express my deepest appreciation to Dr. Ali Nayfeh for his help. Despite his tight schedule he answered all my concerns and guided me in my research work.

Special thanks go to Dr. Nayef Al-Saifi from the chemical department of KFUPM, who advised me in many crucial events in my life. Joining KFUPM as undergraduate student and then continuing as a graduate assistant are two examples of this.

I would like also to thank all my colleagues and friends who helped or supported me in my academic career. I thank Mr. Mohammad Tausiff and Mr. Aalim Mustafa for their kind friendship and all of the efforts they spent on me and they never hesitated to help me whenever I needed assistance.

Table of Contents

Acknowledgments.....	v
List of Tables	ix
List of Figures.....	x
Abstract.....	xiii
ملخص الرسالة.....	xiv
CHAPTER 1: INTRODUCTION.....	1
1.1 Motivation.....	1
1.2 Literature Review.....	3
1.2.1 Solving the Nonlinear Microbeam's Equation	3
1.2.2 Reduced Order Modeling (ROM).....	4
1.2.3 Perturbation Theory	5
1.2.4 Double-Microbeams Configuration in MEMS.....	6
1.3 Thesis Objectives and Organization.....	7
CHAPTER 2: BACKGROUND.....	9
2.1 Parallel-plates Electrostatic Actuation	9
2.2 Electrostatic Force.....	10
2.3 Pull-in Instability.....	11
2.4 Perturbation Theory.....	12
2.5 Galerkin Method	13
2.6 Euler-Bernoulli Beam Model.....	14
2.7 Problem Formulation.....	15
2.7.1 Free Body Diagram (FBD) of a Single Microbeam.....	15
2.7.2 Free Body Diagram (FBD) of Double-microbeams	16
2.7.3 Deriving the System Equations of Motion.....	18
2.7.4 Normalization	20
CHAPTER 3: STATIC ANALYSIS	22
3.1 Static Analysis of a Single Microbeam Based MEMS Actuator	22
3.1.1 Model and ROM	22
3.1.2 Results.....	24
3.2 Static Analysis of Double Microbeams Actuator.....	26

3.2.1	Model and ROM	26
3.2.2	Results	29
3.2.3	Parametric Study	31
CHAPTER 4:	EIGENVALUE PROBLEM	40
4.1	Single Microbeam Case	40
4.1.1	Eigenvalue Problem Equation	40
4.1.2	Results	42
4.2	Double-Microbeams Case	44
4.2.1	Eigenvalue Problem Equation	44
4.2.2	Results	46
CHAPTER 5:	DYNAMIC ANALYSIS	50
5.1	Single Microbeam Case	50
5.1.1	Reduced-Order Modeling (ROM)	50
5.1.2	Perturbation Analysis	51
5.1.3	Results	57
5.2	Double-Microbeams Case	60
5.2.1	Reduced-Order Modeling (ROM)	60
5.2.2	Perturbation Analysis	61
5.2.3	Results	77
5.2.4	Parametric Study	81
CHAPTER 6:	SUMMARY, CONCLUSIONS AND FUTURE WORK	89
6.1	Summary	89
6.2	Conclusions	90
6.3	Future Work	91
References	92
Vitae	98

List of Tables

Table 2.1: Mathematical expression of the forces	18
Table 3.1: Selected parameters for obtaining the static deflection of the single microbeam actuator.....	25
Table 3.2: Selected parameters for obtaining the static deflection of the double-microbeams actuator.....	29
Table 3.3: Microbeams geometrical and material properties.....	32
Table 3.4: Comparison of pull-in voltage	38
Table 4.1: Assumed geometrical and material properties [46]	42
Table 5.1: Assumed geometrical and material properties [34]	59

List of Figures

Figure 2.1: A parallel-plates capacitor configuration [43].....	10
Figure 2.2: 3D schematic of a single microbeam actuator under DC and AC electric loads [46].	12
Figure 2.3: 2D schematic of single microbeam actuator configuration.....	15
Figure 2.4: Free body diagram for the single microbeam of Figure 2.3.....	16
Figure 2.5: 2D schematic of double-microbeams actuator configuration.....	16
Figure 2.6: FBD for the lower microbeam of Figure 2.5.....	17
Figure 2.7: FBD for the upper microbeam of Figure 2.5.....	17
Figure 3.1: Schematic of an electrostatically actuated single microbeam actuator [38]	22
Figure 3.2: Convergence of the maximum deflection for the single microbeam of Table 3.1	25
Figure 3.3: Comparison for the obtained maximum static deflection of the single microbeam with literature results	26
Figure 3.4: Schematic of electrostatically actuated double-microbeams actuator [38].....	26
Figure 3.5: Convergence of the maximum static deflection for the upper microbeam of system of Table 3.2	30
Figure 3.6: Comparison for the maximum static deflection of the upper microbeam of system of Table 3.2.....	31
Figure 3.7: The maximum static deflection for the lower and upper microbeams for the case: when $d_1=d_2$	33
Figure 3.8: Static profile of the lower microbeam for three different voltages and for the case: when $d_1=d_2$	33

Figure 3.9: Static profile of the upper microbeam for three different voltages and for the case: when $d_1=d_2$	34
Figure 3.10: The maximum static deflection for the lower and upper microbeams for the case: when $d_1>d_2$	35
Figure 3.11: Static profile of the lower microbeam for three different voltages and for the case: when $d_1>d_2$	35
Figure 3.12: Static profile of the upper microbeam for three different voltages and for the case: when $d_1>d_2$	36
Figure 3.13: The maximum static deflection for the lower and upper microbeams for the case: when $d_1<d_2$	37
Figure 3.14: Static profile of the lower microbeam for three different voltages and for the case: when $d_1<d_2$	37
Figure 3.15: Static profile of the upper microbeam for three different voltages and for the case: when $d_1<d_2$	38
Figure 3.16: Comparison between the maximum static deflection for the upper microbeam for all three cases with the single microbeam case	39
Figure 4.1: Comparison between the obtained fundamental natural frequencies with literature [46]	43
Figure 4.2: Natural frequencies versus the applied voltage for double-microbeams	47
Figure 4.3: The fundamental natural frequencies for three different cases	48
Figure 4.4: The first coupled mode shape assuming $V_{DC}= 2 \text{ Volt}$	48
Figure 4.5: The second coupled mode shape assuming $V_{DC}= 2 \text{ Volt}$	49

Figure 5.1: Comparison of the obtained normalized nonlinear natural frequency with literature [34] for $V_{DC}= 2 \text{ Volt}$ except for the first two points where $V_{DC}= 1 \text{ Volt}$ 58

Figure 5.2: Comparison of the obtained deflection of the microbeam among the ROM and the perturbation method for $V_{DC}= 8 \text{ Volt}$ and $V_{AC}=0.03 \text{ Volt}$ 59

Figure 5.3: Frequency response curve of the (a) upper microbeam and (b) lower microbeam and assuming both ROM and perturbation method for the case of $d_1=d_2$ 78

Figure 5.4: Frequency response curve of the (a) upper microbeam and (b) lower microbeam and assuming both ROM and perturbation method for the case of $d_1<d_2$ 79

Figure 5.5: Frequency response curve of the (a) upper microbeam and (b) lower microbeam and assuming both ROM and perturbation method for the case of $d_1>d_2$ 80

Figure 5.6: Effect of the microbeam length (L) on the frequency response curve of the (a) lower microbeam and (b) upper microbeam for $V_{DC}= 2 \text{ Volt}$ and $V_{AC}=0.1 \text{ Volt}$ 82

Figure 5.7: Effect of the quality factor (Q) on the frequency response curve of the (a) lower microbeam and (b) upper microbeam for $V_{DC}= 10 \text{ Volt}$ and $V_{AC}=0.5 \text{ Volt}$ 84

Figure 5.8: Effect of the applied DC voltage (V_{DC}) on the frequency response curve of the (a) lower microbeam and (b) upper microbeam for $V_{AC}= 0.1 \text{ Volt}$ 85

Figure 5.9: Effect of the applied DC voltage (V_{DC}) on the frequency response curve of the (a) lower microbeam and (b) upper microbeam for $V_{AC}= 5 \text{ Volt}$ 86

Figure 5.10: Effect of the applied AC voltage (V_{AC}) on the frequency response curve of the (a) lower microbeam and (b) upper microbeam for $V_{DC}= 2 \text{ Volt}$87

Abstract

Full Name : Abdulrahman Mohammed Alofi
Thesis Title : Nonlinear Structural Behavior of Electrically Actuated MEMS
Actuator
Major Field : Mechanical Engineering
Date of Degree : November 2015

In this thesis, the static and dynamic behaviors of micro-electromechanical system (MEMS) double clamped-clamped microbeams are investigated. Two numerical methods were used in this investigation, which are the reduced-order modeling (ROM) and the perturbation method. The ROM was derived based on the Galerkin expansion method and assuming linear undamped mode shapes of straight beam as the basis functions. The perturbation method was generated using the method of multiple scales by direct attack of the equations of motion. The problem was first carried out by reproducing the results of the single microbeam (both static and dynamic). The static analysis for the double-microbeams was performed next using the ROM resulting equations. The results showed that the double-microbeams configuration requires a lower actuation voltage and a lower switching time as compared to the single one. Then, the effects of selection the air gap depths were investigated. The eigenvalue problem was investigated to obtain the fundamental natural frequencies and to study their variation with the applied DC load. Dynamic analyses, assuming the above two numerical methods, were performed and a comparison of the results showed good agreement. Finally, a parametric study was performed using the perturbation on different parameters and the results revealed different interesting features, which hopefully can be useful for some MEMS-based applications.

ملخص الرسالة

الاسم الكامل: عبدالرحمن محمد العوفي

عنوان الرسالة: دراسة في السلوك الغير خطي لأجهزة الميمس المشغلة بواسطة الكهرباء

التخصص: الهندسة الميكانيكية

تاريخ الدرجة العلمية: نوفمبر 2015

في هذه الرسالة, سيتم دراسة السلوك في حالة السكون و أيضا في حالة الحركة لنوع من أنظمة المايكرو (وهو استخدام عامودين) التي تستخدم الكهرباء وتعتمد على حركة ميكانيكية أو مايسمى (بالميمس). تم استخدام طريقتين عددية للتحليل, وهي كالتالي: نموذج الدرجة المخفضة وتحليل الاضطراب. تم اشتقاق نموذج الدرجة المخفضة باستخدام طريقة جالركين بافتراض وضعية الأشكال للنظام الخطي الغير واهن للعامود المستقيم كدوال أساسية عند الاشتقاق. بينما تم صنع طريقة تحليل الاضطراب باستخدام طريقة النطاقات المتعددة بتفعيلها مباشرة على معادلات الحركة. في البداية تم إعادة إيجاد النتائج للعامود الواحد في حالتيه الساكنة والمتحركة. بعد ذلك تم إجراء التحليل العددي للعامودين باستخدام المعادلات الناتجة من نموذج الدرجة المخفضة. أظهرت النتائج أن استخدام عامودين يؤدي إلى احتياج أقل من الجهد الكهربائي للتوليد وأيضاً إلى وقت أقل في التبديل مقارنة مع استخدام عامود واحد. بعد ذلك, تم دراسة تأثير اختيار عمق فراغ الهواء على النظام. ومن ثم تم فحص مسألة القيمة الذاتية وذلك لإيجاد الترددات الأساسية الطبيعية ودراسة تأثير تغييراتها مع الجهد الكهربائي. تم إجراء أيضاً دراسة على التحليل المتحرك باستخدام الطريقتين العدديتين السابقتين, وأظهرت النتائج تطابق جيد بين الطريقتين. أخيراً, تم إجراء دراسة لعدة عوامل متغيرة في المعادلة باستخدام تحليل الاضطراب وأظهرت النتائج عدة خصائص مثيرة للاهتمام, والتي نأمل أن تستخدم لاحقاً لبعض تطبيقات أجهزة الميمس.

CHAPTER 1: INTRODUCTION

1.1 Motivation

Since the 1980s, when micro-electro-mechanical-systems (MEMS) were invented, the demands for these tiny devices have increased dramatically. This is due to their excellent properties (mechanical, electrical etc.) and features (small sizes, easily fabricated etc.). While they were used first as sensors and actuators, they are nowadays used in many other applications in our daily life [1]. For example, MEMS are being used as pressure sensors [2, 3], accelerometers [4, 5], microphones in cellphones [6], micro-mirrors in plasma TVs [7], GPS [8] and many other useful applications. Moreover, they are still being developed by scientists and researchers, and these developments will hopefully lead to more useful features and become even more important in life.

A clamped-clamped microbeam forms one of the basic structures for building MEMS devices. Its desired features in many terms (fabrication, sensitivity, cost etc.) make it attractive in many MEMS-related applications. For example, the process of fabrication is easy and can be done by using bulk and surface micromachining techniques [9, 10]. Moreover, the natural frequencies of the clamped-clamped microbeam are higher relative to other microstructures such as cantilever microbeams. This feature is desirable since it helps in increasing the sensitivity of the microstructures to be used as RF filters [11], RF switches [12] and resonant sensors [13]. Applications of the clamped-clamped microbeam are numerous and examples can be found in projection display arrays [14], optical fibers [15] and thermal actuators [16].

In the MEMS community, there are many different types of structures available and the selection depends on the type of the application. For example, the configuration of a parallel-plates actuator made of a single microbeam provides a long range of travel with high power consumption and switching time. This is needed for many applications but not for others, where more desirable features and better performing structures can be achieved. One of the suggested structures is the use of double-microbeams instead of one in the parallel-plates actuators. Using double-microbeams increases the deflection of the microbeam with the same voltage that is provided in a single microbeam. As a result, it may help reducing the power consumption and the switching time for this type of applications.

Investigating the pull-in voltage is very important in electrically actuated micro-structures. In a static DC field, the microbeam will be actuated by a DC voltage, which will shift its equilibrium position into new one [17]. It is necessary that the microbeam operates far away from the pull-in voltage, otherwise the microstructure will fail, adhering to its down electrode. For double-microbeams there are many previous studies which shed light on this. However, in a dynamic AC field, in addition to the DC voltage, there will be a vibratory motion which excites the microbeam around its natural frequency. Accordingly, the pull-in voltage will change [17]. Further studies are needed, since still the area of dynamic double-microbeams configurations is sparse.

It is clear from the aforementioned few published investigations that studying the static and dynamic behaviors of clamped-clamped double-microbeams type of actuators is important and needs a lot of scope. Also, studying its dynamics may reveal very interesting phenomena, which may be used for inventing new devices or improving existing ones.

1.2 Literature Review

In this section, the main contributions of previously published investigations related to the static and dynamic analysis of double-microbeams are summarized. We will start by summarizing the main contributions in obtaining the deflection of microbeams in a theoretical way. Then, we will discuss more complicated and sophisticated numerical techniques, such as reduced-order modeling based on Galerkin expansion, as well as perturbation techniques. Finally, the literature review will discuss the use of double-microbeams as MEMS devices.

1.2.1 Solving the Nonlinear Microbeam's Equation

One of the main challenges in MEMS is obtaining the deflection of the microbeam until reaching the pull-in voltage. This will help in designing MEMS devices to obtain the desired features in less time, as compared to the trial and error method. However, this is not an easy task and many researchers have tried to find a way in to tackle this problem. The main techniques in solving the problem involve reducing the order of the partial differential governing equation, which is difficult to treat, to ordinary differential equation, which is easier in treatment. Three different approaches are used to obtain the reduction, which are idealization of the microbeam as a rigid body, discretization and constructing the reduced-order model.

The first approach is by idealization of the microbeam as a rigid body. The comparison of this method with a distributed parameter system showed that it under-predicts the pull-in voltage for cantilever [18] and clamped-clamped microbeams [19]. The second method is discretization, which uses an FEM (Finite Element Method), BEM (Boundary Element Method) or FDM (Finite Difference Method). Unlike the previous method, this method is adequate for predicting the pull-in voltage. However, the problem arises when solving for dynamic behavior, since it consumes

too much time, which makes the process computationally expensive. The last method is construction of the reduced-order model, which drew much attention in the previous years. The reduced-order model (ROM) is excellent in predicting the pull-in voltage, and can solve the dynamic deflection of the microbeam in a short time.

1.2.2 Reduced Order Modeling (ROM)

Nowadays, ROM plays an important role in obtaining the structural behavior of MEMS microstructures. There are many available investigations which used the method to solve the non-linear partial differential equation [20, 21] and many researchers tend to use this method, which made it among the most common numerical methods used in the MEMS community.

In 2003, Younis et al. [22] presented a new reduced-order model (macromodel) to solve for the non-linear partial differential equation. The macromodel uses the Galerkin procedure to discretize the distributed parameter system into finite degree of freedom system in the form of ordinary differential equations in time. The linear undamped mode shapes in straight positions are used as basis functions in the Galerkin procedure. The convergence of the method is reached by using only the first few mode shapes of the beam, hence saving both time and computational costs. They compared the macromodel results with results available in the literature, based mainly on finite element softwares and some experimental results, and they found that their method is more attractive than the finite element method in terms of accuracy and cost.

Nayfeh et al. [23] reviewed the work of ROM in MEMS devices. They classified the ROM into two main categories: node and domain methods. The idea of the node method is to evaluate the system equations at each node and then use the obtained lower order approximations, while the domain method uses modal analysis and the Galerkin method to convert the partial-differential-

equations (PDEs) into ordinary differential equations (ODEs) by eliminating the spatial dependence, which will describe the equations in terms of domain-wide modes (eigenfunctions). There are two proposed ways to obtain the basis set in the Galerkin procedure. The first way is to conduct experiments, or by using an FEM or FDM to solve for the PDEs, and then the basis set will be extracted from the time series. The second way is to use the mode shapes obtained by solving the linear undamped eigenvalue problem (EVP) of the device. At the end, they presented a ROM for microbeams and microplates, and presented approaches to deal with two types of damping as well as analytical expressions for the damping coefficient. They validated the results after comparing them with available results in the literature.

1.2.3 Perturbation Theory

There have been several attempts using several different approaches to investigate the dynamic behavior of microbeams [24-26]. For example, ROM was just one of approaches used, Zook et al. [27] investigated the behavior experimentally, others used Rayleigh's energy method [28, 29], and several have made use of the perturbation theory [30-32] in their investigations.

Turner and Andrews [33] used the perturbation method to obtain an approximation for the nonlinear resonance frequency of a microbeam. They modeled the problem by using a spring mass model, and they included a cubic restoring force to represent the mid-plane stretching. They indicated that to achieve high sensitivity it is required to limit the amplitude of vibration at a fixed and small value.

Younis et al. [34] used the method of multiple scales, as a perturbation method, in a model that accounted for the electrical loads (both DC and AC) and for the mid-plane stretching for a clamped-clamped single microbeam resonator. They lumped the parameters into a non-

dimensional form and obtained two equations in the form of nonlinear ODEs. They compared the results with some experimental results, validating their results.

1.2.4 Double-Microbeams Configuration in MEMS

There are a few investigators that discussed the use of double-microbeams as building blocks in several MEMS devices. Abbaspour-Sani et al. [35] proposed a double beam structure where both the contact plates are non-stationary to be used in micro-machined switches applications. They indicated that the proposed structure is able to reduce the actuation voltage by 30% if used with a single beam. Moreover, the structure will reduce the stress which results from the actuation voltage and so the switching life time will be increased.

Chaffey et al. [36] developed an analytical model for cantilever structures. Then, the model was used in a double-cantilever microstructure to investigate the properties. They concluded that the use of a double-cantilever microbeam structure will reduce the pull-in voltage, as compared to a single cantilever microbeam structure.

Samaali et al. [37] proposed a new structure by using double-cantilever microbeams for RF micro-switch applications. They developed the mathematical model for the structure by considering the microbeams as flexible and the microplates as rigid. After examining the static and dynamic behaviors, they indicated that the structure will reduce the actuation voltage by 30% and reduce the switching time by 45%, as compared to a single microbeam configuration.

Ouakad et al. [38] used the Galerkin procedure and an ANSYS software package to calculate the maximum static deflection that can be obtained from an electrically actuated microbeam and an electrically actuated double-microbeams actuator. Their comparison showed that larger

deflections can be obtained by using the double-microbeams scheme. They concluded that it is more desirable to use the double-microbeams whenever large deflections are needed.

So, it is clear from the above-mentioned literature that there is a great need to study the dynamic characteristics of clamped-clamped double-microbeams MEMS-based actuators.

1.3 Thesis Objectives and Organization

In this thesis, there are three major objectives:

- To reproduce the results of the previous work (the static and dynamic behaviors of one microbeam and the static behavior of a double-microbeams MEMS actuator).
- To solve the eigenvalue problem of the double-microbeams MEMS actuator to obtain the natural frequencies and the mode shapes of the system.
- To investigate the dynamic problem of a double-microbeams configuration by using two different methods (the Galerkin procedure and the perturbation theory) and then make a comparison between the approaches.
- Finally, carry out a thorough parametric study for different geometrical cases with concentration more on the dynamic of double-microbeams case.

This paragraph will discuss the organization of the rest of this thesis. The second chapter will present small background about some phenomena and terminologies that are bases in the MEMS community and then show the problem formulation for the proposed model. In Chapter 3, the static analysis of one microbeam will be carried out by using the Galerkin method with a parametric study at the end. In Chapter 4, the analysis of the eigenvalue problem will be carried out for both single and double-microbeams and present the variation of the natural frequencies and mode shapes. Chapter 5 will investigate the dynamic behavior of double-microbeams using

both methods (Galerkin and perturbation) and the comparison between them with a parametric study for several cases. Finally, Chapter 6 will be for the summary and some recommendations for future work.

CHAPTER 2: BACKGROUND

This chapter will present and summarize general concepts about some common terminologies used in the MEMS field. Also, this chapter will summarize some background about two methods which will be used in solving the microbeams equations, which are the Galerkin and the perturbation methods. At the end of the chapter, the problem for single and double-microbeams configurations will be formulated.

2.1 Parallel-plates Electrostatic Actuation

The parallel-plates electrostatic actuation forms one of the most used actuation methods in many MEMS devices [39]. This is due to the powerful advantages that it possesses. For example, it can generate high force with low power consumption and fast actuation [40]. Also, it can be integrated into a standard integrated circuit [41]. A simple model of this system, which is shown in Figure 2.1, can be described as one moving electrode, which is made of a conductive material -usually silicon- and is restrained by a spring, and another fixed electrode made of the same material, which is placed underneath the moving electrode. The distance between the two electrodes is called the gap and it is made of a dielectric medium, usually air. When there is no voltage difference between the two electrodes or no applied voltage, the two electrodes will be held in their initial parallel positions and the separated distance is called the rest gap distance. However, if there is an applied source voltage between the two, there will be potential difference which will make the moving plate travelling toward or away from the fixed plate until the electrostatic force and the spring force are equal to each other. [42]

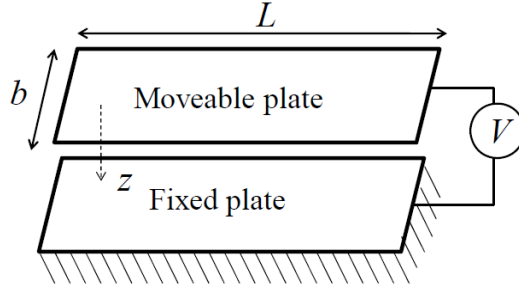


Figure 2.1: A parallel-plates capacitor configuration [43]

2.2 Electrostatic Force

In this section the electrostatic force between two parallel-plates will be derived. A schematic model of this system is shown in Figure 2.1, where it is assumed that the electric field lines between the two plates are perpendicular to them, and no fringing field effects are considered, even close to the edges. Here, we let the electrical charge be (Q) and the source voltage be (V), which is responsible for deriving the capacitor. The electrical charge and the potential energy stored in the capacitor can be written according to Hayt [44] as follows, respectively:

$$Q = C(z)V \quad (2.1)$$

$$E = \frac{V^2}{2} C(z) \quad (2.2)$$

where $C(z)$ is the capacitance between the two electrodes, and for rectangular parallel-plates can be written as [44]:

$$C(z) = \frac{\epsilon_0 L b}{z} \quad (2.3)$$

and where ϵ_0 is the air permittivity and is equal to $8.85 \cdot 10^{-12}$ ($C^2/N.m^2$), and L and b are the length and the width of the plate, respectively.

Since the mathematical expression for the electrostatic force is written as follows [44]:

$$F_e = \frac{V^2}{2} \frac{\partial C(z)}{\partial z} \quad (2.4)$$

the electrostatic force of the rectangular parallel-plates type of capacitor, Figure 2.1, can then be written as:

$$F_e = \frac{-\epsilon_0 L b V^2}{2z^2} \quad (2.5)$$

2.3 Pull-in Instability

Despite the excellent properties and features of electrically-actuated MEMS, they are like any system, in that there are some drawbacks which need to be avoided. One of the main drawbacks of these systems is called the pull-in instability. In order to describe this phenomenon we assume the beam that is shown in Figure 2.2 is subjected to an electrical load. The beam is at rest before the application of the load. By applying a small electrical load, the restoring force of the beam will resist this amount of load, and as a result the beam will move to a new equilibrium position. As the applied load increases the beam will try to resist that and move to another new equilibrium position. This continues until a critical amount of load is reached, the restoring force of the beam will be exceeded and the beam can no longer resist the load. There will be a sudden drop of the beam to the fixed electrode and it will adhere to it, which is known as the pull-in phenomenon [45].

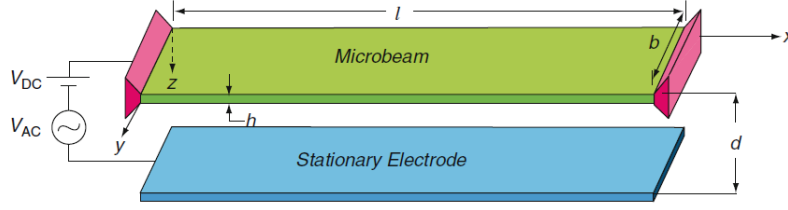


Figure 2.2: 3D schematic of a single microbeam actuator under DC and AC electric loads [46].

2.4 Perturbation Theory

The perturbation theory is usually used to approximate the solution of problems that are difficult to solve computationally. The idea of this technique involves the consideration of a related problem, which can be solved easily, solving the related problem and then using it as a leading term in the solution, which needs to be written as a power series as follows [47]:

$$u(t; \varepsilon) = u_0(t) + \varepsilon^1 u_1(t) + \varepsilon^2 u_2(t) + \dots \quad (2.6)$$

So, according to the previous equation (u_0) is considered to be the leading term and (u_1, u_2, \dots, u_n) are deviations or perturbation from the leading term (or higher order terms) and can be solved by using some systematic procedure.

The letter (ε) is a small parameter which is used to represent the significance of each in the series' term. As a result, the significance of the leading term is always the highest and it decreases as it moves to the right until reaching (u_n), which is the term that has the lowest significance. For most of the problems, it is enough to consider the approximate solution as a summation of the first two terms. So, the approximate solution can be written as follows [47]:

$$u(t; \varepsilon) \approx u_0(t) + \varepsilon^1 u_1(t) \quad (2.7)$$

One of the most common used methods in the perturbation theory is the method of multiple scales. The idea of the method is to convert time (t) into different time scales, as follows:

$$T_0 = t, \quad T_1 = \varepsilon t, \quad T_2 = \varepsilon^2 t, \quad T_n = \varepsilon^n t, \quad (2.8)$$

where the T_n represent different time scales.

Thus, the independent variable is changed from time (t) to T_0, T_1, T_2, \dots . Then, the uniform approximate solution can be written as follows:[47]

$$u(T_0, T_1, T_2, \dots; \varepsilon) = u_0(T_0, T_1, T_2, \dots) + \varepsilon^1 u_1(T_0, T_1, T_2, \dots) + \dots \quad (2.9)$$

2.5 Galerkin Method

The Galerkin method is a helpful method for converting a continuous system into a discrete one. It was first discovered by Walther Ritz, but it is usually ascribed to the mathematician scientist Boris Galerkin [48]. There are many examples of the Galerkin method and one of the most common methods is called “the Galerkin method of weighted residuals”, which can be used to solve differential equations. The idea of the method is to first consider the solution of the differential equation according to the finite element method as a polynomial in this form:

$$u(x) = \sum_{i=1}^m a_i \phi_i(x) \quad (2.10)$$

where, $\{\phi_i | i = 1, \dots, m\}$ are called basis functions (or trial functions), which should satisfy the boundary conditions. These functions should be continuously differentiable and chosen carefully, since the accuracy of the solution is highly dependent on them. The Galerkin method is concerned with finding the unknown coefficients of the equation i.e. $\{a_i | i = 1, \dots, m\}$, which is done by making every solution $u_i(x)$ $\{u_i | i = 1, \dots, m\}$ orthogonal to $L\{y(x)\}$, which is the differential operator to $u(x)$. [49]

2.6 Euler-Bernoulli Beam Model

The Euler-Bernoulli beam is so named for the contribution of two scientists, Leonhard Euler and Daniel Bernoulli. The beam can be considered as a special case of the Timoshenko beam theory after following some assumptions. Though the theory was developed long ago, around 1750, it was not considered trustworthy until its validation on large scales, which was in the late 19th century [50]. The equation of the beam relates the deflection of the beam with the applied load in a 4th order differential equation. In dealing with static load, the equation will be an ordinary differential equation and can be written as [51]:

$$\frac{d^2}{dx^2} \left(EI \frac{d^2 w}{dx^2} \right) = q(x) \quad (2.11)$$

where E is the modulus of elasticity, I is the second moment of area which is calculated with respect to the axis that is perpendicular to the applied load and passing through the centroid of the cross section, w is the deflection of the microbeam in the z -axis and it is function of x (position) and $q(x)$ is the distributed load. The equation can be simplified by considering the

product EI as being independent of the position (x), which is often the case, so equation (2.12) will simply be:

$$EI \frac{d^4 w}{dx^4} = q(x) \quad (2.12)$$

In the dynamic case, the Euler-Bernoulli beam equation will be a partial differential equation with respect to the position (x) and the time (t) variables, which can be written as:

$$EI \frac{\partial^4 w}{\partial x^4} + \mu \frac{\partial^2 w}{\partial t^2} = q(x, t) \quad (2.13)$$

where, μ is the mass per unit length.

2.7 Problem Formulation

This section will discuss the problem formulation and derivation of the equations for the chosen system of single and double-microbeams MEMS based actuators.

2.7.1 Free Body Diagram (FBD) of a Single Microbeam

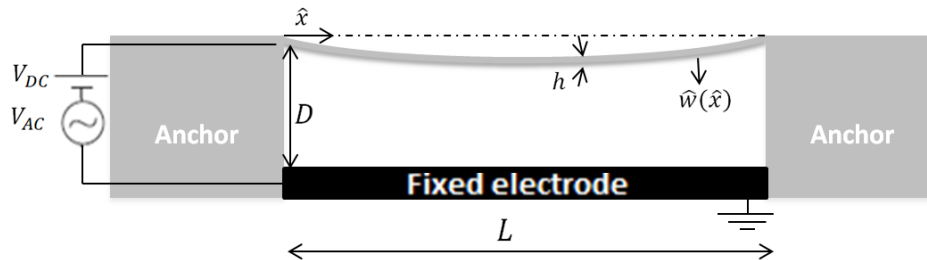


Figure 2.3: 2D schematic of single microbeam actuator configuration

It is clear from Figure 2.3 that, the model is a microbeam which is clamped-clamped at both ends and electrically actuated by a DC bias (V_{DC}) and a harmonic excitation (V_{AC}). The free body diagram (FBD) of the microbeam is shown below:

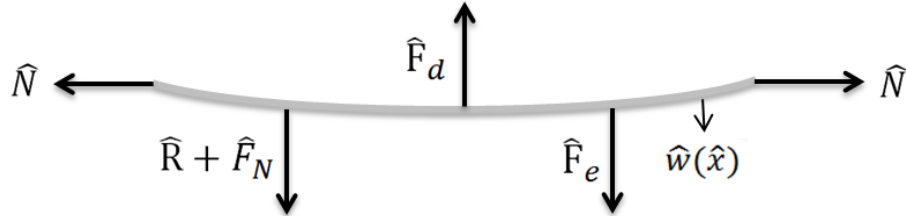


Figure 2.4: Free body diagram for the single microbeam of Figure 2.3

where:

\hat{N} is the normal forces at the boundaries, \hat{F}_d is the damping force on the microbeam, \hat{R} is the mid-plane stretching term, \hat{F}_N is the force that results from the axial load on the microbeam, and \hat{F}_e is the electrostatic force that acts on the microbeam from the fixed electrode, where the separated distance at any point on the lower microbeam to the fixed electrode is the initial gap between them (D) minus its deflection ($\hat{w}(\hat{x})$).

2.7.2 Free Body Diagram (FBD) of Double-microbeams

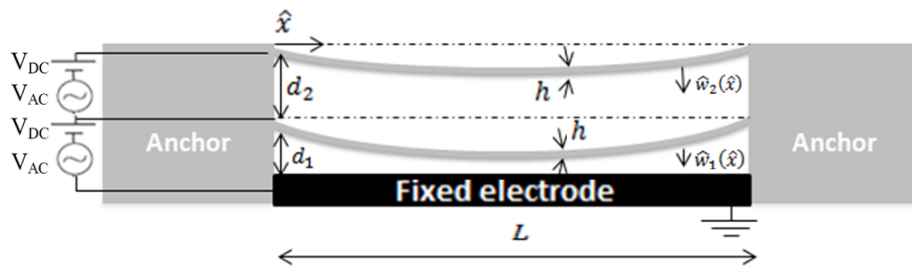


Figure 2.5: 2D schematic of double-microbeams actuator configuration

The chosen model for the double-microbeams, which is shown in Figure 2.5, is clamped-clamped for both ends of both microbeams and it is electrically actuated by a DC bias (V_{DC}) and a harmonic excitation (V_{AC}). The free body diagrams (FBD) for the two microbeams are shown below:

- For the lower microbeam:

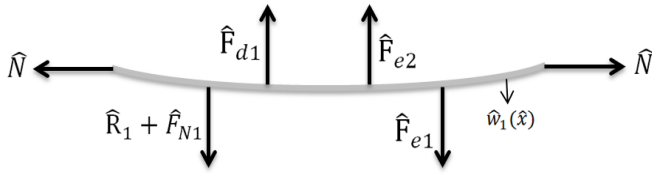


Figure 2.6: FBD for the lower microbeam of Figure 2.5

- For the upper microbeam:

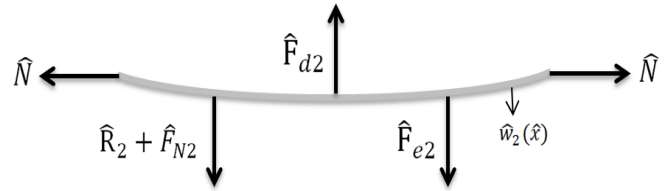


Figure 2.7: FBD for the upper microbeam of Figure 2.5

where:

\hat{F}_{d1} , \hat{F}_{d2} , \hat{R}_1 , \hat{R}_2 , \hat{F}_{N1} and \hat{F}_{N2} are the same definition in one microbeam with the subscripts of (1) and (2) to indicate the lower and upper microbeams, respectively.

\hat{F}_{e1} is the electrostatic force that actuates the lower microbeam from the fixed electrode, where the separation distance at any point on the lower microbeam to the fixed electrode is the initial gap between them (d_1) minus its deflection ($\hat{w}_1(\hat{x})$).

\hat{F}_{e2} is the electrostatic force that each microbeams is mutually applying to each other, where the separated distance between two points at different microbeams is the initial gap between them (d_2) to which is added the deflection of the lower microbeam ($\hat{w}_1(\hat{x})$) and from which is subtracted ($\hat{w}_2(\hat{x})$).

2.7.3 Deriving the System Equations of Motion

The followed method used in deriving the equations is Newton's second law where:

$$\sum \vec{F} = m\vec{a} \quad (2.14)$$

The mathematical expression for each force is shown in the next table:

Table 2.1: Mathematical expression of the forces

Force	Expression	Force	Expression
F_d	$\hat{c} \frac{\partial \hat{w}}{\partial \hat{t}}$	F_{d1}	$\hat{c} \frac{\partial \hat{w}_1}{\partial \hat{t}}$
F_{d2}	$\hat{c} \frac{\partial \hat{w}_2}{\partial \hat{t}}$	R	$\frac{EA}{2L} \int_0^L \left(\frac{\partial \hat{w}}{\partial \hat{x}} \right)^2 d\hat{x} \frac{\partial^2 \hat{w}}{\partial \hat{x}^2}$
R_1	$\frac{EA}{2L} \int_0^L \left(\frac{\partial \hat{w}_1}{\partial \hat{x}} \right)^2 d\hat{x} \frac{\partial^2 \hat{w}_1}{\partial \hat{x}^2}$	R_2	$\frac{EA}{2L} \int_0^L \left(\frac{\partial \hat{w}_2}{\partial \hat{x}} \right)^2 d\hat{x} \frac{\partial^2 \hat{w}_2}{\partial \hat{x}^2}$
F_N	$\hat{N} \frac{\partial^2 \hat{w}}{\partial \hat{x}^2}$	F_{N1}	$\hat{N} \frac{\partial^2 \hat{w}_1}{\partial \hat{x}^2}$
F_{N2}	$\hat{N} \frac{\partial^2 \hat{w}_2}{\partial \hat{x}^2}$	F_e	$\frac{\varepsilon_0 b (V_{DC} + V_{AC} \cos(\hat{\Omega} \hat{t}))^2}{2(D - \hat{w})^2}$
F_{e1}	$\frac{\varepsilon_0 b (V_{DC} + V_{AC} \cos(\hat{\Omega} \hat{t}))^2}{2(d_1 - \hat{w}_1)^2}$	F_{e2}	$\frac{\varepsilon_0 b (V_{DC} + V_{AC} \cos(\hat{\Omega} \hat{t}))^2}{2(d_2 + \hat{w}_1 - \hat{w}_2)^2}$

where \hat{c} is the viscous damping coefficient; E is Young's modulus of elasticity; A is the cross sectional area and is equal to bh , where b and h are the width and the height of the microbeam, respectively; L is the length of the beam; \hat{N} is the axial load; ε_0 is the dielectric constant; V_{DC} and V_{AC} are, respectively, the applied DC and AC voltages and $\hat{\Omega}$ is the frequency.

Using Newton's second law with Euler Bernoulli's beam equation, we obtain:

- For a single microbeam:

$$EI \frac{\partial^4 \hat{w}}{\partial \hat{x}^4} + \rho b h \frac{\partial^2 \hat{w}}{\partial \hat{t}^2} + \hat{c} \frac{d\hat{w}}{d\hat{t}} = \left(\frac{EA}{2L} \int_0^L \left(\frac{\partial \hat{w}}{\partial \hat{x}} \right)^2 d\hat{x} + \hat{N} \right) \frac{\partial^2 \hat{w}}{\partial \hat{x}^2} + \frac{\varepsilon_0 b (V_{DC} + V_{AC} \cos(\hat{\Omega} \hat{t}))^2}{2(D - \hat{w})^2} \quad (2.15)$$

and the associated boundary conditions:

$$\hat{w}(0, t) = 0 \quad \hat{w}(L, t) = 0 \quad \frac{\partial \hat{w}}{\partial \hat{x}}(0, t) = 0 \quad \frac{\partial \hat{w}}{\partial \hat{x}}(L, t) = 0 \quad (2.16)$$

- For double-microbeams:

$$\left\{ \begin{array}{l} \rightarrow EI \frac{\partial^4 \hat{w}_1}{\partial \hat{x}^4} + \rho b h \frac{\partial^2 \hat{w}_1}{\partial \hat{t}^2} + \hat{c} \frac{\partial \hat{w}_1}{\partial \hat{t}} = \left(\frac{EA}{2L} \int_0^L \left(\frac{\partial \hat{w}_1}{\partial \hat{x}} \right)^2 d\hat{x} + \hat{N} \right) \frac{\partial^2 \hat{w}_1}{\partial \hat{x}^2} + \\ + \frac{\varepsilon_0 b (V_{DC} + V_{AC} \cos(\hat{\Omega} \hat{t}))^2}{2(d_1 - \hat{w}_1)^2} - \frac{\varepsilon_0 b (V_{DC} + V_{AC} \cos(\hat{\Omega} \hat{t}))^2}{2(d_2 + \hat{w}_1 - \hat{w}_2)^2} \end{array} \right. \quad (2.17)$$

$$\left\{ \begin{array}{l} \rightarrow EI \frac{\partial^4 \hat{w}_2}{\partial \hat{x}^4} + \rho b h \frac{\partial^2 \hat{w}_2}{\partial \hat{t}^2} + \hat{c} \frac{\partial \hat{w}_2}{\partial \hat{t}} = \left(\frac{EA}{2L} \int_0^L \left(\frac{\partial \hat{w}_2}{\partial \hat{x}} \right)^2 d\hat{x} + \hat{N} \right) \frac{\partial^2 \hat{w}_2}{\partial \hat{x}^2} + \\ + \frac{\varepsilon_0 b (V_{DC} + V_{AC} \cos(\hat{\Omega} \hat{t}))^2}{2(d_2 + \hat{w}_1 - \hat{w}_2)^2} \end{array} \right. \quad (2.18)$$

and the associated boundary conditions are:

$$\hat{w}_1(0, t) = 0 \quad \hat{w}_1(L, t) = 0 \quad \frac{\partial \hat{w}_1}{\partial \hat{x}}(0, t) = 0 \quad \frac{\partial \hat{w}_1}{\partial \hat{x}}(L, t) = 0 \quad (2.19)$$

$$\hat{w}_2(0,t) = 0 \quad \hat{w}_2(L,t) = 0 \quad \frac{\partial \hat{w}_2}{\partial \hat{x}}(0,t) = 0 \quad \frac{\partial \hat{w}_2}{\partial \hat{x}}(L,t) = 0 \quad (2.20)$$

where ρ is the mass density and I is the moment of inertia, which is equal to $\frac{1}{12}bh^3$.

2.7.4 Normalization

In order to deal with these types of equations in the micro-scale, it is more convenient to write these equations in non-dimensional form; this can be done by considering the following non-dimensional variables:

$$w_1 = \frac{\hat{w}_1}{d_1} \quad w_2 = \frac{\hat{w}_2}{d_1} \quad w_3 = \frac{\hat{w}_3}{d_1} \quad x = \frac{\hat{x}}{L} \quad t = \frac{\hat{t}}{T} \quad (2.21)$$

where T is a time scale parameter and is chosen to be $T = \sqrt{\frac{\rho b h L^4}{E I}}$

So, substituting equation (2.21) into equations (2.17), (2.18), (2.19) and (2.20) will give:

- For a single microbeam:

$$\frac{\partial^4 w}{\partial x^4} + \frac{\partial^2 w}{\partial t^2} + c \frac{\partial w}{\partial t} = (\alpha_1 \Gamma + N) \frac{\partial^2 w}{\partial x^2} + \frac{\alpha_2 (V_{DC} + V_{AC} \cos(\Omega t))^2}{(1-w)^2} \quad (2.22)$$

$$w(0,t) = 0 \quad w(1,t) = 0 \quad \frac{\partial w}{\partial x}(0,t) = 0 \quad \frac{\partial w}{\partial x}(1,t) = 0 \quad (2.23)$$

- For double-microbeams:

$$\frac{\partial^4 w_1}{\partial x^4} + \frac{\partial^2 w_1}{\partial t^2} + c \frac{\partial w_1}{\partial t} = (\alpha_3 \Gamma_1 + N) \frac{\partial^2 w_1}{\partial x^2} + \frac{\alpha_4 (V_{DC} + V_{AC} \cos(\Omega t))^2}{(1 - w_1)^2} - \frac{\alpha_4 (V_{DC} + V_{AC} \cos(\Omega t))^2}{(d_2/d_1 + w_1 - w_2)^2} \quad (2.24)$$

$$\frac{\partial^4 w_2}{\partial x^4} + \frac{\partial^2 w_2}{\partial t^2} + c \frac{\partial w_2}{\partial t} = (\alpha_3 \Gamma_2 + N) \frac{\partial^2 w_2}{\partial x^2} + \frac{\alpha_4 (V_{DC} + V_{AC} \cos(\Omega t))^2}{(d_2/d_1 + w_1 - w_2)^2} \quad (2.25)$$

$$w_1(0, t) = 0 \quad w_1(1, t) = 0 \quad \frac{\partial w_1}{\partial x}(0, t) = 0 \quad \frac{\partial w_1}{\partial x}(1, t) = 0 \quad (2.26)$$

$$w_2(0, t) = 0 \quad w_2(1, t) = 0 \quad \frac{\partial w_2}{\partial x}(0, t) = 0 \quad \frac{\partial w_2}{\partial x}(1, t) = 0 \quad (2.27)$$

where the nondimensional parameters are defined as follows:

$$c = \frac{\hat{c}L^4}{TEI} \quad \alpha_1 = 6 \left(\frac{D}{h} \right)^2 \quad \alpha_2 = \frac{6\varepsilon_0 L^4}{Eh^3 D^3} \quad \alpha_3 = 6 \left(\frac{d_1}{h} \right)^2 \quad \alpha_4 = \frac{6\varepsilon_0 L^4}{Eh^3 d_1^3}$$

$$N = \frac{\hat{N}L^2}{EI} \quad \Gamma = \int_0^1 \left(\frac{\partial w}{\partial x} \right)^2 dx \quad \Gamma_i = \int_0^1 \left(\frac{\partial w_i}{\partial x} \right)^2 dx$$

So from now on, equations (2.22) and (2.23) will be used to solve for the single microbeam whereas for double-microbeams equations (2.24), (2.25), (2.26) and (2.27) will be used.

CHAPTER 3: STATIC ANALYSIS

In this chapter, the static analysis of straight clamped-clamped and double-microbeams actuated by electrostatic force will be carried out. The results obtained will be compared to the results that are available in the literature. The method used to evaluate the deflection of the microbeam is ROM and the procedure is described in the coming chapter's sections.

3.1 Static Analysis of a Single Microbeam Based MEMS Actuator

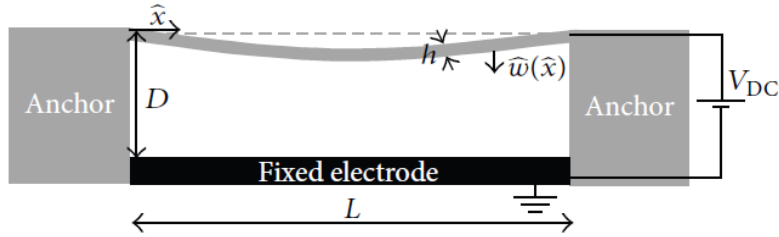


Figure 3.1: Schematic of an electrostatically actuated single microbeam actuator [38]

3.1.1 Model and ROM

As in the aforementioned, equation (2.22) expresses the equation of a clamped-clamped straight microbeam actuated by electrical force. In dealing with the static behavior, the equation will be independent of time. As a result, the inertia, damping and the harmonic force terms will be dropped. So, the equation of the microbeam will be reduced to:

$$\frac{d^4 w}{dx^4} = (\alpha_1 \Gamma + N) \frac{d^2 w}{dx^2} + \frac{\alpha_2 V_{DC}^2}{(1-w)^2} \quad (3.1)$$

The boundary conditions will remain the same. In order to get the (ROM), the previous equation will be discretized using Galerkin method. This can be done by letting the static deflection be:

$$w(x, t) = \sum_{i=1}^N k_i \phi_i(x) \quad (3.2)$$

where the coefficients k_i are constants independent of the time and $\phi_i(x)$ are the symmetric mode shapes of the linear undamped microbeam.

To solve for the constants k_i it is required to substitute equation (3.2) into equation (3.1), then multiply the outcome by $\phi_j(x)$, and finally integrate the outcome from $x=0$ to $x=1$. Following the previous procedure will give:

$$\int_{x=0}^1 \phi_j(x) \sum_{i=1}^N k_i \phi_i^{iv}(x) dx = \int_{x=0}^1 \phi_j \left(\left(\alpha_1 \int_0^1 \left(\sum_{i=1}^N k_i \phi_i'(x) \right)^2 dx + N \right) \sum_{i=1}^N k_i \phi_i''(x) + \alpha_2 \frac{V_{DC}^2}{\left(1 - \sum_{i=1}^N k_i \phi_i(x) \right)^2} \right) dx \quad (3.3)$$

It can be seen that the previous equation is an algebraic equation with the constants k_i being the only unknowns. The number of equations here is equal to the number of modes that are considered in equation (3.2). In order to know the dominant number of modes we need to start with one mode and then increase the number of modes; for each number of modes we solve for

the unknowns k_i and then evaluate the maximum deflection until the solution is converged. To reduce the computational cost it is better to multiply the previous equation by $\left(1 - \sum_{i=1}^N k_i \phi_i(x)\right)^2$ to get rid of the unknowns k_i in the denominator when integrating [22]. So, the method in getting the deflection at any point on the microbeam can be summarized as follows:

- 1- Start with assuming only one mode in the ROM, find the k_i by solving equation (3.3).
- 2- Evaluate and plot the maximum nondimensional deflection by substituting the k_i 's in equation (3.2) for various DC voltages.
- 3- Increase the number of modes by one
- 4- Repeat the previous steps until the maximum deflection is converged
- 5- The deflection of the microbeam at any point can be obtained by evaluating equation (3.2) and then multiplying it by the air gap width (D).

3.1.2 Results

Younis [46] investigated a similar problem by considering the parameters summarized in Table 3.1. To validate our analysis, we would like to reproduce the same results by considering the same selected parameters.

Table 3.1: Selected parameters for obtaining the static deflection of the single microbeam actuator

Parameter	Value	Parameter	Value
Beam Length (L)	100 μm	Effective young's modulus (E)	124 GPa
Beam thickness (h)	0.5 μm	Density (ρ)	2,332 kg/m^3
Beam width (b)	10 μm	Air gap width (D)	1.0 μm
Axial load (N)	0		

The maximum deflection of the microbeam is plotted versus the applied DC voltage, as seen in Figure 3.2, up to four modes. It can be noticed from the graph that increasing the number of modes will converge the solution and three modes seems to be sufficient for convergence.

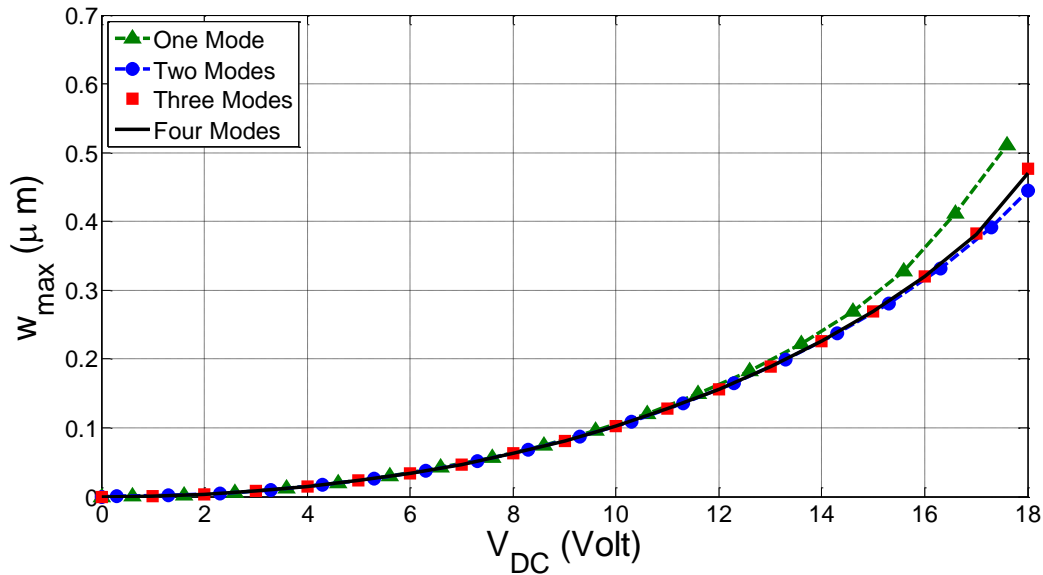


Figure 3.2: Convergence of the maximum deflection for the single microbeam of Table 3.1

A comparison between the obtained results and the results available in the literature using three modes is shown in Figure 3.3, which shows excellent agreement.

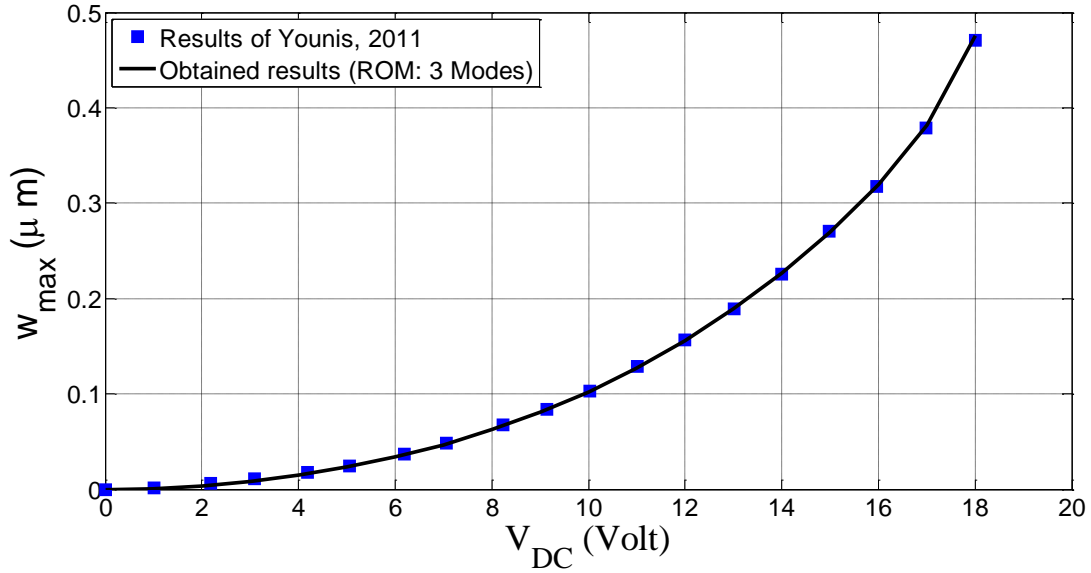


Figure 3.3: Comparison for the obtained maximum static deflection of the single microbeam with literature results

3.2 Static Analysis of Double Microbeams Actuator

3.2.1 Model and ROM

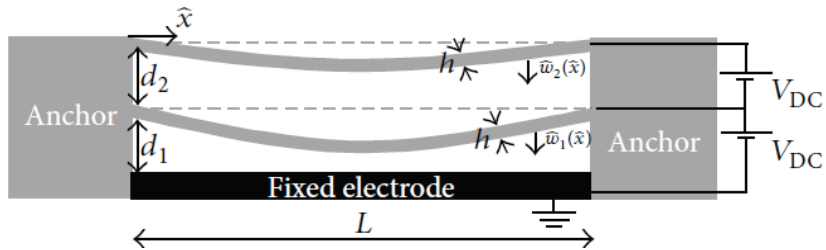


Figure 3.4: Schematic of electrostatically actuated double-microbeams actuator [38]

The equations of double clamped-clamped straight microbeams actuated by an electrostatic force are given in equations (2.24) and (2.25). As in the previous section, the equations will be independent of time since we are dealing with a static problem. After cancelling the time dependent terms the equations will be reduced to:

$$\frac{d^4 w_1}{dx^4} = (\alpha_3 \Gamma_1 + N) \frac{d^2 w_1}{dx^2} + \frac{\alpha_4 V_{DC}^2}{(1-w_1)^2} - \frac{\alpha_4 V_{DC}^2}{(d_2/d_1 + w_1 - w_2)^2} \quad (3.4)$$

$$\frac{d^4 w_2}{dx^4} = (\alpha_3 \Gamma_2 + N) \frac{d^2 w_2}{dx^2} + \frac{\alpha_4 V_{DC}^2}{(d_2/d_1 + w_1 - w_2)^2} \quad (3.5)$$

The reduced-order model can be obtained by discretizing the previous two equations using the Galerkin expansion. So, the static deflection for the two microbeams will be discretized as follows:

$$w_1(x, t) = \sum_{i=1}^N f_i \phi_i(x) \quad (3.6)$$

$$w_2(x, t) = \sum_{i=1}^N g_i \phi_i(x) \quad (3.7)$$

where, the f_i and the g_i are unknown constants that are independent of time.

To solve for the constants f_i and g_i , it is required to substitute equations (3.6) and (3.7) into equations (3.4) and (3.5), then multiply the outcome by $\phi_j(x)$, and finally integrate the outcome from $x=0$ to $x=1$ to get the following equations:

$$\int_{x=0}^1 \phi_j(x) \sum_{i=1}^N f_i \phi_i^{iv}(x) dx = \int_{x=0}^1 \phi_j \left(\left(\alpha_3 \int_0^1 \left(\sum_{i=1}^N f_i \phi_i'(x) \right)^2 dx + N \right) \sum_{i=1}^N f_i \phi_i''(x) \right) dx + \int_{x=0}^1 \phi_j \left(\alpha_4 \frac{V_{DC}^2}{\left(1 - \sum_{i=1}^N f_i \phi_i(x) \right)^2} - \frac{\alpha_4 V_{DC}^2}{\left(d_2/d_1 + \sum_{i=1}^N f_i \phi_i(x) - \sum_{i=1}^N g_i \phi_i(x) \right)^2} \right) dx \quad (3.8)$$

$$\int_{x=0}^1 \phi_j(x) \sum_{i=1}^N g_i \phi_i^{iv}(x) dx = \int_{x=0}^1 \phi_j \left(\left(\alpha_3 \int_0^1 \left(\sum_{i=1}^N g_i \phi_i'(x) \right)^2 dx + N \right) \sum_{i=1}^N g_i \phi_i''(x) \right) dx + \int_{x=0}^1 \phi_j \left(\frac{\alpha_4 V_{DC}^2}{\left(d_2/d_1 + \sum_{i=1}^N f_i \phi_i(x) - \sum_{i=1}^N g_i \phi_i(x) \right)^2} \right) dx \quad (3.9)$$

In the previous algebraic equations we have to set the unknowns f_i and g_i . In this instance, the number of equations will be double that of the number of modes that we considered. The procedure in getting the dominant number of modes is similar to that of the single beam, except that the number of constants will be double. We propose to verify the convergence of the beam that has maximum deflection, since the other converges by default. We can reduce the computational cost by multiplying the first equation by

$\left(1 - \sum_{i=1}^N f_i \phi_i(x)\right)^2 \left(d_2/d_1 + \sum_{i=1}^N f_i \phi_i(x) - \sum_{i=1}^N g_i \phi_i(x)\right)^2$ and the second by
 $\left(d_2/d_1 + \sum_{i=1}^N f_i \phi_i(x) - \sum_{i=1}^N g_i \phi_i(x)\right)^2$, which will help in getting rid of the unknown constants in the denominator when integrating with space.

3.2.2 Results

This problem was investigated first by Ouakad et al. [38]. Here we considered the same parameters to reproduce the same results. The chosen parameters are shown in Table 3.2. To check the convergence, the maximum deflection of the upper microbeam is plotted versus the applied DC voltage, since it has the maximum deflection, as seen in Figure 3.5. Again, as in the single microbeam case, it can be noted from the graph that when the number of modes is increased the solution is converging, until convergence is reached for three modes.

Table 3.2: Selected parameters for obtaining the static deflection of the double-microbeams actuator

Parameter	Value	Parameter	Value
Beam Length (L)	150 μm	Effective young's modulus (E)	124 GPa
Beam thickness (h)	1.0 μm	Density (ρ)	2,332 kg/m^3
Beam width (b)	4.0 μm	Air gap width (d_1 and d_2)	1.0 μm

Axial Load (N)	0		
--------------------	---	--	--

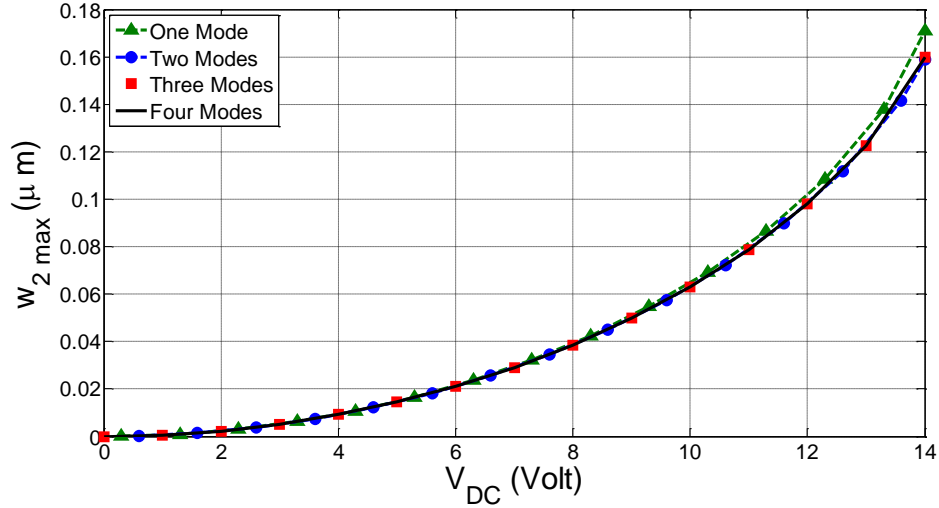


Figure 3.5: Convergence of the maximum static deflection for the upper microbeam of system of Table 3.2

A comparison between the obtained results and the results available in literature is shown in Figure 3.6, which shows somehow a dis-agreement. This is mainly due to a non-correct equations of motion that were used by Ouakad et al. in their recently published work [38] and that we adjusted in our present investigation.

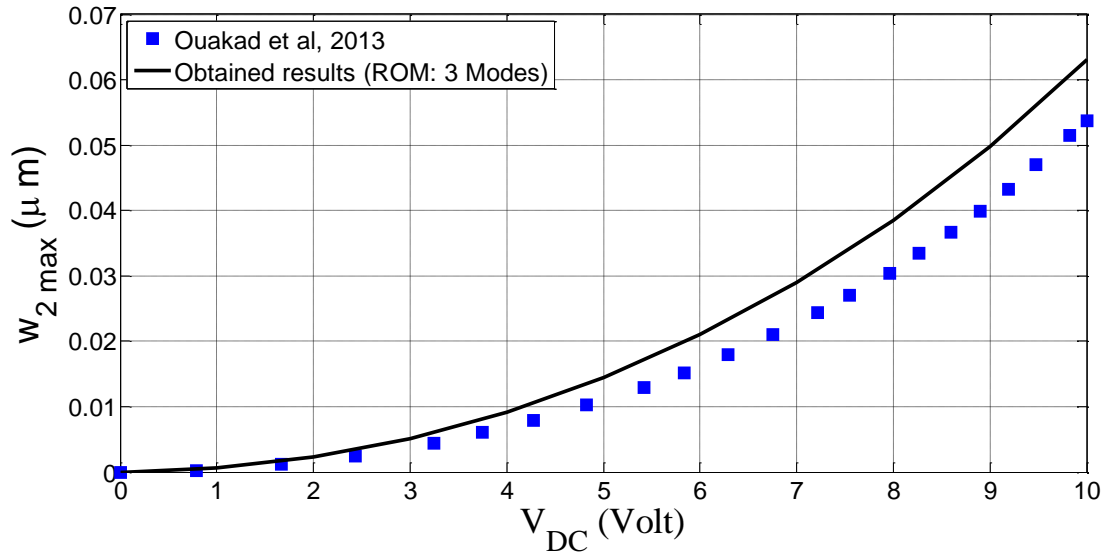


Figure 3.6: Comparison for the maximum static deflection of the upper microbeam of system of Table 3.2

3.2.3 Parametric Study

In this section, a parametric study will be carried out to investigate the effect of changing the air gaps between the movable microbeams on their static profiles. Three different air gaps were assumed, which are: 1.0, 1.25 and 1.5 μm and they were restricted by the following condition:

$$d_1 + d_2 + h = 4 \mu\text{m} \quad (3.10)$$

Accordingly, three different cases were considered, which are:

- ✓ Case 1: $d_1=d_2$ (where both of the gaps =1.25 μm)
- ✓ Case 2: $d_1>d_2$ (where $d_1=1.5 \mu\text{m}$ and $d_2=1.0 \mu\text{m}$)
- ✓ Case 3: $d_1<d_2$ (where $d_1=1.0 \mu\text{m}$ and $d_2=1.5 \mu\text{m}$)

The other assumed geometric properties are summarized in Table 3.3.

Table 3.3: Microbeams geometrical and material properties

Parameter	Value	Parameter	Value
Beam Length (L)	210 μm	Effective young's modulus (E)	169 GPa
Beam thickness (h)	1.5 μm	Density (ρ)	2,332 kg/m^3
Beam width (b)	20 μm	Axial Load (N)	0

a) Case 1 ($d_1=d_2$)

The maximum static deflection versus the applied DC voltage for both microbeams is plotted in Figure 3.7. It is clear from the figure that, the upper microbeam is deflected downward (positive value in Figure 3.7), which seems to be reasonable since the upper microbeam is affected by the force from the lower microbeam, which pulls it downward. By contrast, the lower microbeam is deflected upward (negative value in Figure 3.7), which means that the force which results due to the potential between the two microbeams is higher than the force from the fixed electrode. Also, the deflection for the upper microbeam is higher than the lower microbeam and it reaches pull-in first, which is about 23 *Volt*. The static profiles for the lower and upper microbeams along the beams for three different voltages (5, 10 and 14 *Volt*) are plotted in Figure 3.8 and Figure 3.9 respectively.

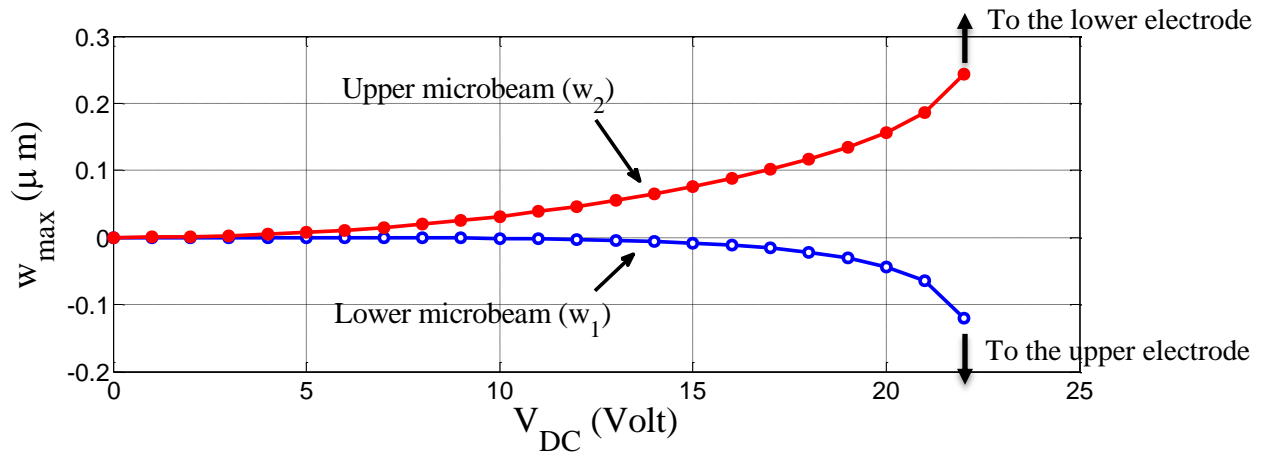


Figure 3.7: The maximum static deflection for the lower and upper microbeams for the case:

when $d_1=d_2$

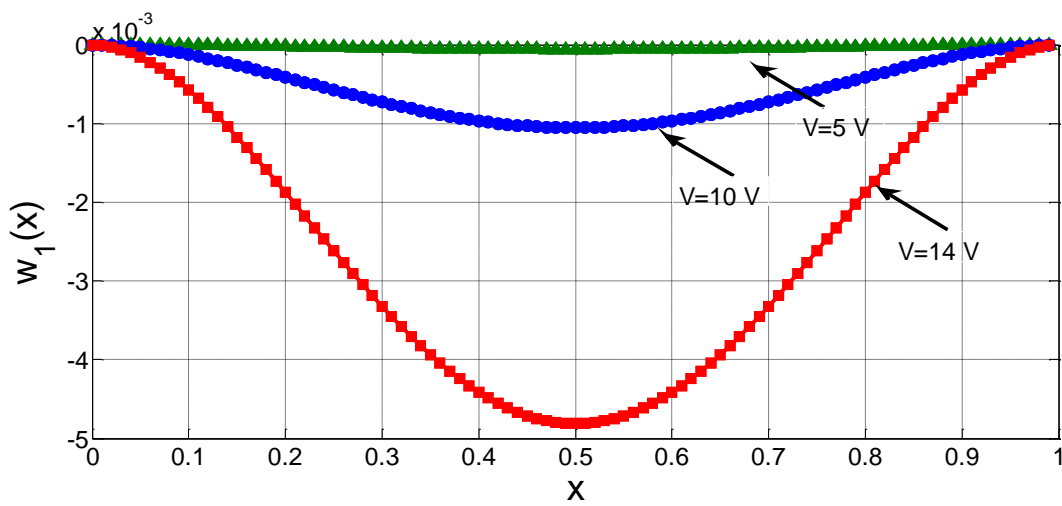


Figure 3.8: Static profile of the lower microbeam for three different voltages and for the case:

when $d_1=d_2$

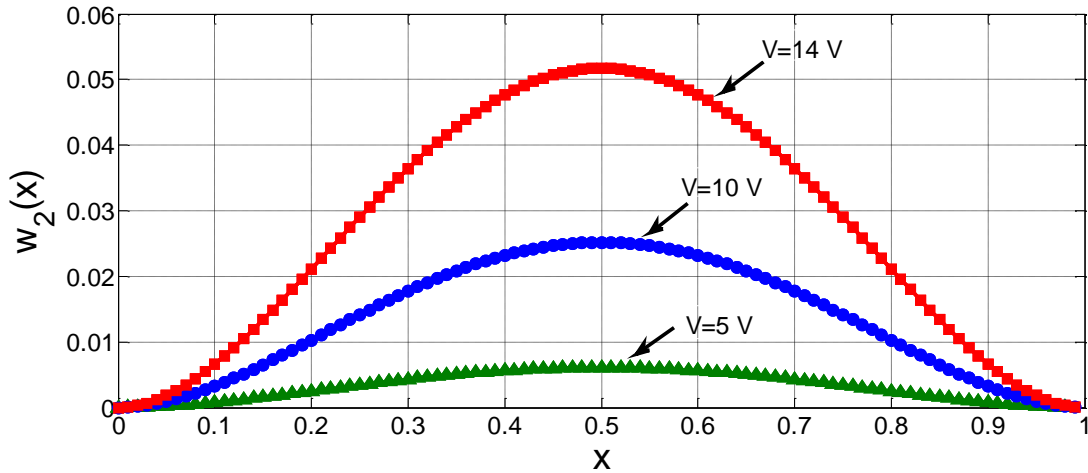


Figure 3.9: Static profile of the upper microbeam for three different voltages and for the case:
when $d_1=d_2$

b) Case 2 ($d_1>d_2$)

In this particular case, the behavior of the maximum static deflection for both microbeams is similar to the previous case, as shown in Figure 3.10. Again, the upper microbeam reaches the pull-in instability first at about 15 Volt. Figure 3.11 and Figure 3.12 show the static profile of the lower and upper microbeams, respectively, for three different applied DC voltages. As compared to the previous case, the pull-in voltage is reduced and more deflection will occur if similar voltages are used.

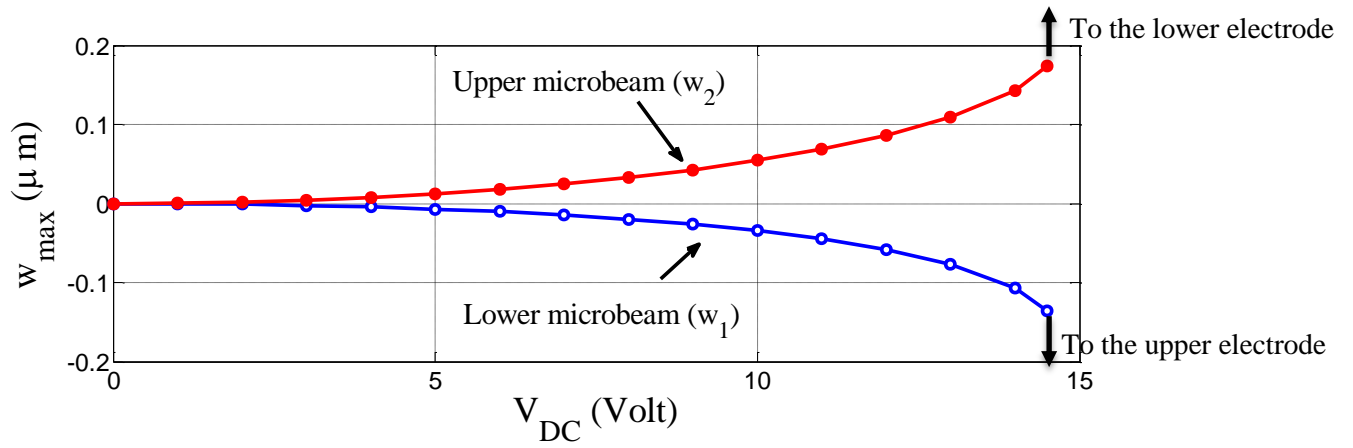


Figure 3.10: The maximum static deflection for the lower and upper microbeams for the case:

when $d_1 > d_2$

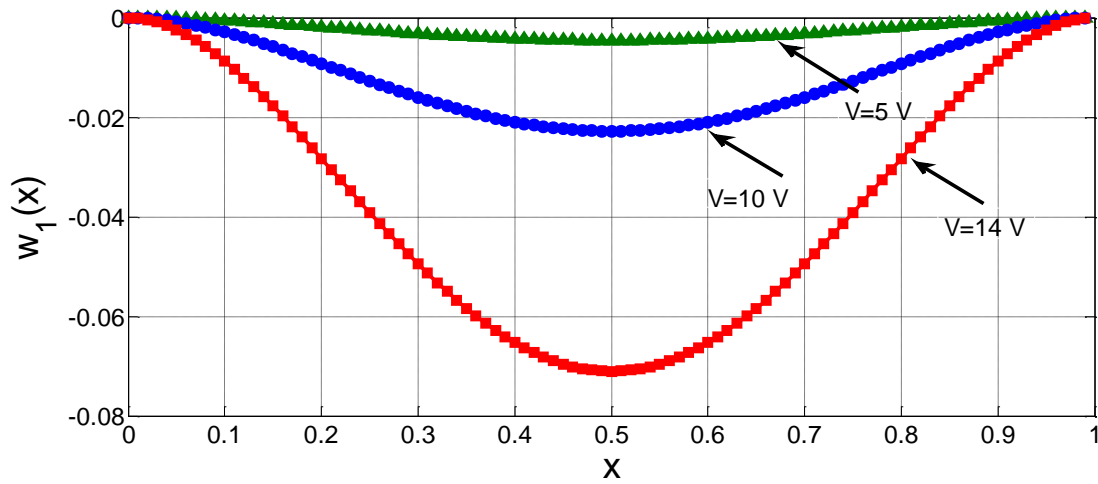


Figure 3.11: Static profile of the lower microbeam for three different voltages and for the case:

when $d_1 > d_2$

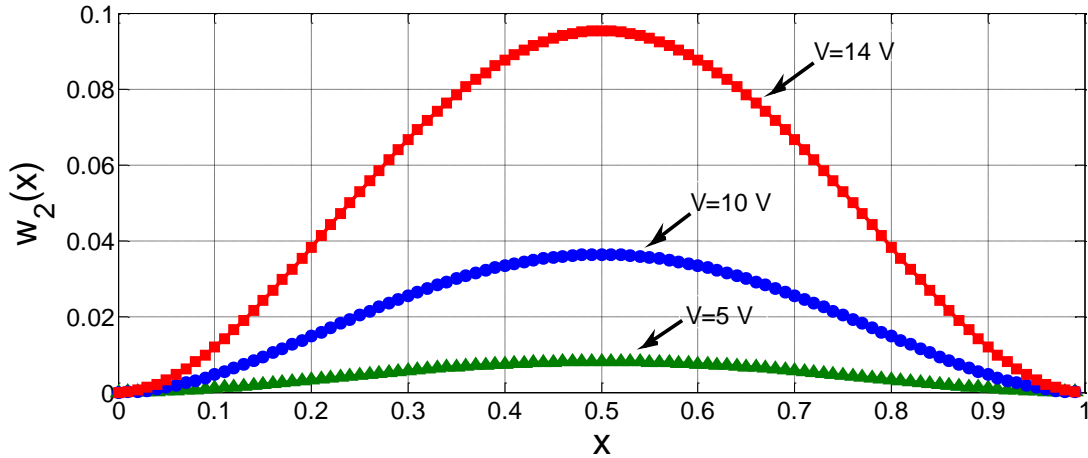


Figure 3.12: Static profile of the upper microbeam for three different voltages and for the case:

when $d_1 > d_2$

c) Case 3 ($d_1 < d_2$)

By plotting the maximum static deflection versus the applied voltage, as shown in Figure 3.13, we can recognize some interesting results that differ from the previous investigated cases. For example, the lower microbeam is deflected downward this time, which means the force resulting from the fixed electrode is higher than the force exerted by the upper microbeam. Furthermore, the magnitude of the deflection for the lower microbeam is higher than the upper and it reaches the pull-in instability first at about 23 Volt. The static profiles for the lower and upper microbeams for the same chosen voltages in the previous cases are shown in Figure 3.14 and Figure 3.15, respectively.

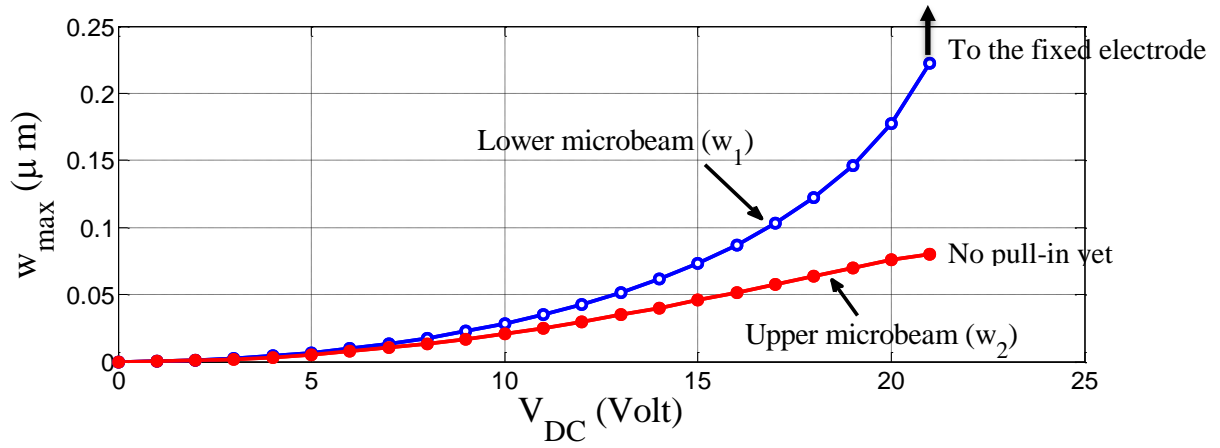


Figure 3.13: The maximum static deflection for the lower and upper microbeams for the case:
when $d_1 < d_2$

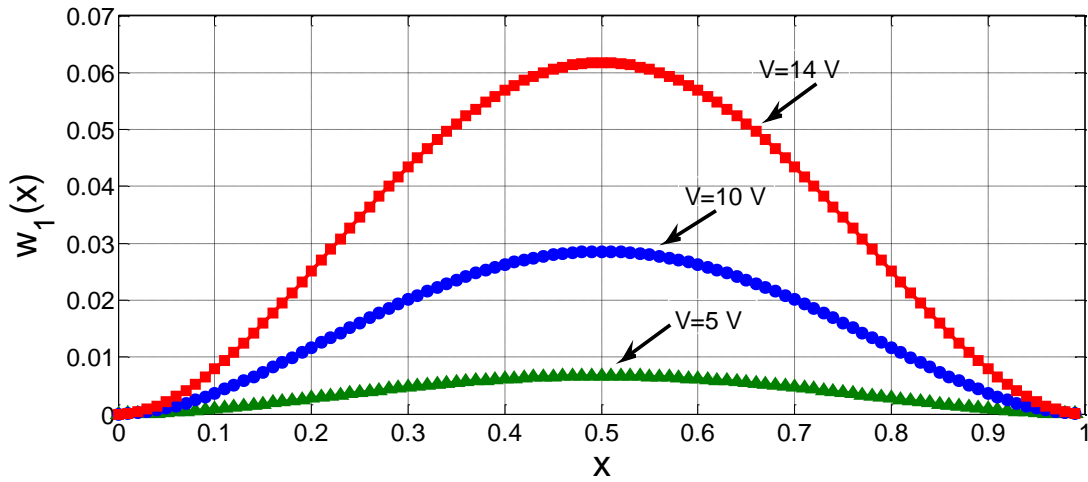


Figure 3.14: Static profile of the lower microbeam for three different voltages and for the case:
when $d_1 < d_2$

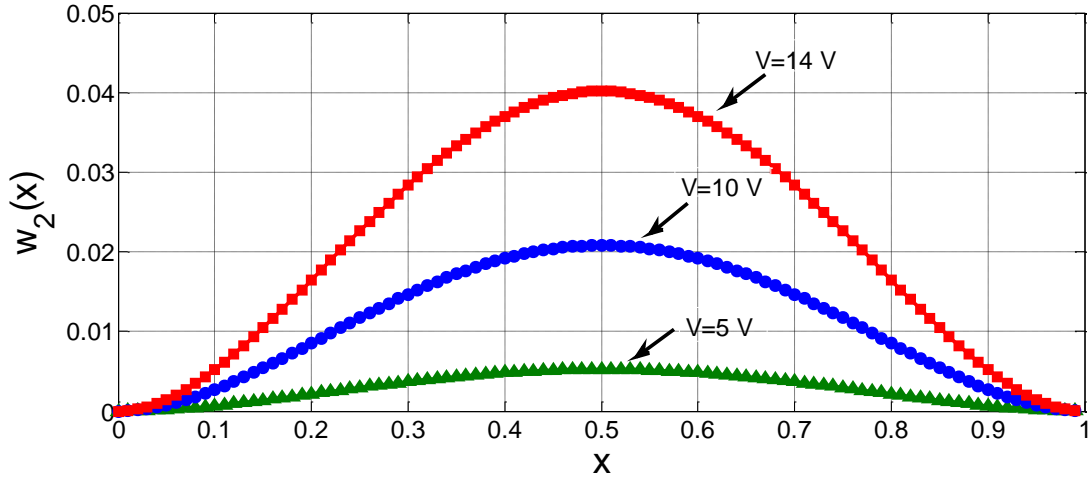


Figure 3.15: Static profile of the upper microbeam for three different voltages and for the case:
when $d_1 < d_2$

A comparison between the static deflection for the upper microbeam, when considering all three investigated cases as well as the case considering only one microbeam is shown in Figure 3.16. So, in all of the three cases more deflection will be provided at the same voltage if using double-microbeams rather than a single microbeam. However, the pull-in voltage is reduced by a significant amount, since for a single microbeam the pull-in voltage is about 236 Volt.

The table below compares the pull-in voltage for the three cases with the single microbeam.

Table 3.4: Comparison of pull-in voltage

Configuration		Pull-in Voltage
Double-microbeams	Case $d_1 = d_2$	23 Volt
	Case $d_1 > d_2$	15 Volt
	Case $d_1 < d_2$	23 Volt
Single microbeam		236 Volt

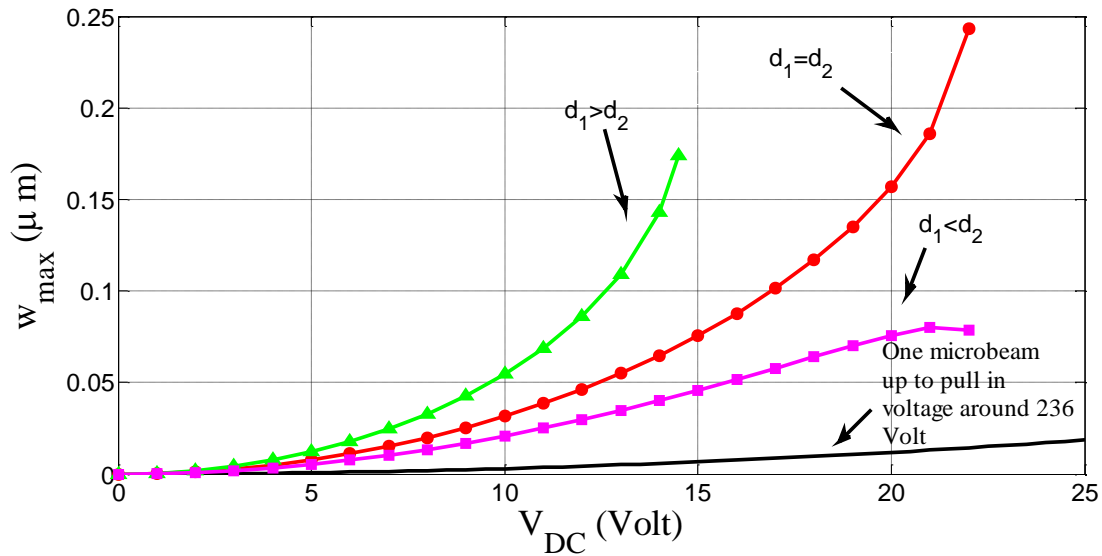


Figure 3.16: Comparison between the maximum static deflection for the upper microbeam for all three cases with the single microbeam case

Also, a closer look to Figure 3.16 reveals an interesting behavior. While, in all of the configurations, increasing the voltage makes the upper microbeam approach the pull-in voltage faster, it can be seen that for the last point (case of $d_1 < d_2$) there is no such tendency. This strange behavior may be because the lower microbeam in this case is very close to the pull-in instability from the applied force from the fixed electrode. As a result, the lower microbeam gets closer to the fixed electrode and the distance between the two microbeams will be higher. This makes the force between the two microbeams lower, and so the upper microbeam will be far from the pull-in instability.

CHAPTER 4: EIGENVALUE PROBLEM

Determining the natural frequencies and mode shapes of microbeams is important in the MEMS field, since it will help in investigating their dynamic characteristics. The method used to determine the natural frequencies will be described in this section and variations of their values with the applied DC voltages will be carried out.

4.1 Single Microbeam Case

4.1.1 Eigenvalue Problem Equation

In determining the natural frequencies of microbeams, it is necessary to cancel the time-dependent forces in the equation of motion. As a result, the damping force and the harmonic force will be dropped from equation (2.22). Hence, the equation of the microbeam will be reduced to:

$$\frac{\partial^4 w}{\partial x^4} + \frac{\partial^2 w}{\partial t^2} = (\alpha_1 \Gamma + N) \frac{\partial^2 w}{\partial x^2} + \frac{\alpha_2 V_{DC}^2}{(1-w)^2} \quad (4.1)$$

In order to develop the ROM, the deflection of the microbeam will be assumed as:

$$w(x, t) = \sum_{i=1}^N U_i(t) \phi_i(x) \quad (4.2)$$

where: $\phi_i(x)$ are the undamped linear mode shapes of the system and $U_i(t)$ are some unknown functions depending on the time, and can be written as follows: $U_i(t) = k_i + \eta_i(t)$ where k_i are the

same constants that were calculated in the static analysis and $\eta_i(t)$ are unknown functions that are dependent on time.

Substituting equation (4.2) into equation (4.1) will give:

$$\begin{aligned} & \sum_{i=1}^N (k_i + \eta_i(t)) \phi_i^{iv}(x) + \sum_{i=1}^N \ddot{\eta}_i(t) \phi_i(x) = \\ & \left(\alpha_1 \int_{x=0}^1 (\sum_{i=1}^N (k_i + \eta_i(t)) \phi_i'(x))^2 dx + N \right) \sum_{i=1}^N (k_i + \eta_i(t)) \phi_i''(x) + \\ & \frac{\alpha_2 V_{DC}^2}{\left(1 - \sum_{i=1}^N (k_i + \eta_i(t)) \phi_i(x)\right)^2} \end{aligned} \quad (4.3)$$

Expanding the electrostatic force term using a Taylor series expansion, assuming a small variation of $\eta_i(t)$ about (0) and dropping the higher order terms of $\eta_i(t)$, will result in:

$$\frac{\alpha_2 V_{DC}^2}{\left(1 - \sum_{i=1}^N (k_i + \eta_i(t)) \phi_i(x)\right)^2} \approx \frac{\alpha_2 V_{DC}^2}{\left(1 - \sum_{i=1}^N k_i \phi_i(x)\right)^2} + \frac{2\alpha_2 V_{DC}^2}{\left(1 - \sum_{i=1}^N k_i \phi_i(x)\right)^3} \sum_{i=1}^N \eta_i(t) \phi_i(x) \quad (4.4)$$

After plugging equation (4.4) into equation (4.3), canceling all the terms that verify the static equation and writing the resultant equation in state space representation, the equation can be written in the following matrix form:

$$M(k_i) \bar{\eta} = J(k_i) \bar{\eta} \quad (4.5)$$

where $\bar{\eta}$ and $\bar{\eta}$ have the form of $[\dot{\eta}_1 \dot{\eta}_2 \dots]'$ and $[\eta_1 \eta_2 \dots]'$, respectively. Also, $M(k_i)$ is a matrix representing the coefficients multiplying $\bar{\eta}$, and finally, $J(k_i)$ is known as the Jacobian matrix. The natural frequencies of the beam for a given voltage can be obtained by taking the square roots of the eigenvalues that can be obtained by solving the following algebraic equation:

$$\text{Determinant}(M(k_i)^{-1}J(k_i) - \lambda I) = 0 \quad (4.6)$$

The mode shapes of the system can be obtained by evaluating the eigenvectors of $M^{-1}J$. So, it is clear from the previous equation, that the number of natural frequencies obtained will be similar to the number of modes, and also equal to the number of mode shapes assumed in the Galerkin expansion.

4.1.2 Results

Table 4.1: Assumed geometrical and material properties [46]

Parameter	Value	Parameter	Value
Beam Length (L)	210 μm	Effective Young's Modulus (E)	169 GPa
Beam Thickness (h)	1.5 μm	Density (ρ)	2,332 kg/m^3
Beam Width (b)	100 μm	Air Gap Width (D)	1.18 μm
Axial Load (\hat{N})	0.0009 <i>Newton</i>		

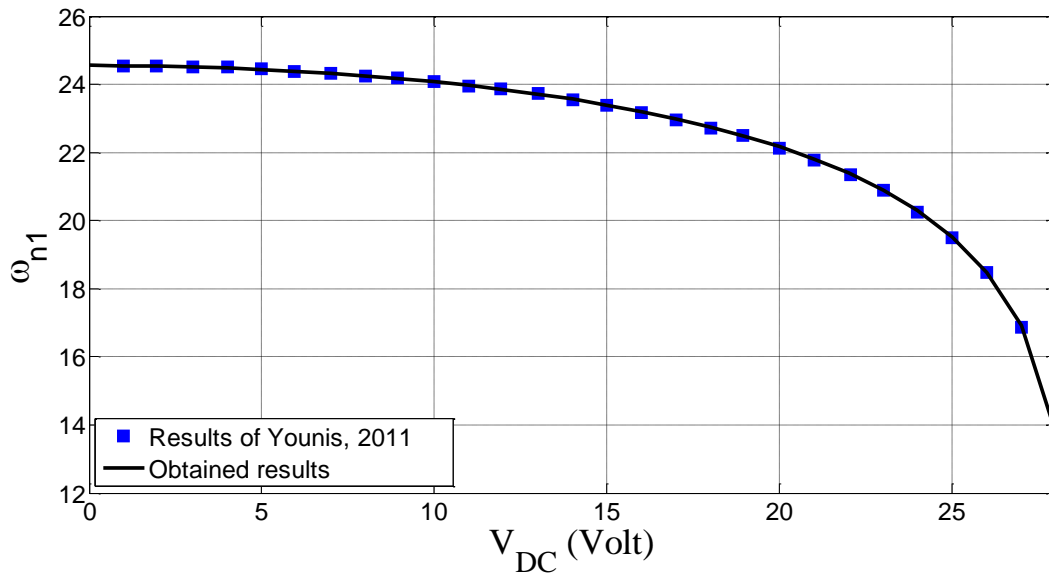


Figure 4.1: Comparison between the obtained fundamental natural frequencies with literature [46]

Younis [46] calculated the natural frequencies for a single microbeam configuration. The selected parameters of this actuator are shown in Table 4.1. Here, the same parameters were considered to reproduce the same results. A comparison between the two results for the fundamental natural frequency is shown in Figure 4.1, which shows excellent agreement.

At zero voltage, the fundamental natural frequency will be the same as the fundamental natural frequency of the microbeam, as no load is applied. However, increasing the voltage slowly reduces the stiffness of the microbeams a little as well as the fundamental natural frequency, until it gets very close to the pull-in voltage, where a small increase in the voltage will result in a dramatic decrease in the fundamental frequency, which will result in a failure in the system at the pull-in voltage.

4.2 Double-Microbeams Case

4.2.1 Eigenvalue Problem Equation

Recall equations (2.24) and (2.25), which represent the governing equations of motion for the model of double-microbeams actuators. In order to find the natural frequencies for the model, all of the time-dependent forces will be dropped from the two equations, which will lead to:

$$\frac{\partial^4 w_1}{\partial x^4} + \frac{\partial^2 w_1}{\partial t^2} = (\alpha_3 \Gamma_1 + N) \frac{\partial^2 w_1}{\partial x^2} + \frac{\alpha_4 V_{DC}^2}{(1-w_1)^2} - \frac{\alpha_4 V_{DC}^2}{(d_2/d_1 + w_1 - w_2)^2} \quad (4.7)$$

$$\frac{\partial^4 w_2}{\partial x^4} + \frac{\partial^2 w_2}{\partial t^2} = (\alpha_3 \Gamma_2 + N) \frac{\partial^2 w_2}{\partial x^2} + \frac{\alpha_4 V_{DC}^2}{(d_2/d_1 + w_1 - w_2)^2} \quad (4.8)$$

In order to develop the ROM, the deflection of the lower and upper microbeams will be assumed as, respectively:

$$w_1(x, t) = \sum_{i=1}^N P_i(t) \phi_i(x) \quad (4.9)$$

$$w_2(x, t) = \sum_{i=1}^N Q_i(t) \phi_i(x) \quad (4.10)$$

where: $P_i(t)$ and $Q_i(t)$ are some unknown functions that are dependent on time and can be written as follows: $P_i(t) = f_i + \mu_i(t)$ and $Q_i(t) = g_i + \nu_i(t)$, where f_i and g_i are the constants calculated in the static analysis and $\mu_i(t)$ and $\nu_i(t)$ are unknown functions that are dependent on time.

Substituting equations (4.9) and (4.10) into equations (4.7) and (4.8) results in:

$$\begin{aligned} & \sum_{i=1}^N P_i(t) \phi_i^{iv}(x) + \sum_{i=1}^N \ddot{P}_i(t) \phi_i(x) = \\ & \left(\alpha_3 \int_{x=0}^1 (\sum_{i=1}^N P_i(t) \phi_i'(x))^2 dx + N \right) \sum_{i=1}^N P_i(t) \phi_i''(x) + \frac{\alpha_4 V_{DC}^2}{\left(1 - \sum_{i=1}^N P_i(t) \phi_i(x)\right)^2} - \end{aligned} \quad (4.11)$$

$$\frac{\alpha_4 V_{DC}^2}{\left(d_2/d_1 + \sum_{i=1}^N P_i(t) \phi_i(x) - \sum_{i=1}^N Q_i(t) \phi_i(x)\right)^2}$$

$$\begin{aligned} & \sum_{i=1}^N Q_i(t) \phi_i^{iv}(x) + \sum_{i=1}^N \ddot{Q}_i(t) \phi_i(x) = \\ & \left(\alpha_3 \int_{x=0}^1 (\sum_{i=1}^N Q_i(t) \phi_i'(x))^2 dx + N \right) \sum_{i=1}^N Q_i(t) \phi_i''(x) + \end{aligned} \quad (4.12)$$

$$\frac{\alpha_4 V_{DC}^2}{\left(d_2/d_1 + \sum_{i=1}^N P_i(t) \phi_i(x) - \sum_{i=1}^N Q_i(t) \phi_i(x)\right)^2}$$

Expanding the two electrostatic force terms in equations (4.11) and (4.12) using a Taylor series expansion and assuming $\mu_i(t)$ and $(\mu_i(t) - v_i(t))$ are very small around (0), respectively, and dropping the higher order terms of $\mu_i(t)$ and $v_i(t)$ gives:

$$\begin{aligned} & \frac{\alpha_4 V_{DC}^2}{\left(1 - \sum_{i=1}^N P_i(t) \phi_i(x)\right)^2} = \frac{\alpha_4 V_{DC}^2}{\left(1 - \sum_{i=1}^N (f_i + \mu_i(t)) \phi_i(x)\right)^2} \approx \\ & \frac{\alpha_2 V_{DC}^2}{\left(1 - \sum_{i=1}^N f_i \phi_i(x)\right)^2} + \frac{2\alpha_2 V_{DC}^2}{\left(1 - \sum_{i=1}^N f_i \phi_i(x)\right)^3} \sum_{i=1}^N \mu_i(t) \phi_i(x) \end{aligned} \quad (4.13)$$

$$\begin{aligned}
& \frac{\alpha_4 V_{DC}^2}{\left(d_2/d_1 + \sum_{i=1}^N P_i(t)\phi_i(x) - \sum_{i=1}^N Q_i(t)\phi_i(x)\right)^2} = \\
& \frac{\alpha_4 V_{DC}^2}{\left(d_2/d_1 + \sum_{i=1}^N (f_i + \mu_i(t))\phi_i(x) - \sum_{i=1}^N (g_i + \nu_i(t))\phi_i(x)\right)^2} \approx \\
& - \frac{\alpha_4 V_{DC}^2}{\left(d_2/d_1 + \sum_{i=1}^N f_i\phi_i(x) - \sum_{i=1}^N g_i\phi_i(x)\right)^2} + \frac{2\alpha_4 V_{DC}^2 \sum_{i=1}^N (\mu_i(t) - \nu_i(t))\phi_i(x)}{\left(d_2/d_1 + \sum_{i=1}^N f_i\phi_i(x) - \sum_{i=1}^N g_i\phi_i(x)\right)^3}
\end{aligned} \tag{4.14}$$

Following the same method for a single microbeam, plugging equations (4.13) and (4.14) into equations (4.11) and (4.12), then canceling all of the static terms, and then writing the resultant equation in matrix form gives:

$$M(f_i, g_i)\bar{\eta} = J(f_i, g_i)\bar{\eta} \tag{4.15}$$

where: $\bar{\eta}$ and $\bar{\eta}$ have the form of $[\ddot{\mu}_1 \dot{\nu}_1 \ddot{\mu}_2 \dot{\nu}_2 \dots]'$ and $[\mu_1 \nu_1 \mu_2 \nu_2 \dots]'$, respectively, and $M(f_i, g_i)$ is a matrix representing the coefficients multiplying $\bar{\eta}$. The natural frequencies and the mode shapes of the system can be obtained by taking the square root of the eigenvalues and evaluating the eigenvectors of $M^{-1}J$, respectively. So, this time the number of natural frequencies and the mode shapes obtained is double that of the number used in the assumed modes in the Galerkin expansion.

4.2.2 Results

The selected parameters are the same we assumed in the static analysis for the double-microbeams, which is shown in Table 3.3 with the case of $d_1=d_2$. The natural frequencies were obtained by using three symmetric modes and were plotted versus the applied voltage as shown

in Figure 4.2. The obtained results indicate that all of the natural frequencies do not change with the applied voltage, with the exception of the fundamental. The fundamental natural frequency starts at its maximum position (when no electrical load is applied) and then decreases gradually with an increase in the applied voltage until it gets close to the pull-in voltage, at which point it drops sharply to zero. Also, it can be noted that each odd natural frequency, when paired with the consecutive one are the same, except for the fundamental frequency, especially at high voltages.

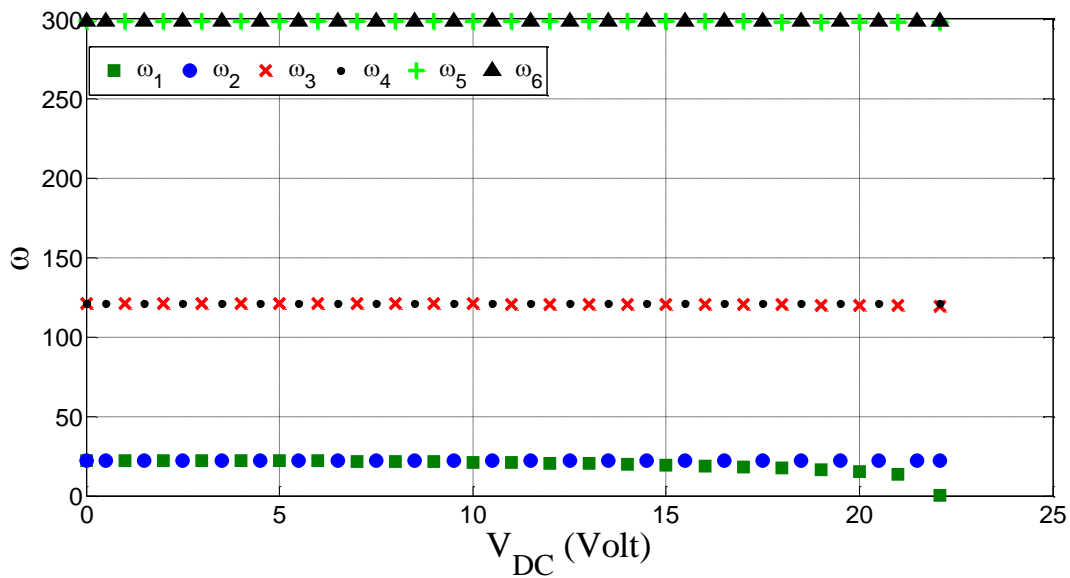


Figure 4.2: Natural frequencies versus the applied voltage for double-microbeams

A comparison between the fundamental natural frequencies among the three cases considered in the static section is shown in Figure 4.3. The results here seem to follow the static analysis outcomes, since in the case with the lowest pull-in voltage the fundamental frequency reaches zero first (when: $d_1 > d_2$). Moreover, the other two cases reach the pull-in voltage at about the same value (23 Volt) and accordingly their fundamental natural frequency drops to zero or close to it.

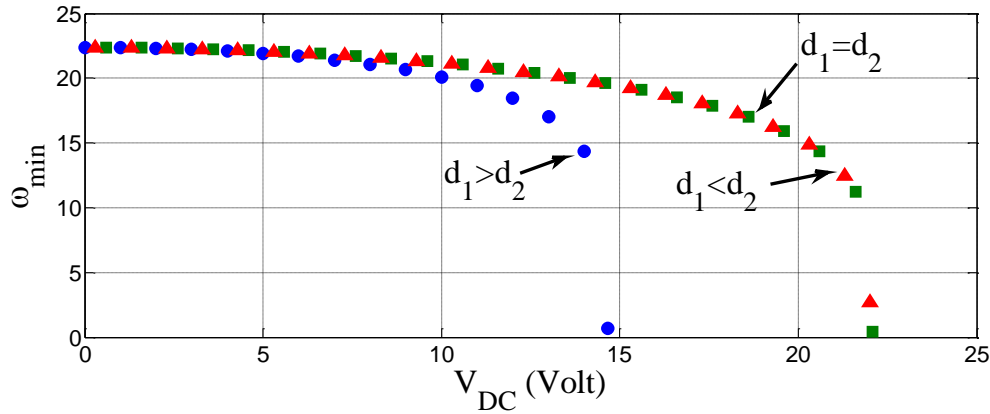


Figure 4.3: The fundamental natural frequencies for three different cases

The first and second coupled mode shapes for the case of $d_1=d_2$ at $V_{DC} = 2 \text{ Volt}$ are presented in Figure 4.4 and Figure 4.5, respectively. The results show that for the first mode shape Φ_1 the coupled modes (Φ_{11} and Φ_{12}) are opposite to each other, sharing an out-of-phase motion. Conversely, for the second mode shape (Φ_2) the two coupled modes (Φ_{21} and Φ_{22}) have almost the same magnitude as the first in an absolute value and both of them share an in-phase-motion.

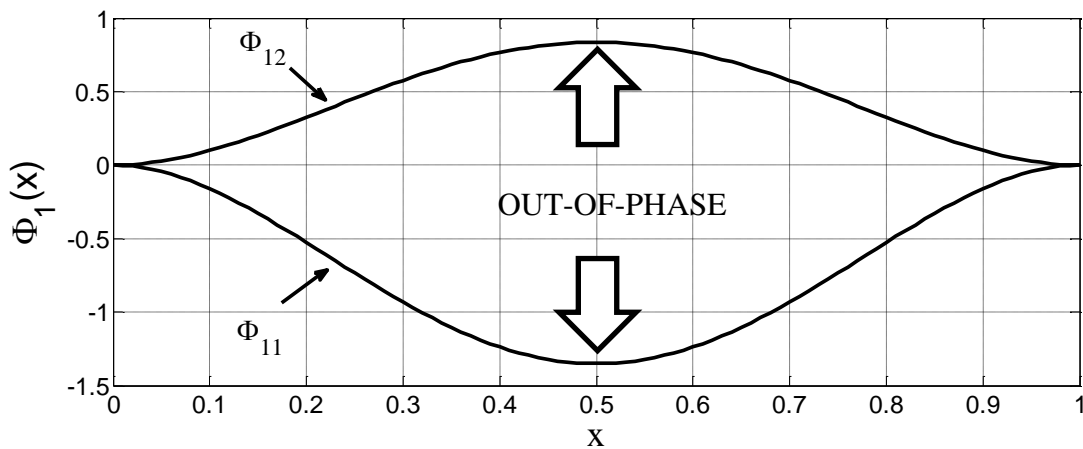


Figure 4.4: The first coupled mode shape assuming $V_{DC} = 2 \text{ Volt}$

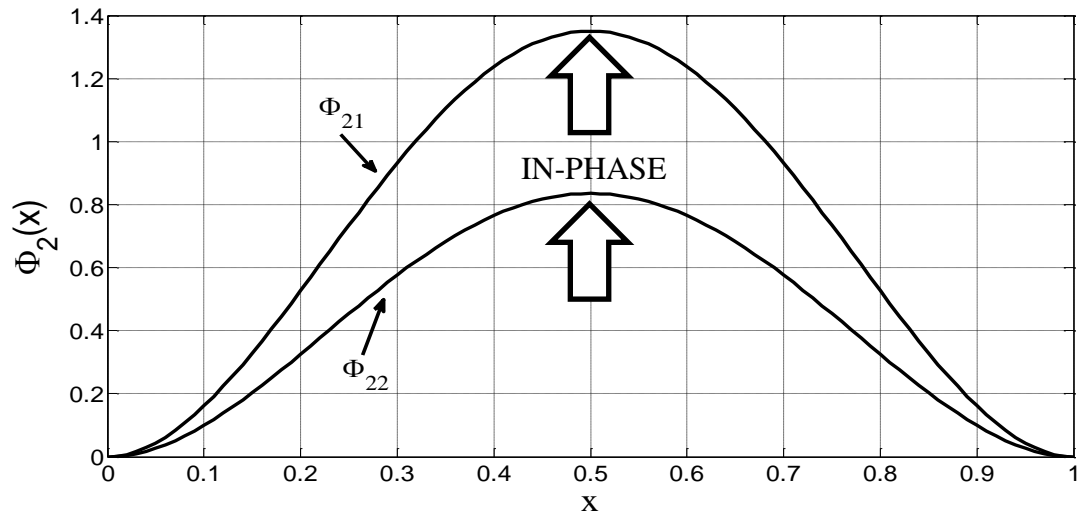


Figure 4.5: The second coupled mode shape assuming $V_{DC} = 2$ Volt

CHAPTER 5: DYNAMIC ANALYSIS

This chapter will discuss the dynamic analysis of single and double-microbeams based actuators by using two different approaches: Reduced-Order Modeling (ROM) and perturbation analysis. A comparison will be carried out for each method to validate both approaches. Finally, a parametric study will be done for the double-microbeams configuration to investigate some dynamical features for the micro-actuator.

5.1 Single Microbeam Case

5.1.1 Reduced-Order Modeling (ROM)

Equation (2.22) represents the equation of motion of electrically actuated single microbeam based-actuator. In order to get the reduced-order model (ROM), the equation will be discretized using the Galerkin expansion. Therefore, the deflection for the microbeam will have the following form:

$$w(x,t) = \sum_{i=1}^N u_i(t) \phi_i(x) \quad (5.1)$$

where $u_i(t)$ are the modal amplitudes which are functions of time that need to be evaluated. As in the static analysis, it is desirable to multiply equation (2.22) by $(1 - w)^2$. In fact, this will reduce the computational cost. Therefore, the resultant equation will be multiplied by $\phi_j(x)$ and then integrated from $x=0$ to $x=I$ to give:

$$\int_{x=0}^1 \phi_j(x) \left(1 - \sum_{i=1}^N u_i(t) \phi_i(x)\right)^2 \left(\sum_{i=1}^N u_i(t) \phi_i^{iv}(x) + \sum_{i=1}^N \ddot{u}_i(t) \phi_i(x) + c \sum_{i=1}^N \dot{u}_i(t) \phi_i(x)\right) dx = \int_{x=0}^1 \phi_j(x) \left(\left(1 - \sum_{i=1}^N u_i(t) \phi_i(x)\right)^2 (\alpha_1 \Gamma + N) \sum_{i=1}^N u_i(t) \phi_i''(x) + \alpha_2 (V_{DC} + V_{AC} \cos(\Omega t))^2\right) dx \quad (5.2)$$

5.1.2 Perturbation Analysis

Younis et al. [34] discussed this technique in solving the deflection for a single microbeam based-actuator. The following method, which is the method of multiple scales by direct attack of the equation of motion, will be discussed in this section. The variable for the time scale and its derivatives are defined as follows:

$$T_0 = t, \quad D_0 = \frac{\partial}{\partial T_0}, \quad T_1 = \varepsilon t, \quad D_1 = \frac{\partial}{\partial T_1}, \quad T_2 = \varepsilon^2 t, \quad D_2 = \frac{\partial}{\partial T_2}, \quad (5.3)$$

Next, the damping coefficient c and the forcing amplitude V_{AC} are scaled so that their nonlinearity effect will be balanced in the modulation equations [34, 47]. Hence,

$$c = \varepsilon^2 c, \quad V_{AC} = \varepsilon^3 V_{AC}, \quad (5.4)$$

where ε is a bookkeeping parameter.

We then seek a solution of the microbeam dynamic deflection in the following form:

$$\begin{aligned}
w(x, t, \varepsilon) &= w_s(x) + u(x, t) \\
&= w_s(x) + \varepsilon u_1(x, T_0, T_2) + \varepsilon^2 u_2(x, T_0, T_2) + \varepsilon^3 u_3(x, T_0, T_2) + \dots,
\end{aligned} \tag{5.5}$$

where w_s is the static component of the microbeam deflection, and u is its dynamic component.

Substituting equation (5.5) into equation (2.22) gives:

$$\frac{\partial^4 w_s}{\partial x^4} + \frac{\partial^4 u}{\partial x^4} + \frac{\partial^2 u}{\partial t^2} + c \frac{\partial u}{\partial t} = (\alpha_1 \Gamma(w_s + u, w_s + u) + N) \left(\frac{\partial^2 w_s}{\partial x^2} + \frac{\partial^2 u}{\partial x^2} \right) + \frac{\alpha_2 (V_{DC} + V_{AC} \cos(\Omega t))^2}{(1 - w_s - u)^2} \tag{5.6}$$

To deal with the nonlinearity of the electrical force, it is required to expand it around the microbeam deflection dynamic component (u). Also, the expression of $(V_{DC} + V_{AC} \cos(\Omega t))^2$ can be approximated to $V_{DC}^2 + 2V_{DC}V_{AC} \cos(\Omega t)$, since, generally, in the resonant sensors $V_{AC}^2 \cos^2(\Omega t) \ll V_{DC}^2$. Assuming the aforementioned relations and canceling the static equation and small terms, while equating the coefficients of like powers of ε , the following equations can be obtained:

- **Order ε^1 :**

$$\mathcal{L}(u_1) = 0 \tag{5.7}$$

- **Order ε^2 :**

$$\mathcal{L}(u_2) = \alpha_1 w_s'' \Gamma(u_1, u_1) + 2\alpha_1 u_1' \Gamma(w_s, u_1) + \frac{3\alpha_2 V_{DC}^2 u_1^2}{(1 - w_s)^4} \tag{5.8}$$

- **Order ε^3 :**

$$\begin{aligned} \mathcal{L}(u_3) = & -2D_0D_2u_1 - cD_0u_1 + 2\alpha_1w_s'\Gamma(u_1, u_2) + 2\alpha_1u_1'\Gamma(w_s, u_2) + \\ & 2\alpha_1u_2''\Gamma(w_s, u_1) + \alpha_1\Gamma(u_1, u_1)u_1'' + \frac{6\alpha_2V_{DC}^2u_1u_2}{(1-w_s)^4} + \frac{4\alpha_2V_{DC}^2u_1^3}{(1-w_s)^5} + 2\tilde{F}\cos(\Omega T_0) \end{aligned} \quad (5.9)$$

where \mathcal{L} is a linear differential operator defined for any function (f) by:

$$\mathcal{L}(f) = D_0^2 f + f^{iv} - \alpha_1\Gamma(w_s, w_s)f'' - Nf'' - 2\alpha_1w_s'\Gamma(w_s, f) - \frac{2\alpha_2V_{DC}^2f}{(1-w_s)^3} = 0$$

and where $\tilde{F} = \frac{\alpha_2V_{DC}V_{AC}}{(1-w_s)^2}$.

Assuming no possibility of internal resonances, the solutions of equation (5.7) is assumed to consist of only the directly excited fundamental modes, $\Phi(x)$, since the indirectly excited modes will die out in the presence of damping. As a result, the solution of the dynamic component u_1 will be:

$$u_1(x, T_0, T_2) = \left[A(T_2)e^{i\omega T_0} + \bar{A}(T_2)e^{-i\omega T_0} \right] \Phi(x), \quad (5.10)$$

where $A(T_2)$ is a complex-valued function that is determined by imposing the solvability condition at the third order, equation (5.9). The over-bar denotes the complex conjugate, and ω and $\Phi(x)$ are the natural frequency and corresponding eigenfunction of the directly excited modes, respectively. By substituting equation (5.10) into equation (5.7) we obtain:

$$-\omega^2\Phi + \Phi^{iv} - \alpha_1\Gamma(w_s, w_s)\Phi'' - N\Phi'' - 2\alpha_1w_s''\Gamma(w_s, \Phi) - \frac{2\alpha_2V_{DC}^2\Phi}{(1-w_s)^3} = 0 \quad (5.11)$$

In order to solve for the mode shape function $\Phi(x)$, we propose to use the Galerkin-based discretization technique to solve the nonlinear eigenvalue problem (EVP), equation (5.11).

Hence, we assume the following:

$$\Phi(x) = \sum_{i=1}^N a_i \phi_i(x) \quad (5.12)$$

Substituting equation (5.12) into equation (5.11), the resulting equation is then multiplied by ϕ_j , and the outcome equations are integrated from $x=0$ to $x=1$, which will give an eigenvalue problem. The mode shapes can be obtained by evaluating the eigenvectors of the resulting EVP, the number of modes is equal to the number of chosen modes in the ROM expansion.

Next, the solution u_1 will be substituted in the second order equation (ε^2), which will give:

$$\mathcal{L}(u_2) = (A^2 e^{2i\omega T_0} + 2A\bar{A} + \bar{A}^2 e^{-2i\omega T_0})h(x) \quad (5.13)$$

where:

$$h(x) = \alpha_1 w_s'' \Gamma(\Phi, \Phi) + 2\alpha_1 \Phi'' \Gamma(w_s, \Phi) + \frac{3\alpha_2 V_{DC}^2 \Phi^2}{(1-w_s)^4} \quad (5.14)$$

Assuming the particular solution of u_2 :

$$u_2 = A^2 e^{2i\omega T_0} \Psi_1 + 2A\bar{A}\bar{\Psi}_2 + \bar{A}^2 e^{-2i\omega T_0} \Psi_1 \quad (5.15)$$

where Ψ_i are the solutions of the following boundary value problems:

$$M(\Psi_i, 2\omega\delta_{ij}) = h(x) \quad (5.16)$$

$$\Psi_j = 0 \quad \Psi'_j = 0 \quad \text{At } x=0 \text{ and } x=l \text{ for } j=1 \text{ to } 2 \quad (5.17)$$

where δ is the Kronecker delta and M is a linear differential operator defined as:

$$M(\Psi, \omega) = \Psi^{iv} - \omega^2 \Psi - \alpha_1 \Gamma(w_s, w_s) \Psi'' - N \Psi'' - 2\alpha_1 w_s' \Gamma(w_s, \Psi) - \frac{2\alpha_2 V_{DC}^2 \Psi}{(1-w_s)^3} \quad (5.18)$$

Introducing the detuning parameter σ to describe the nearness of the excitation frequency Ω to the fundamental excited natural frequency ω as:

$$\Omega = \omega + \varepsilon^2 \sigma \quad (5.19)$$

The solutions of the first and second order equations (5.10) and (5.15), respectively, are then substituted into equation (5.9), which will lead to:

$$\mathcal{L}(u_3) = (-2i\omega A' \Phi(x) - i c \omega \Phi(x) A + \chi(x) A^2 \bar{A} + \tilde{F} e^{i\omega T_2}) e^{i\omega T_0} + cc + NST \quad (5.20)$$

where NST stands for the non-secular terms and the function χ is defined as:

$$\begin{aligned} \chi_1(x) = & 2\alpha_1 w_s'' (\Gamma(\Phi, \Psi_1) + 2\Gamma(\Phi, \Psi_2)) + 2\alpha_1 \Phi'' (\Gamma(w_s, \Psi_1) + 2\Gamma(w_s, \Psi_2)) + \\ & 2\alpha_1 \Gamma(w_s, \Phi) (\Psi_1'' + 2\Psi_2'') + 3\alpha_1 \Gamma(\Phi, \Phi) \Phi'' + \frac{6\alpha_2 V_{DC}^2}{(1-w_s)^4} (\Psi_1 \Phi + 2\Psi_2 \Phi) + \frac{4\alpha_2 V_{DC}^2}{(1-w_s)^5} \Phi^3 \end{aligned} \quad (5.21)$$

Since we seek a solution for the second order approximation, there is no need to solve for u_3 . However, we need to impose the solvability condition to get $A(T_2)$. The solvability condition can be obtained by multiplying equation (5.20) by $\Phi(x)e^{-i\omega T_0}$ and then integrating the result from $x=0$ to $x=1$, which will result in the following:

$$2i\omega(D_2 A + \mu A) + 8SA^2 \bar{A} - F e^{i\omega T_2} = 0 \quad (5.22)$$

where $S = -\frac{1}{8} \int_{x=0}^1 \chi \Phi dx$, $\mu = \frac{1}{2} \int_{x=0}^1 c \Phi^2 dx$, $F = \int_{x=0}^1 \tilde{F} \Phi dx$,

$A(T_2)$ can be expressed in a polar form, such as: $A = (1/2)a e^{i\beta}$, where a and β are the amplitude and phase of the microbeam deflection amplitude, respectively and they are real-valued functions. Equation (5.22) will lead to two equations after separating the real and imaginary parts. Letting ($\gamma = \sigma T_2 - \beta$) the two equations are given as:

$$a' = -\mu A + \frac{F}{\omega} \sin \gamma \quad (5.23)$$

$$a\gamma' = a\sigma - \frac{Sa^3}{\omega} + \frac{F}{\omega} \cos \gamma \quad (5.24)$$

Since a and γ refer to fixed points they will be replaced by a_0 and γ_0 , respectively; therefore their derivatives are equal to zero (i.e. $a' = \gamma' = 0$). The nonlinear equation governing the amplitude can be then obtained by squaring both sides of equations (5.23) and (5.24), adding them together, which will result in:

$$a_0^2 \left[\mu^2 + \left(\sigma - \frac{Sa_0^2}{\omega} \right)^2 \right] = \frac{F^2}{\omega^2} \quad (5.25)$$

5.1.3 Results

We start by solving the nonlinear equation of motion assuming the ROM technique. For that, we solve for the coefficients $u_i(t)$ in equation (5.2) then substitute them back into equation (5.1). For the perturbation technique, starting by the first order, we solve equation (5.11) for function $\Phi(x)$. Then, we substitute it in the second order equation (5.16) then solve for both functions $\Psi_1(x)$ and $\Psi_2(x)$, respectively. After that, we solve for the amplitude from equation (5.25) and the phase from either equation (5.23) or (5.24). Finally, the deflection of the lower and upper microbeams can be numerically calculated using equation (5.5).

Figure 5.1 shows a comparison between the obtained results for the normalized nonlinear resonance frequency with the literature [34]. The selected parameters are summarized in Table 5.1 for an applied DC voltage of $V_{DC} = 2 \text{ Volt}$, except for the first two points where $V_{DC} = 1 \text{ Volt}$. As it can be seen, the obtained curves show excellent agreement with the literature.

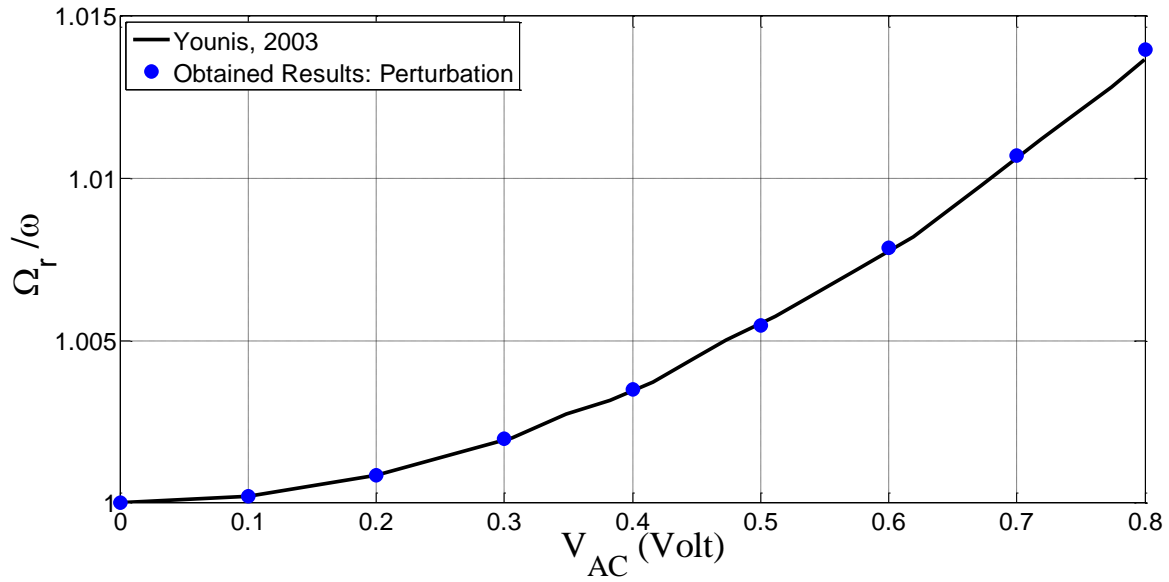


Figure 5.1: Comparison of the obtained normalized nonlinear natural frequency with literature [34] for $V_{DC} = 2$ Volt except for the first two points where $V_{DC} = 1$ Volt

Figure 5.2 shows a comparison between the ROM and the perturbation method. The selected parameters are shown in Table 5.1 with the difference in the quality factor, where it is assumed to be 1000. The applied DC and AC voltages were assumed as $V_{DC} = 8$ Volt and $V_{AC} = 0.03$ Volt, respectively. The obtained results are in good agreement among the two assumed methods. It can be noticed from the figure that in the presence of nonlinearity, the ROM is not capable in obtaining all of the branches. In the other hand, the perturbation method can perform this task and hence it is better to use it in the case of non-zero nonlinearity.

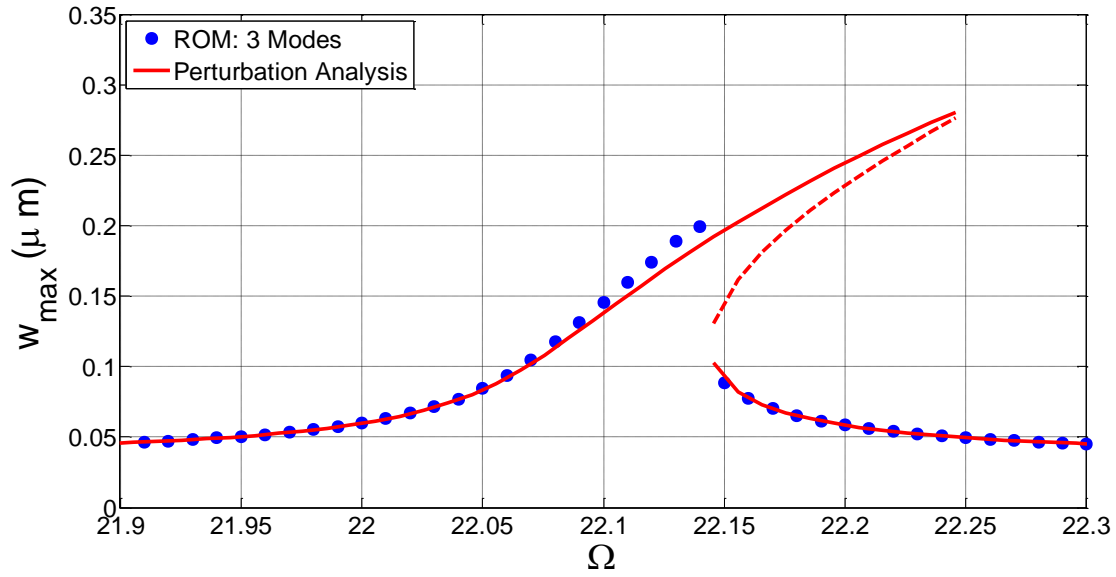


Figure 5.2: Comparison of the obtained deflection of the microbeam among the ROM and the perturbation method for $V_{DC}= 8 \text{ Volt}$ and $V_{AC}=0.03 \text{ Volt}$

Table 5.1: Assumed geometrical and material properties [34]

Parameter	Value	Parameter	Value
Beam Length (L)	$210 \mu m$	Effective Young's Modulus (E)	151 GPa
Beam Thickness (h)	$1.5 \mu m$	Density (ρ)	$2,332 \text{ kg/m}^3$
Beam Width (b)	$100 \mu m$	Air Gap Width (D)	$1.0 \mu m$
Axial Load (\hat{N})	0.00011 Newton	Quality factor (Q)	816.6

5.2 Double-Microbeams Case

5.2.1 Reduced-Order Modeling (ROM)

As with the single microbeam analysis, the ROM can be obtained by discretizing equations (2.24) and (2.25) using the Galerkin expansion. Therefore, the deflection for the lower and upper microbeams will have the following forms, respectively:

$$w_1(x, t) = \sum_{i=1}^N p_i(t) \phi_i(x) \quad (5.26)$$

$$w_2(x, t) = \sum_{i=1}^N q_i(t) \phi_i(x) \quad (5.27)$$

where $\phi_i(x)$ are the linear undamped mode shapes of a clamped-clamped micro-beam, which are orthogonal. As in the previous case of a single microbeam, equation (2.24) will be multiplied by $(1 - w_1)^2 \left(\frac{d_2}{d_1} - w_1 - w_2 \right)^2$ and equation (2.25) will be multiplied by $\left(\frac{d_2}{d_1} - w_1 - w_2 \right)^2$. After that, the outcome will be multiplied by $\phi_j(x)$ and then integrated from $x=0$ to $x=1$ to give the following equations:

$$\begin{aligned}
& \int_{x=0}^1 \phi_j(x) \left(1 - \sum_{i=1}^N p_i(t) \phi_i(x) \right)^2 \left(d_2/d_1 + \sum_{i=1}^N p_i(t) \phi_i(x) - \sum_{i=1}^N q_i(t) \phi_i(x) \right)^2 * \\
& \left(\sum_{i=1}^N p_i(t) \phi_i^{iv}(x) + \sum_{i=1}^N \ddot{p}_i(t) \phi_i(x) + c \sum_{i=1}^N \dot{p}_i(t) \phi_i(x) \right) dx = \\
& \int_{x=0}^1 \phi_j(x) \left(1 - \sum_{i=1}^N p_i(t) \phi_i(x) \right)^2 \left(d_2/d_1 + \sum_{i=1}^N p_i(t) \phi_i(x) - \sum_{i=1}^N q_i(t) \phi_i(x) \right)^2 * \quad (5.28) \\
& \left(\alpha_3 \Gamma_1 + N \right) \sum_{i=1}^N p_i(t) \phi_i''(x) + \left(d_2/d_1 + \sum_{i=1}^N p_i(t) \phi_i(x) - \sum_{i=1}^N q_i(t) \phi_i(x) \right)^2 \alpha_4 (V_{DC} + \\
& V_{AC} \cos(\Omega t))^2 - \left(1 - \sum_{i=1}^N p_i(t) \phi_i(x) \right)^2 \alpha_4 (V_{DC} + V_{AC} \cos(\Omega t))^2 dx
\end{aligned}$$

$$\begin{aligned}
& \int_{x=0}^1 \phi_j(x) \left(d_2/d_1 + \sum_{i=1}^N p_i(t) \phi_i(x) - \sum_{i=1}^N q_i(t) \phi_i(x) \right)^2 \left(\sum_{i=1}^N q_i(t) \phi_i^{iv}(x) + \right. \\
& \left. \sum_{i=1}^N \ddot{q}_i(t) \phi_i(x) + c \sum_{i=1}^N \dot{q}_i(t) \phi_i(x) \right) dx = \int_{x=0}^1 \phi_j(x) \left(\left(d_2/d_1 + \sum_{i=1}^N p_i(t) \phi_i(x) - \right. \right. \quad (5.29) \\
& \left. \left. \sum_{i=1}^N q_i(t) \phi_i(x) \right)^2 \left(\alpha_3 \Gamma_2 + N \right) \sum_{i=1}^N q_i(t) \phi_i''(x) + \alpha_4 (V_{DC} + V_{AC} \cos(\Omega t))^2 \right) dx
\end{aligned}$$

5.2.2 Perturbation Analysis

Numerical solutions of the ROM dynamical equations provide good results for low nonlinearity values. However, when tuning the system's geometrical parameters as well as the forcing amplitudes, one can increase the source of the nonlinearity, leading to nonlinear frequency responses which cannot be fully captured by ROM. As a result, perturbation theory was investigated to find the resonance of the double-microbeams especially for any high nonlinearity factors. The method of multiple scales was used by direct attack of the equations of motion [34, 47]. So, the variable for the time scales and its derivatives were defined as follows:

$$T_0 = t, \quad D_0 = \frac{\partial}{\partial T_0}, \quad T_1 = \varepsilon t, \quad D_1 = \frac{\partial}{\partial T_1}, \quad T_2 = \varepsilon^2 t, \quad D_2 = \frac{\partial}{\partial T_2}, \quad (5.30)$$

Next, the damping coefficient c and the forcing amplitude V_{AC} were scaled so that their nonlinearity effect will be balanced in the modulation equations [34, 47]. Hence,

$$c = \varepsilon^2 c, \quad V_{AC} = \varepsilon^3 V_{AC}, \quad (5.31)$$

where ε is a bookkeeping parameter.

We seek a solution for the lower and upper electrodes in the following form, respectively:

$$\begin{aligned} w_1(x, t, \varepsilon) &= w_{s1}(x) + u_1(x, t) \\ &= w_{s1}(x) + \varepsilon u_{11}(x, T_0, T_2) + \varepsilon^2 u_{12}(x, T_0, T_2) + \varepsilon^3 u_{13}(x, T_0, T_2) + \dots, \end{aligned} \quad (5.32)$$

$$\begin{aligned} w_2(x, t, \varepsilon) &= w_{s2}(x) + u_2(x, t) \\ &= w_{s2}(x) + \varepsilon u_{21}(x, T_0, T_2) + \varepsilon^2 u_{22}(x, T_0, T_2) + \varepsilon^3 u_{23}(x, T_0, T_2) + \dots, \end{aligned} \quad (5.33)$$

where w_{s1} and w_{s2} are the static components of the microbeams' deflection and u_1 and u_2 are their dynamic components for the lower and upper microbeams, respectively. Substituting equations (5.32) and (5.33) into equations (2.24) and (2.25) gives:

$$\begin{aligned} \frac{\partial^4 w_{s1}}{\partial x^4} + \frac{\partial^4 u_1}{\partial x^4} + \frac{\partial^2 u_1}{\partial t^2} + c \frac{\partial u_1}{\partial t} &= (\alpha_3 \Gamma(w_{s1} + u_1, w_{s1} + u_1) + N) \left(\frac{\partial^2 w_{s1}}{\partial x^2} + \frac{\partial^2 u_1}{\partial x^2} \right) + \\ \frac{\alpha_4 (V_{DC} + V_{AC} \cos(\Omega t))^2}{(1 - w_{s1} - u_1)^2} &- \frac{\alpha_4 (V_{DC} + V_{AC} \cos(\Omega t))^2}{\left(\frac{d_2}{d_1} + w_{s1} + u_1 - w_{s2} - u_2\right)^2} \end{aligned} \quad (5.34)$$

$$\begin{aligned} \frac{\partial^4 w_{s2}}{\partial x^4} + \frac{\partial^4 u_2}{\partial x^4} + \frac{\partial^2 u_2}{\partial t^2} + c \frac{\partial u_2}{\partial t} &= (\alpha_3 \Gamma(w_{s2} + u_2, w_{s2} + u_2) + N) \left(\frac{\partial^2 w_{s2}}{\partial x^2} + \frac{\partial^2 u_2}{\partial x^2} \right) + \\ \frac{\alpha_4 (V_{DC} + V_{AC} \cos(\Omega t))^2}{\left(\frac{d_2}{d_1} + w_{s1} + u_1 - w_{s2} - u_2\right)^2} & \end{aligned} \quad (5.35)$$

As in the single microbeam configuration, the electrical forces $\frac{\alpha_4 (V_{DC} + V_{AC} \cos(\Omega t))^2}{(1 - w_{s1} - u_1)^2}$ and

$\frac{\alpha_4 (V_{DC} + V_{AC} \cos(\Omega t))^2}{\left(\frac{d_2}{d_1} + w_{s1} + u_1 - w_{s2} - u_2\right)^2}$ are expanded around (u_1) and $(u_1 - u_2)$ using a Taylor-series expansion,

respectively. Further, the expression of $(V_{DC} + V_{AC} \cos(\Omega t))^2$ will be approximated as $V_{DC}^2 + 2V_{DC}V_{AC} \cos(\Omega t)$. Using the aforementioned expressions and canceling the static equations and neglecting all small terms while equating the coefficients of like powers of ε , the following equations are obtained:

For equation (5.34):

- **Order ε^1 :**

$$\mathcal{L}_1(u_{11}, u_{21}) = 0 \quad (5.36)$$

- **Order ε^2 :**

$$\mathcal{L}_1(u_{12}, u_{22}) = \alpha_3 w_{s1}'' \Gamma(u_{11}, u_{11}) + 2\alpha_3 u_{11}'' \Gamma(w_{s1}, u_{11}) + \frac{3\alpha_4 V_{DC}^2 u_{11}^2}{(1-w_{s1})^4} - \frac{3\alpha_4 V_{DC}^2 (u_{11}^2 - 2u_{11}u_{21} + u_{21}^2)}{(d_2/d_1 + w_{s1} - w_{s2})^4} \quad (5.37)$$

- **Order ε^3 :**

$$\begin{aligned} \mathcal{L}_1(u_{13}, u_{23}) = & -2D_0 D_2 u_{11} - cD_0 u_{11} + 2\alpha_3 w_{s1}'' \Gamma(u_{11}, u_{12}) + 2\alpha_3 u_{11}'' \Gamma(w_{s1}, u_{12}) + \\ & 2\alpha_3 u_{12}'' \Gamma(w_{s1}, u_{11}) + \alpha_3 \Gamma(u_{11}, u_{11}) u_{11}'' + \frac{6\alpha_4 V_{DC}^2 u_{11} u_{12}}{(1-w_{s1})^4} + \frac{4\alpha_4 V_{DC}^2 u_{11}^3}{(1-w_{s1})^5} + \\ & \frac{6\alpha_4 V_{DC}^2 (-u_{11}u_{12} + u_{11}u_{22} + u_{12}u_{21} - u_{21}u_{22})}{\left(\frac{d_2}{d_1} + w_{s1} - w_{s2}\right)^4} + \frac{4\alpha_4 V_{DC}^2 (u_{11}^3 - 3u_{11}^2 u_{21} + 3u_{11} u_{21}^2 - u_{21}^3)}{\left(\frac{d_2}{d_1} + w_{s1} - w_{s2}\right)^5} + \\ & 2\tilde{F}_1 \cos(\Omega T_0) - 2\tilde{F}_2 \cos(\Omega T_0) \end{aligned} \quad (5.38)$$

where \mathcal{L}_1 is a linear differential operator defined for any two functions (f and g) by:

$$\begin{aligned} \mathcal{L}_1(f, g) = & D_0^2 f + f^{iv} - \alpha_3 \Gamma(w_{s1}, w_{s1}) f'' - N f'' - 2\alpha_3 w_{s1}'' \Gamma(w_{s1}, f) - \frac{2\alpha_4 V_{DC}^2 f}{(1-w_{s1})^3} - \frac{2\alpha_4 V_{DC}^2 f}{\left(\frac{d_2}{d_1} + w_{s1} - w_{s2}\right)^3} + \\ & \frac{2\alpha_4 V_{DC}^2 g}{\left(\frac{d_2}{d_1} + w_{s1} - w_{s2}\right)^3} = 0 \end{aligned}$$

and where: $\tilde{F}_1 = \frac{\alpha_4 V_{DC} V_{AC}}{(1-w_{s1})^2}$ $\tilde{F}_2 = \frac{\alpha_4 V_{DC} V_{AC}}{\left(\frac{d_2}{d_1} + w_{s1} - w_{s2}\right)^2}$

For equation (5.35):

- **Order ε^1 :**

$$\mathcal{L}_2(u_{11}, u_{21}) = 0 \quad (5.39)$$

- **Order ε^2 :**

$$\mathcal{L}_2(u_{12}, u_{22}) = \alpha_3 w_{s2}'' \Gamma(u_{21}, u_{21}) + 2\alpha_3 u_{21}'' \Gamma(w_{s2}, u_{21}) + \frac{3\alpha_4 V_{DC}^2 (u_{11}^2 - 2u_{11}u_{21} + u_{21}^2)}{\left(\frac{d_2}{d_1} + w_{s1} - w_{s2}\right)^4} \quad (5.40)$$

- **Order ε^3 :**

$$\begin{aligned} \mathcal{L}_2(u_{13}, u_{23}) = & -2D_0 D_2 u_{21} - cD_0 u_{21} + 2\alpha_3 w_{s2}'' \Gamma(u_{21}, u_{22}) + 2\alpha_3 u_{21}'' \Gamma(w_{s2}, u_{22}) + \\ & 2\alpha_3 u_{22}'' \Gamma(w_{s2}, u_{21}) + \alpha_3 \Gamma(u_{21}, u_{21}) u_{21}'' + \frac{6\alpha_4 V_{DC}^2 (u_{11}u_{12} - u_{11}u_{22} - u_{12}u_{21} + u_{21}u_{22})}{\left(\frac{d_2}{d_1} + w_{s1} - w_{s2}\right)^4} + \\ & \frac{4\alpha_4 V_{DC}^2 (-u_{11}^3 + 3u_{11}^2 u_{21} - 3u_{11}u_{21}^2 + u_{21}^3)}{\left(\frac{d_2}{d_1} + w_{s1} - w_{s2}\right)^5} + 2\tilde{F}_2 \cos(\Omega T_0) \end{aligned} \quad (5.41)$$

where \mathcal{L}_2 is a linear differential operator defined for any two functions (f and g) by:

$$\begin{aligned} \mathcal{L}_2(f, g) = & D_0^2 g + g^{iv} - \alpha_3 \Gamma(w_{s2}, w_{s2}) g'' - N g'' - 2\alpha_3 w_{s2}'' \Gamma(w_{s2}, g) + \frac{2\alpha_4 V_{DC}^2 f}{\left(\frac{d_2}{d_1} + w_{s1} - w_{s2}\right)^3} - \\ & \frac{2\alpha_4 V_{DC}^2 g}{\left(\frac{d_2}{d_1} + w_{s1} - w_{s2}\right)^3} \end{aligned}$$

Assuming no internal resonances scenarios, the solutions of equations (5.36) and (5.39) are assumed to consist of only the directly excited modes, $\Phi(x)$, since the indirectly excited modes will die out in the presence of damping. As a result, the solution of the dynamic components u_{1l} and u_{2l} of the lower and upper microbeams, respectively, are:

$$u_{1l}(x, T_0, T_2) = \left[A(T_2)e^{i\omega T_0} + \bar{A}(T_2)e^{-i\omega T_0} \right] \Phi_1(x), \quad (5.42)$$

$$u_{2l}(x, T_0, T_2) = \left[A(T_2)e^{i\omega T_0} + \bar{A}(T_2)e^{-i\omega T_0} \right] \Phi_2(x), \quad (5.43)$$

where $A(T_2)$ is a complex-valued function that is determined by imposing the solvability condition at the third order, the over bar denotes the complex conjugate, and ω and $\Phi(x)$ are the natural frequency and corresponding eigenfunction of the directly excited modes, respectively. Here, the complex-valued function is considered to be the same for both microbeams, while the mode shapes will compensate for the resulting difference. This will help in obtaining the eigenvalue problem. Substituting equations (5.42) and (5.43) into equations (5.36) and (5.39) we obtain the following nonlinear coupled eigenvalue problem (EVP):

$$\begin{aligned} & -\omega^2\Phi_1 + \Phi_1^{iv} - \alpha_3\Gamma(w_{s1}, w_{s1})\Phi_1'' - N\Phi_1'' - 2\alpha_3w_{s1}''\Gamma(w_{s1}, \Phi_1) - \\ & \frac{2\alpha_4V_{DC}^2\Phi_1}{(1-w_{s1})^3} - \frac{2\alpha_4V_{DC}^2\Phi_1}{\left(\frac{d_2}{d_1} + w_{s1} - w_{s2}\right)^3} + \frac{2\alpha_4V_{DC}^2\Phi_2}{\left(\frac{d_2}{d_1} + w_{s1} - w_{s2}\right)^3} = 0 \end{aligned} \quad (5.44)$$

$$\begin{aligned}
& -\omega^2\Phi_2 + \Phi_2^{iv} - \alpha_3\Gamma(w_{s2}, w_{s2})\Phi_2'' - N\Phi_2'' - 2\alpha_3w_{s2}''\Gamma(w_{s2}, \Phi_2) - \\
& \frac{2\alpha_4V_{DC}^2\Phi_2}{\left(\frac{d_2}{d_1} + w_{s1} - w_{s2}\right)^3} + \frac{2\alpha_4V_{DC}^2\Phi_1}{\left(\frac{d_2}{d_1} + w_{s1} - w_{s2}\right)^3} = 0
\end{aligned} \tag{5.45}$$

In order to solve for the coupled mode shapes Φ_1 and Φ_2 the eigenfunctions of the coupled EVP of equations (5.44) and (5.45), both functions are expanded assuming the Galerkin discretization method, as follows:

$$\Phi_1(x) = \sum_{i=1}^N a_{1i}\phi_i(x) \tag{5.46}$$

$$\Phi_2(x) = \sum_{i=1}^N a_{2i}\phi_i(x) \tag{5.47}$$

Substituting equations (5.46) and (5.47) into equations (5.44) and (5.45), the resulting equations are then multiplied by ϕ_j , and the resulting equations are then integrated from $x=0$ to $x=1$. The coupled mode shapes can be then obtained by evaluating the eigenvectors of the resulting equations, where their number will be double that of the chosen number of modes. Next, the solutions u_{11} and u_{21} will be substituted in the second order equations (ε^2), which will give:

$$\mathcal{L}_1(u_{12}, u_{22}) = (A^2 e^{2i\omega T_0} + 2A\bar{A} + \bar{A}^2 e^{-2i\omega T_0})h_1(x) \tag{5.48}$$

$$\mathcal{L}_2(u_{12}, u_{22}) = (A^2 e^{2i\omega T_0} + 2A\bar{A} + \bar{A}^2 e^{-2i\omega T_0})h_2(x) \quad (5.49)$$

where:

$$h_1(x) = \alpha_3 w_{s1}'' \Gamma(\Phi_1, \Phi_1) + 2\alpha_3 \Phi_1' \Gamma(w_{s1}, \Phi_1) + \frac{3\alpha_4 V_{DC}^2 \Phi_1^2}{(1-w_{s1})^4} - \frac{3\alpha_4 V_{DC}^2 \Phi_1^2}{(\frac{d_2}{d_1} + w_{s1} - w_{s2})^4} + \frac{6\alpha_4 V_{DC}^2 \Phi_1 \Phi_2}{(\frac{d_2}{d_1} + w_{s1} - w_{s2})^4} - \frac{3\alpha_4 V_{DC}^2 \Phi_2^2}{(\frac{d_2}{d_1} + w_{s1} - w_{s2})^4} \quad (5.50)$$

$$h_2(x) = \alpha_3 w_{s2}'' \Gamma(\Phi_2, \Phi_2) + 2\alpha_3 \Phi_2' \Gamma(w_{s2}, \Phi_2) + \frac{3\alpha_4 V_{DC}^2 \Phi_1^2}{(\frac{d_2}{d_1} + w_{s1} - w_{s2})^4} - \frac{6\alpha_4 V_{DC}^2 \Phi_1 \Phi_2}{(\frac{d_2}{d_1} + w_{s1} - w_{s2})^4} + \frac{3\alpha_4 V_{DC}^2 \Phi_2^2}{(\frac{d_2}{d_1} + w_{s1} - w_{s2})^4} \quad (5.51)$$

Assuming the particular solution of u_{12} and u_{22} as:

$$u_{12} = (A^2 e^{2i\omega T_0} \Psi_{11} + 2A\bar{A} \Psi_{12} + \bar{A}^2 e^{-2i\omega T_0} \Psi_{11}) \quad (5.52)$$

$$u_{22} = (A^2 e^{2i\omega T_0} \Psi_{21} + 2A\bar{A} \Psi_{22} + \bar{A}^2 e^{-2i\omega T_0} \Psi_{21}) \quad (5.53)$$

where Ψ_{ij} are the solutions of the boundary value problems:

$$M_1(\Psi_{1i}, 2\omega\delta_{1i}) = h_1(x) \quad (5.54)$$

$$M_2(\Psi_{2i}, 2\omega\delta_{1i}) = h_2(x) \quad (5.55)$$

$$\Psi_{1j} = 0 \quad \Psi'_{1j} = 0 \quad \Psi_{2j} = 0 \quad \Psi'_{2j} = 0 \quad (5.56)$$

At $x=0$ and $x=l$ for $j=1$ to 2

where δ is the Kronecker delta operator and the two linear differential operators M_1 and M_2 are defined as:

$$M_1(\Psi_{1i}, \omega) = \Psi_{1i}^{iv} - \omega^2 \Psi_{1i} - \alpha_3 \Gamma(w_{s1}, w_{s1}) \Psi_{1i}'' - N \Psi_{1i}'' - 2\alpha_3 w_{s1}'' \Gamma(w_{s1}, \Psi_{1i}) - \frac{2\alpha_4 V_{DC}^2 \Psi_{1i}}{(1 - w_{s1})^3} - \frac{2\alpha_4 V_{DC}^2 \Psi_{1i}}{(\frac{d_2}{d_1} + w_{s1} - w_{s2})^3} + \frac{2\alpha_4 V_{DC}^2 \Psi_{2i}}{(\frac{d_2}{d_1} + w_{s1} - w_{s2})^3} \quad (5.57)$$

$$M_2(\Psi_{2i}, \omega) = \Psi_{2i}^{iv} - \omega^2 \Psi_{2i} - \alpha_3 \Gamma(w_{s2}, w_{s2}) \Psi_{2i}'' - N \Psi_{2i}'' - 2\alpha_3 w_{s2}'' \Gamma(w_{s2}, \Psi_{2i}) + \frac{2\alpha_4 V_{DC}^2 \Psi_{1i}}{(\frac{d_2}{d_1} + w_{s1} - w_{s2})^3} - \frac{2\alpha_4 V_{DC}^2 \Psi_{2i}}{(\frac{d_2}{d_1} + w_{s1} - w_{s2})^3} \quad (5.58)$$

Introducing the detuning parameter σ_1 and σ_2 to describe the nearness of the excitation frequency Ω_1 and Ω_2 , respectively, to the fundamental natural frequency of the excited mode ω as:

$$\Omega_1 = \omega + \varepsilon^2 \sigma_1 \quad (5.59)$$

$$\Omega_2 = \omega + \varepsilon^2 \sigma_2 \quad (5.60)$$

The solutions of the first and second order are then substituted in equations (5.38) and (5.41), leading to:

$$\begin{aligned} \mathcal{L}_1(u_{13}, u_{23}) &= D_0^2 u_{13} + u_{13}^{iv} - \alpha_3 \Gamma(w_{s1}, w_{s1}) u_{13}'' - N u_{13}'' - 2\alpha_3 w_{s1}'' \Gamma(w_{s1}, u_{13}) \\ &- \frac{2\alpha_4 V_{DC}^2 u_{13}}{(1-w_{s1})^3} - \frac{2\alpha_4 V_{DC}^2 u_{13}}{\left(\frac{d_2}{d_1} + w_{s1} - w_{s2}\right)^3} + \frac{2\alpha_4 V_{DC}^2 u_{23}}{\left(\frac{d_2}{d_1} + w_{s1} - w_{s2}\right)^3} = (-2i\omega A' \Phi_1(x) - \\ &ic\omega \Phi_1(x) A + \chi_1(x) A^2 \bar{A} + \tilde{F}_1 e^{i\omega_1 T_2} - \tilde{F}_2 e^{i\omega_2 T_2}) e^{i\omega T_0} + cc + NST \end{aligned} \quad (5.61)$$

$$\begin{aligned} \mathcal{L}_2(u_{13}, u_{23}) &= D_0^2 u_{23} + u_{23}^{iv} - \alpha_3 \Gamma(w_{s2}, w_{s2}) u_{23}'' - N u_{23}'' - 2\alpha_3 w_{s2}'' \Gamma(w_{s2}, u_{23}) + \\ &\frac{2\alpha_4 V_{DC}^2 u_{13}}{\left(\frac{d_2}{d_1} + w_{s1} - w_{s2}\right)^3} - \frac{2\alpha_4 V_{DC}^2 u_{23}}{\left(\frac{d_2}{d_1} + w_{s1} - w_{s2}\right)^3} = (-2i\omega A' \Phi_2(x) - ic\omega A \Phi_2(x) + \\ &A^2 \bar{A} \chi_2(x) + \tilde{F}_2 e^{i\omega_2 T_2}) e^{i\omega T_0} + cc + NST \end{aligned} \quad (5.62)$$

where NST stands for the non-secular terms and the functions χ_i are defined as:

$$\begin{aligned}
\chi_1(x) = & 2\alpha_3 w_{s1}'' (\Gamma(\Phi_1, \Psi_{11}) + 2\Gamma(\Phi_1, \Psi_{12})) + 2\alpha_3 \Phi_1'' (\Gamma(w_{s1}, \Psi_{11}) + 2\Gamma(w_{s1}, \Psi_{12})) + \\
& 2\alpha_3 \Gamma(w_{s1}, \Phi_1) (\Psi_{11}'' + 2\Psi_{12}'') + 3\alpha_3 \Gamma(\Phi_1, \Phi_1) \Phi_1'' + \frac{6\alpha_4 V_{DC}^2}{(1-w_{s1})^4} (\Psi_{11} \Phi_1 + 2\Psi_{12} \Phi_1) + \\
& \frac{12\alpha_4 V_{DC}^2}{(1-w_{s1})^5} \Phi_1^3 + \frac{6\alpha_4 V_{DC}^2}{((d_2/d_1) + w_{s1} - w_{s2})^4} (-\Phi_1 \Psi_{11} - 2\Phi_1 \Psi_{12} + \Phi_1 \Psi_{21} + 2\Phi_1 \Psi_{22} + \\
& \Phi_2 \Psi_{11} + 2\Phi_2 \Psi_{12} - \Phi_2 \Psi_{21} - 2\Phi_2 \Psi_{22}) + \frac{12\alpha_4 V_{DC}^2}{((d_2/d_1) + w_{s1} - w_{s2})^5} (\Phi_1^3 - 3\Phi_1^2 \Phi_2 + 3\Phi_1 \Phi_2^2 - \Phi_2^3)
\end{aligned} \tag{5.63}$$

$$\begin{aligned}
\chi_2(x) = & 2\alpha_3 w_{s2}'' (\Gamma(\Phi_2, \Psi_{21}) + 2\Gamma(\Phi_2, \Psi_{22})) + 2\alpha_3 \Phi_2'' (\Gamma(w_{s2}, \Psi_{21}) + 2\Gamma(w_{s2}, \Psi_{22})) + \\
& 2\alpha_3 \Gamma(w_{s2}, \Phi_2) (\Psi_{21}'' + 2\Psi_{22}'') + 3\alpha_3 \Gamma(\Phi_2, \Phi_2) \Phi_2'' + \frac{6\alpha_4 V_{DC}^2}{((d_2/d_1) + w_{s1} - w_{s2})^4} (\Phi_1 \Psi_{11} + \\
& 2\Phi_1 \Psi_{12} - \Phi_1 \Psi_{21} - 2\Phi_1 \Psi_{22} - \Phi_2 \Psi_{11} - 2\Phi_2 \Psi_{12} + \Phi_2 \Psi_{21} + 2\Phi_2 \Psi_{22}) + \\
& \frac{12\alpha_4 V_{DC}^2}{((d_2/d_1) + w_{s1} - w_{s2})^5} (-\Phi_1^3 + 3\Phi_1^2 \Phi_2 - 3\Phi_1 \Phi_2^2 + \Phi_2^3)
\end{aligned} \tag{5.64}$$

Hence, we need to eliminate the secular terms in equations (5.61) and (5.62) by seeking a particular solution free of secular terms in the form:

$$u_{13}(x, T_0, T_2) = \Upsilon_1(x, T_2) e^{i\omega T_0} \tag{5.65}$$

$$u_{23}(x, T_0, T_2) = \Upsilon_2(x, T_2) e^{i\omega T_0} \tag{5.66}$$

Then, equations (5.65) and (5.66) are substituted into equations (5.61) and (5.62), which will give:

$$\begin{aligned}
\mathcal{L}_1(u_{13}, u_{23}) &= e^{i\omega T_0} (-\omega^2 \Upsilon_1 + \Upsilon_1^{iv} - \alpha_3 \Gamma(w_{s1}, w_{s1}) \Upsilon_1'' - N \Upsilon_1'' - 2\alpha_3 w_{s1}'' \Gamma(w_{s1}, \Upsilon_1) - \\
&\frac{2\alpha_4 V_{DC}^2 \Upsilon_1}{(1-w_{s1})^3} - \frac{2\alpha_4 V_{DC}^2 \Upsilon_1}{\left(\frac{d_2}{d_1} + w_{s1} - w_{s2}\right)^3} + \frac{2\alpha_4 V_{DC}^2 \Upsilon_2}{\left(\frac{d_2}{d_1} + w_{s1} - w_{s2}\right)^3}) = (-2i\omega A' \Phi_1(x) - ic\omega \Phi_1(x) A + \\
&\chi_1(x) A^2 \bar{A} + \tilde{F}_1 e^{i\sigma_1 T_2} - \tilde{F}_2 e^{i\sigma_2 T_2}) e^{i\omega T_0} + cc + NST
\end{aligned} \tag{5.67}$$

$$\begin{aligned}
\mathcal{L}_2(u_{13}, u_{23}) &= e^{i\omega T_0} (-\omega^2 \Upsilon_2 + \Upsilon_2^{iv} - \alpha_1 \Gamma(w_{s2}, w_{s2}) \Upsilon_2'' - N \Upsilon_2'' - 2\alpha_1 w_{s2}'' \Gamma(w_{s2}, \Upsilon_2) + \\
&\frac{2\alpha_2 V_{DC}^2 \Upsilon_1}{\left(\frac{d_2}{d_1} + w_{s1} - w_{s2}\right)^3} - \frac{2\alpha_2 V_{DC}^2 \Upsilon_2}{\left(\frac{d_2}{d_1} + w_{s1} - w_{s2}\right)^3}) = (-2i\omega A' \Phi_2(x) - ic\omega A \Phi_2(x) + \\
&A^2 \bar{A} \chi_2(x) + \tilde{F}_2 e^{i\sigma_2 T_2}) e^{i\omega T_0} + cc + NST
\end{aligned} \tag{5.68}$$

Next, the coefficients of $e^{i\omega T_0}$ in equations (5.67) and (5.68) will be equated. The resulting two equations will be then multiplied by two adjoints functions $P(x)$ and $Q(x)$, respectively, and then integrated by parts to transfer the derivatives from Υ to the adjoints, leading to:

$$\begin{aligned}
& - \int_{x=0}^1 \omega^2 \Upsilon_1 P dx + [P \Upsilon_1''' - P' \Upsilon_1'' + P'' \Upsilon_1' - P''' \Upsilon_1]_{x=0}^1 + \int_{x=0}^1 P^{iv} \Upsilon_1 dx - \\
& \alpha_3 \Gamma(w_{s1}, w_{s1}) ([P \Upsilon_1']_0^1 - [P' \Upsilon_1]_0^1 + \int_{x=0}^1 P'' \Upsilon_1 dx) - ([NP \Upsilon_1' - NP' \Upsilon_1]_{x=0}^1 + \int_{x=0}^1 NP'' \Upsilon_1 dx) - \\
& 2\alpha_3 ([w_{s1}'^2 P \Upsilon_1]_0^1 - [w_{s1}' P]_0^1 \int_{x=0}^1 \Upsilon_1 w_{s1}'' dx - [w_{s1}' \Upsilon_1]_0^1 \Gamma(P, w_{s1}) + \int_{x=0}^1 \Upsilon_1 w_{s1}'' \Gamma(P, w_{s1}) dx) - \\
& \int_{x=0}^1 \frac{2\alpha_4 V_{DC}^2 \Upsilon_1 P}{(1-w_{s1})^3} dx - \int_{x=0}^1 \frac{2\alpha_4 V_{DC}^2 \Upsilon_1 P}{\left(\frac{d_2}{d_1} + w_{s1} - w_{s2}\right)^3} dx + \int_{x=0}^1 \frac{2\alpha_4 V_{DC}^2 \Upsilon_2 P}{\left(\frac{d_2}{d_1} + w_{s1} - w_{s2}\right)^3} dx = \\
& \int_{x=0}^1 P (-2i\omega A' \Phi_1(x) - ic\omega \Phi_1(x) A + \chi_1(x) A^2 \bar{A} + \tilde{F}_1 e^{i\sigma_1 T_2} - \tilde{F}_2 e^{i\sigma_2 T_2}) dx
\end{aligned} \tag{5.69}$$

$$\begin{aligned}
& - \int_{x=0}^1 \omega^2 \Upsilon_2 Q dx + [Q \Upsilon_2''' - Q' \Upsilon_2'' + Q'' \Upsilon_2' - Q''' \Upsilon_2]_{x=0}^1 + \int_{x=0}^1 Q^{iv} \Upsilon_2 dx - \\
& \alpha_3 \Gamma(w_{s2}, w_{s2}) ([Q \Upsilon_2']_0^1 - [Q' \Upsilon_2]_0^1 + \int_{x=0}^1 Q'' \Upsilon_2 dx) - ([N Q \Upsilon_2' - N Q' \Upsilon_2]_{x=0}^1 + \\
& \int_{x=0}^1 N Q'' \Upsilon_2 dx) - (2\alpha_3 ([w_{s2}'^2 Q \Upsilon_2]_0^1 - [w_{s2}' Q]_0^1 \int_{x=0}^1 \Upsilon_2 w_{s2}'' dx - [w_{s2}' \Upsilon_2]_0^1 \Gamma(Q, w_{s2}) + \\
& \int_{x=0}^1 \Upsilon_2 w_{s2}'' \Gamma(Q, w_{s2}) dx) + \int_{x=0}^1 \frac{2\alpha_4 V_{DC}^2 \Upsilon_1}{\left(\frac{d_2}{d_1} + w_{s1} - w_{s2}\right)^3} Q dx - \int_{x=0}^1 \frac{2\alpha_4 V_{DC}^2 \Upsilon_2}{\left(\frac{d_2}{d_1} + w_{s1} - w_{s2}\right)^3} Q dx = \\
& \int_{x=0}^1 (-2i\omega A' \Phi_2(x) - ic\omega A \Phi_2(x) + A^2 \bar{A} \chi_2(x) + \tilde{F}_2 e^{i\sigma_2 T_2}) Q dx
\end{aligned} \tag{5.70}$$

which then can be simplified as:

$$\begin{aligned}
& \int_{x=0}^1 \Upsilon_1 (-\omega^2 P + P^{iv} - \alpha_3 \Gamma(w_{s1}, w_{s1}) P'' - NP'' - 2\alpha_3 w_{s1}' \Gamma(P, w_{s1}) - \\
& \frac{2\alpha_4 V_{DC}^2 P}{(1-w_{s1})^3} - \frac{2\alpha_4 V_{DC}^2 P}{\left(\frac{d_2}{d_1} + w_{s1} - w_{s2}\right)^3}) dx + [P \Upsilon_1''' - P' \Upsilon_1'' + P'' \Upsilon_1' - P''' \Upsilon_1 - \\
& \alpha_3 \Gamma(w_{s1}, w_{s1}) (P \Upsilon_1' - P' \Upsilon_1) - NP \Upsilon_1' + NP' \Upsilon_1 + 2\alpha_3 w_{s1}' P \int_{x=0}^1 w_{s1}'' \Upsilon_1 dx - \\
& 2\alpha_3 w_{s1}'^2 P \Upsilon_1 + 2\alpha_3 w_{s1}' \Upsilon_1 \Gamma(P, w_{s1})]_{x=0}^1 + \int_{x=0}^1 \Upsilon_2 \frac{2\alpha_4 V_{DC}^2 P}{\left(\frac{d_2}{d_1} + w_{s1} - w_{s2}\right)^3} dx = \\
& \int_{x=0}^1 P (-2i\omega A' \Phi_1(x) - ic\omega \Phi_1(x) A + \chi_1(x) A^2 \bar{A} + \tilde{F}_1 e^{i\sigma_1 T_2} - \tilde{F}_2 e^{i\sigma_2 T_2}) dx
\end{aligned} \tag{5.71}$$

$$\begin{aligned}
& \int_{x=0}^1 \Upsilon_2 (-\omega^2 Q + Q^{iv} - \alpha_3 \Gamma(w_{s_2}, w_{s_2}) Q'' - NQ'' - 2\alpha_3 w_{s_2}'' \Gamma(Q, w_{s_2}) - \frac{2\alpha_4 V_{DC}^2 Q}{\left(\frac{d_2}{d_1} + w_{s_1} - w_{s_2}\right)^3}) dx + \\
& \int_{x=0}^1 \Upsilon_1 \frac{2\alpha_4 V_{DC}^2 Q}{\left(\frac{d_2}{d_1} + w_{s_1} - w_{s_2}\right)^3} dx + [Q\Upsilon_2''' - Q'\Upsilon_2'' + Q''\Upsilon_2' - Q'''\Upsilon_2 - \alpha_3 \Gamma(w_{s_2}, w_{s_2})(Q\Upsilon_2' - Q'\Upsilon_2) - \\
& NQ\Upsilon_2' + NQ'\Upsilon_2 + 2\alpha_3 w_{s_2}' Q \int_{x=0}^1 w_{s_2}'' \Upsilon_2 dx - 2\alpha_3 w_{s_2}'^2 Q\Upsilon_2 + 2\alpha_3 w_{s_2}' \Upsilon_2 \Gamma(Q, w_{s_2})]_{x=0}^1 = \\
& \int_{x=0}^1 Q(-2i\omega A'\Phi_2(x) - ic\omega A\Phi_2(x) + A^2 \bar{A}\chi_2(x) + \tilde{F}_2 e^{i\sigma_2 T_2}) dx
\end{aligned} \tag{5.72}$$

By adding equations (5.71) and (5.72) and re-arranging the terms, we obtain:

$$\begin{aligned}
& \int_{x=0}^1 \Upsilon_1 (-\omega^2 P + P^{iv} - \alpha_1 \Gamma(w_{s_1}, w_{s_1}) P'' - NP'' - 2\alpha_3 w_{s_1}'' \Gamma(P, w_{s_1}) - \frac{2\alpha_4 V_{DC}^2 P}{(1-w_{s_1})^3} - \\
& \frac{2\alpha_4 V_{DC}^2 P}{\left(\frac{d_2}{d_1} + w_{s_1} - w_{s_2}\right)^3} + \frac{2\alpha_4 V_{DC}^2 Q}{\left(\frac{d_2}{d_1} + w_{s_1} - w_{s_2}\right)^3}) dx + \int_{x=0}^1 \Upsilon_2 (-\omega^2 Q + Q^{iv} - \alpha_3 \Gamma(w_{s_2}, w_{s_2}) Q'' - \\
& NQ'' - 2\alpha_3 w_{s_2}'' \Gamma(Q, w_{s_2}) - \frac{2\alpha_4 V_{DC}^2 Q}{\left(\frac{d_2}{d_1} + w_{s_1} - w_{s_2}\right)^3} + \frac{2\alpha_4 V_{DC}^2 P}{\left(\frac{d_2}{d_1} + w_{s_1} - w_{s_2}\right)^3}) dx + \\
& [P\Upsilon_1''' - P'\Upsilon_1'' + P''\Upsilon_1' - P'''\Upsilon_1 - \alpha_1 \Gamma(w_{s_1}, w_{s_1})(P\Upsilon_1' - P'\Upsilon_1) - NP\Upsilon_1' + NP'\Upsilon_1 + \\
& 2\alpha_1 w_{s_1}' P \int_0^1 \Upsilon_1 w_{s_1}'' dx]_{x=0}^1 + [-2\alpha_1 w_{s_1}'^2 P\Upsilon_1 + 2\alpha_1 w_{s_1}' \Upsilon_1 \Gamma(P, w_{s_1}) + Q\Upsilon_2''' - Q'\Upsilon_2'' + \\
& Q''\Upsilon_2' - Q'''\Upsilon_2 - \alpha_3 \Gamma(w_{s_2}, w_{s_2})(Q\Upsilon_2' - Q'\Upsilon_2)]_{x=0}^1 + [-NQ\Upsilon_2' + NQ'\Upsilon_2 + \\
& 2\alpha_3 w_{s_2}' Q \int_0^1 \Upsilon_2 w_{s_2}'' dx - 2\alpha_3 w_{s_2}'^2 Q\Upsilon_2 + 2\alpha_3 w_{s_2}' \Upsilon_2 \Gamma(Q, w_{s_2})]_{x=0}^1 = \\
& \int_{x=0}^1 (-2i\omega A'(P\Phi_1 + Q\Phi_2) - ic\omega A(P\Phi_1 + Q\Phi_2) + A^2 \bar{A}(P\chi_1 + Q\chi_2) + \\
& \tilde{F}_1 P e^{i\sigma_1 T_1} + \tilde{F}_2 e^{i\sigma_2 T_2} (Q - P)) dx
\end{aligned} \tag{5.73}$$

Finally, the two adjoints equations governing both functions $P(x)$ and $Q(x)$ can be written as:

$$\begin{aligned}
& -\omega^2 P + P^{iv} - \alpha_3 \Gamma(w_{s1}, w_{s1}) P'' - NP'' - 2\alpha_3 w_{s1}'' \Gamma(P, w_{s1}) - \frac{2\alpha_4 V_{DC}^2 P}{(1-w_{s1})^3} - \frac{2\alpha_4 V_{DC}^2 P}{\left(\frac{d_2}{d_1} + w_{s1} - w_{s2}\right)^3} + \\
& \frac{2\alpha_4 V_{DC}^2 Q}{\left(\frac{d_2}{d_1} + w_{s1} - w_{s2}\right)^3} = 0
\end{aligned} \tag{5.74}$$

$$\begin{aligned}
& -\omega^2 Q + Q^{iv} - \alpha_3 \Gamma(w_{s2}, w_{s2}) Q'' - NQ'' - 2\alpha_3 w_{s2}'' \Gamma(Q, w_{s2}) - \frac{2\alpha_4 V_{DC}^2 Q}{\left(\frac{d_2}{d_1} + w_{s1} - w_{s2}\right)^3} + \\
& \frac{2\alpha_4 V_{DC}^2 P}{\left(\frac{d_2}{d_1} + w_{s1} - w_{s2}\right)^3} = 0
\end{aligned} \tag{5.75}$$

which are the same as the first order equations ((5.44) and (5.45)) so we call them self-adjoints equations. The solvability condition can be then obtained as:

$$\begin{aligned}
& \int_{x=0}^1 (-2i\omega A'(P\Phi_1 + Q\Phi_2) - ic\omega A(P\Phi_1 + Q\Phi_2) + A^2 \bar{A}(P\chi_1 + Q\chi_2) + \\
& \tilde{F}_1 P e^{i\sigma_1 T_2} + \tilde{F}_2 e^{i\sigma_2 T_2} (Q - P)) dx = 0
\end{aligned} \tag{5.76}$$

Using Euler's formula for $e^{i\sigma_1 T_2}$ and $e^{i\sigma_2 T_2}$, then separating the real and imaginary parts of the solvability condition will give the following two coupled equations:

$$\beta' a(z_1 + z_2) + \frac{1}{8\omega} a^3(S_1 + S_2) = -\frac{F_1}{\omega} \cos \gamma_1 - \frac{1}{\omega} (F_{22} - F_{21}) \cos \gamma_2 \quad (5.77)$$

$$a'(z_1 + z_2) + \frac{c}{2} a(z_1 + z_2) = \frac{F_1}{\omega} \sin \gamma_1 + \frac{1}{\omega} (F_{22} - F_{21}) \sin \gamma_2 \quad (5.78)$$

where:

$$z_1 = \int_{x=0}^1 P\Phi_1 dx \quad z_2 = \int_{x=0}^1 Q\Phi_2 dx \quad S_1 = \int_{x=0}^1 P\chi_1 dx \quad S_2 = \int_{x=0}^1 Q\chi_2 dx$$

$$F_1 = \int_{x=0}^1 \tilde{F}_1 P dx \quad F_{21} = \int_{x=0}^1 \tilde{F}_2 P dx \quad F_{22} = \int_{x=0}^1 \tilde{F}_2 Q dx \quad \gamma_1 = \sigma_1 T_2 - \beta$$

$$\gamma_2 = \sigma_2 T_2 - \beta$$

By setting ($\sigma_1 = \sigma_2 = \sigma$), which will give ($\gamma_1 = \gamma_2 = \gamma$), squaring both sides of equations (5.77) and (5.78), then adding the results, while remembering that ($\beta' = \sigma - \gamma'$), we get:

$$a_0^2 ((\sigma(z_1 + z_2) + \frac{1}{8\omega} a^2(S_1 + S_2))^2 + \frac{c^2}{4} (z_1 + z_2)^2) = \frac{(F_1 + F_{22} - F_{21})^2}{\omega^2} \quad (5.79)$$

Since the quality factor is related to the damping coefficient (c) by:

$$Q = \frac{\omega}{c(z_1 + z_2)} \quad (5.80)$$

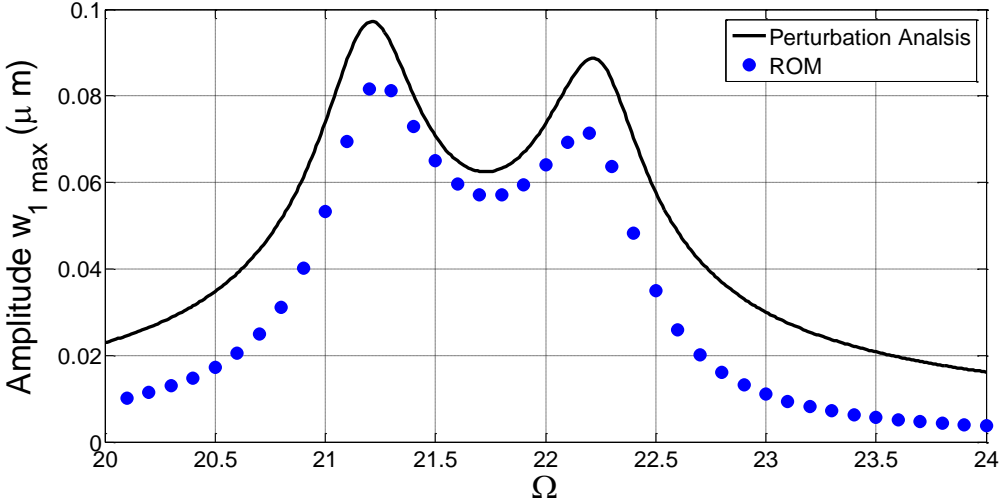
it can be replaced in the solvability equation (5.79) to examine the effect of the quality factor on the system dynamics.

5.2.3 Results

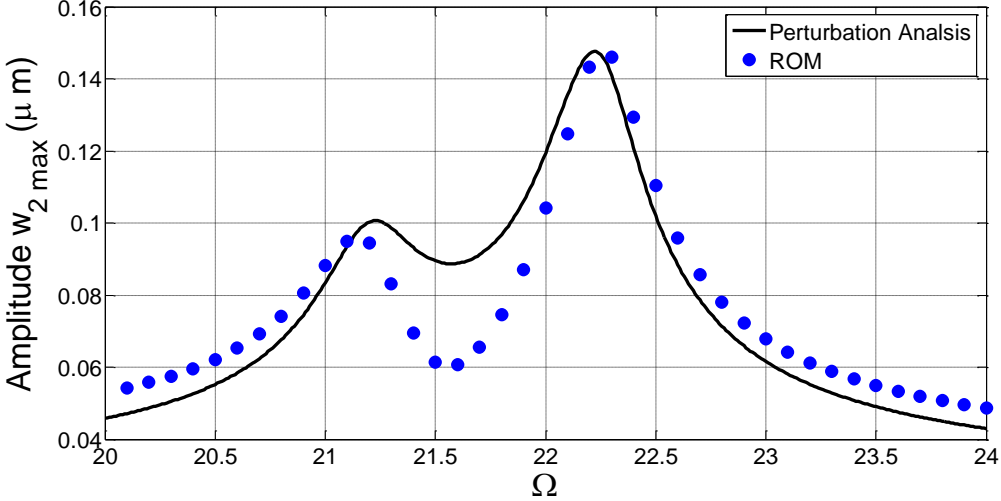
To solve for the coupled equations of motion of both the lower and upper microbeams using the ROM, it is necessary to solve for the unknown functions $p_i(t)$ and $q_i(t)$ in equations (5.28) and (5.29) then substituting them back into equations (5.26) and (5.27), which will give the deflection of both microbeams. For the perturbation technique, we start first by scaling the first order coupled equations, equations (5.44) and (5.45) for both functions Φ_1 and Φ_2 . Then, we substitute them into the second order equations, equations (5.54) and (5.55), to solve for the functions Ψ_{11} , Ψ_{12} , Ψ_{21} and Ψ_{22} . Then, we solve for the unknown dynamic amplitude from equation (5.79) and the phase from either equation (5.77) or (5.78). Finally, the deflection of the lower and upper microbeams can be calculated using equations (5.32) and (5.33), respectively. Since each two consecutive natural frequencies of this system are very close to each other, the equations of the perturbation will be solved twice for each one of those two, and then the deflections around the two natural frequencies for each microbeam will be added to give the resultant deflections of both microbeams.

A comparison of the obtained results for the two above described methods for the case of double-microbeams is shown in Figures 5.3-5.5. The selected parameters were the same as assumed in the static analysis (i.e. Table 3.3) with the only difference being the applied voltages, $V_{DC}=10$ Volt and $V_{AC}=0.5$ Volt. In this present case, it can be seen from all figures that overall both assumed numerical methods are in good agreement for all different cases. While the perturbation analysis technique is less accurate than the ROM, it showed better global results in the presence of gross nonlinearity. It can predict all of the stable and unstable branches which the ROM is not capable of capturing. Also, it gives a better global and local dynamical picture about the

microsystem's behavior. Hence, the perturbation technique will be used in the following parametric study.

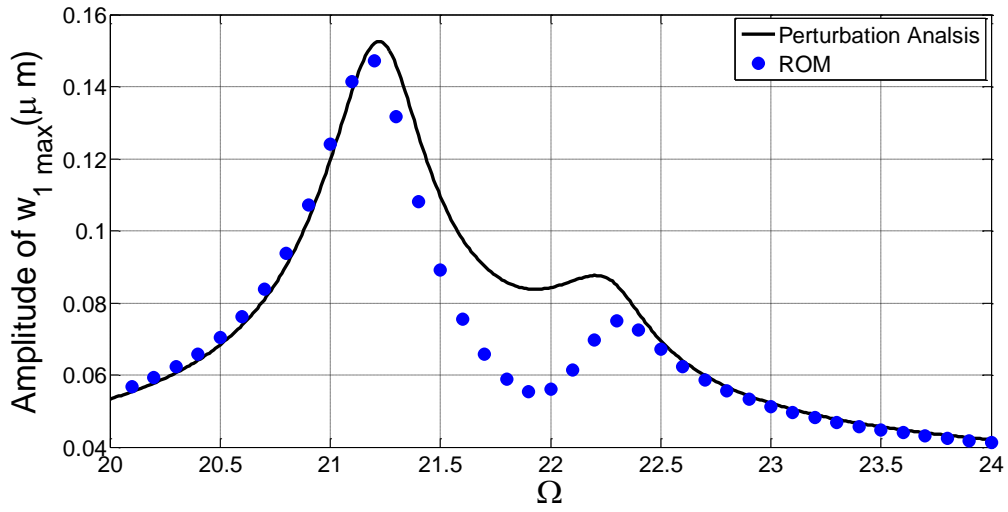


(a)

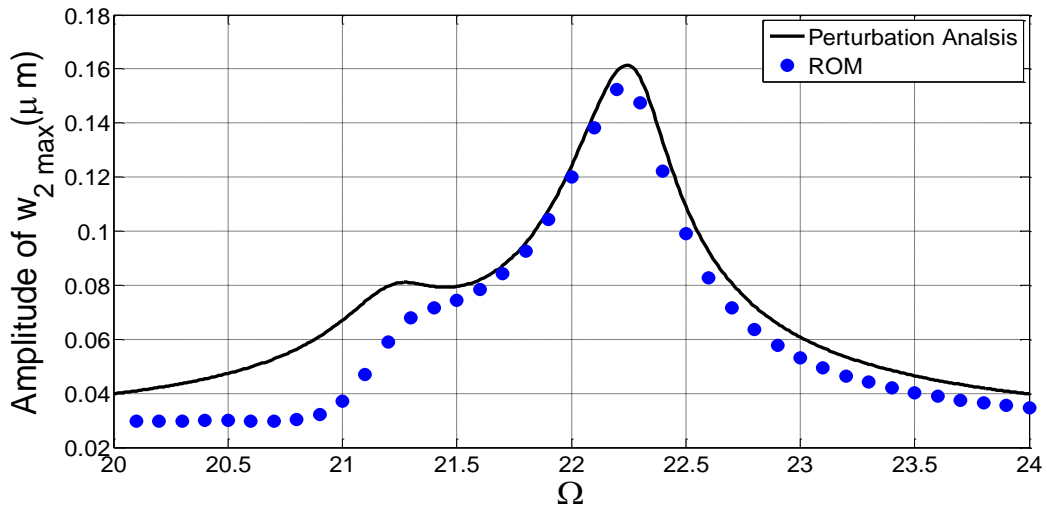


(b)

Figure 5.3: Frequency response curve of the (a) upper microbeam and (b) lower microbeam and assuming both ROM and perturbation method for the case of $d_1=d_2$

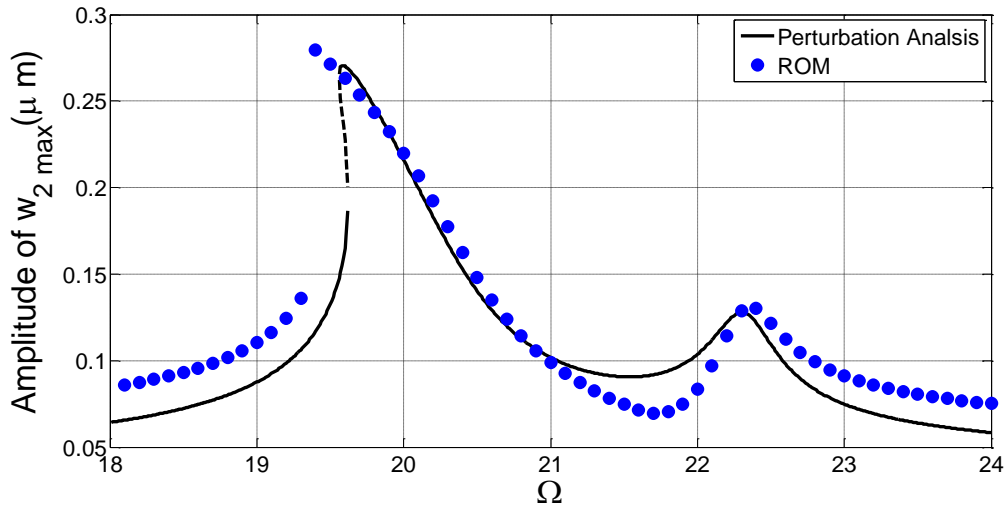


(a)

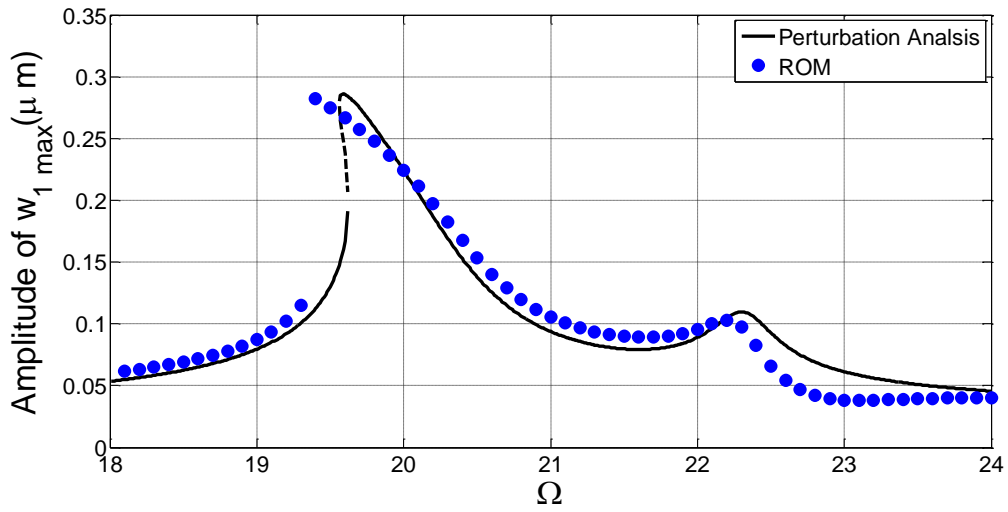


(b)

Figure 5.4: Frequency response curve of the (a) upper microbeam and (b) lower microbeam and assuming both ROM and perturbation method for the case of $d_1 < d_2$



(a)



(b)

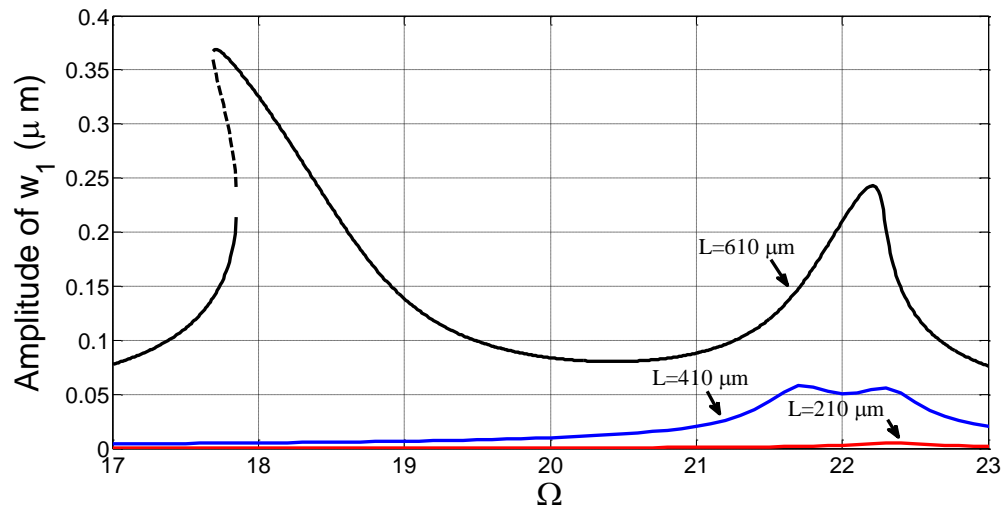
Figure 5.5: Frequency response curve of the (a) upper microbeam and (b) lower microbeam and assuming both ROM and perturbation method for the case of $d_1 > d_2$

5.2.4 Parametric Study

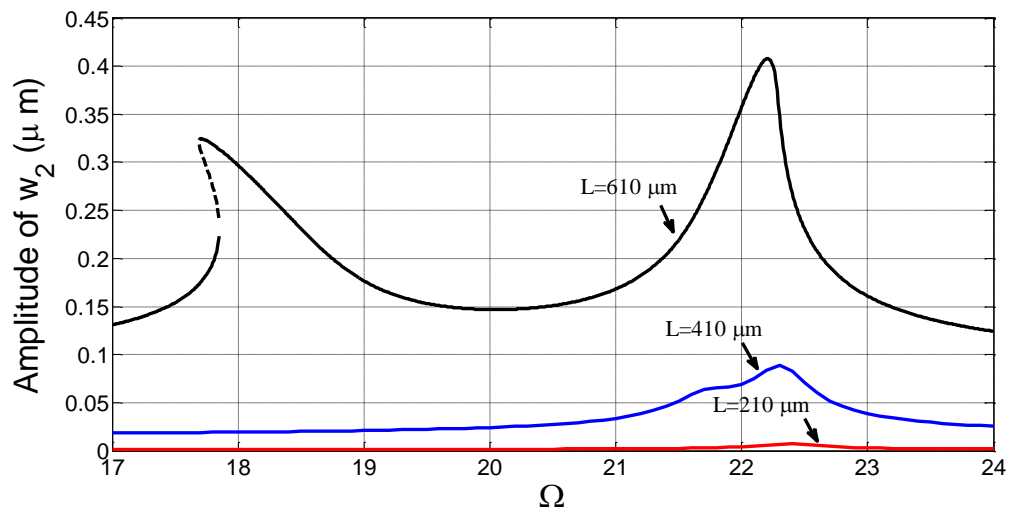
In order to investigate the effect of different physical and geometrical parameters on the dynamical amplitude of the double-microbeams based actuator, three different values were selected (low, medium and high) for each chosen parameter then the frequency response curve was generated for each microbeam to investigate the effects of each tuned parameter. The selected parameters are the length, the quality factor, and the DC and AC voltages. For all those cases, the depth of both air gaps are kept equal ($d_1=d_2=1.25 \mu m$) and the width (b) and height (h) for both microbeams are initially assumed to be $20 \mu m$ and $1.5 \mu m$, respectively. The length (L) and the quality factor (Q) were equal to $210 \mu m$ and 50, respectively, for all the cases except when they are intentionally varied.

a) Effect of the Microbeam Length (L)

Figure 5.6 shows the amplitude versus the excitation frequency for three different lengths ($210 \mu m$, $410 \mu m$ and $610 \mu m$). From both figures, the significance of changing the length on the dynamical amplitude, even when small voltages were applied (i.e. $V_{DC}=2 \text{ Volt}$ and $V_{AC}=0.1 \text{ Volt}$), is clear. When the length is of a small value ($L=210 \mu m$), the two resonance peaks are very close to each other, which means that the applied voltages have a slight effect on the microstructure and so do not change its fundamental frequencies. However, when the value of the microbeam length is increased ($L=410$ and $610 \mu m$), the distance between the two peaks becomes larger, meaning the fundamental frequency becomes lowered and the system is prone to experience a pull-in instability. Also, with a high value of the microbeam length, the nonlinearity becomes more dominant, producing a softening-type of behavior at the fundamental frequency for both microbeams.



(a)



(b)

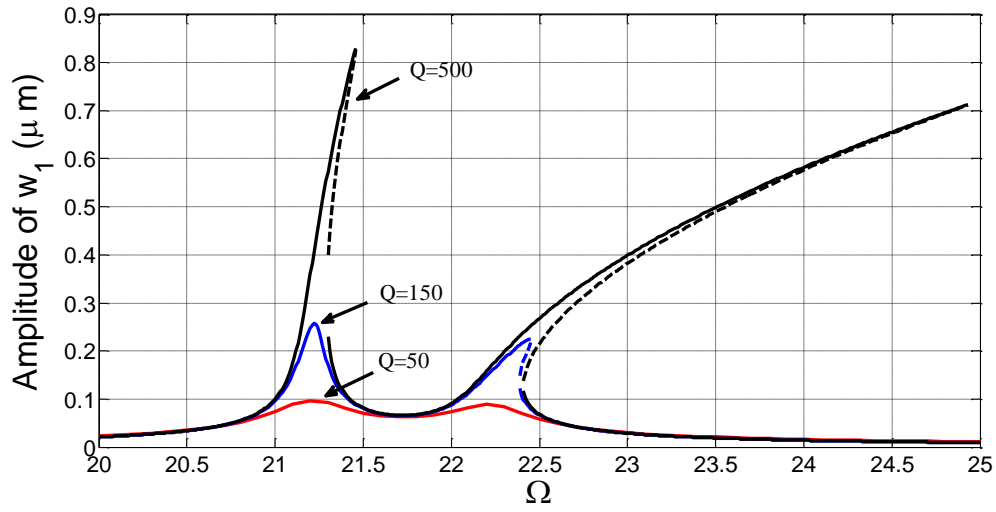
Figure 5.6: Effect of the microbeam length (L) on the frequency response curve of the (a) lower microbeam and (b) upper microbeam for $V_{DC} = 2$ Volt and $V_{AC} = 0.1$ Volt

b) Effect of the Quality Factor (Q)

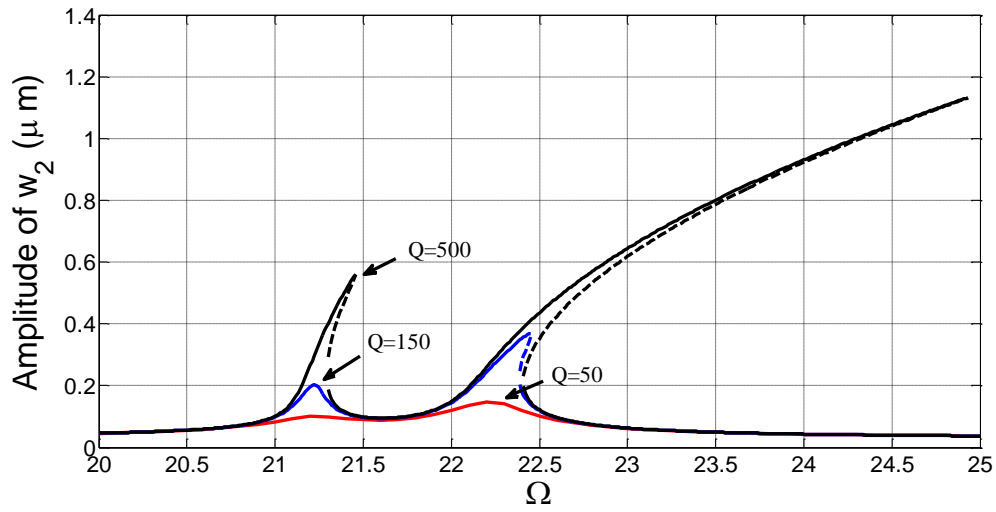
Figure 5.7 shows the amplitude versus the excitation frequency for three different quality factors (50, 150 and 500) at high DC and AC voltages (i.e. $V_{DC}=10$ Volt and $V_{AC}=0.5$ Volt). It can be noticed that there is no effect for the quality factor on the resonance locations, which is reasonable since increasing the quality factor will decrease the damping which has no effect on the natural frequencies. However, the quality factor is shown to maximize the amplitude and with a high quality factor the nonlinearity becomes prominent (see *hardening behavior* in both figures).

c) Effect of the DC Load (V_{DC})

The effects of the applied DC voltage on the amplitude are shown in Figure 5.8. Three different voltages were selected, which are 5, 10 and 15 Volt. At a low DC voltage, the fundamental frequency is not affected by the applied voltage, so it is very close to its consecutive one. However, an increase in the value of the DC voltage causes the fundamental frequency to shift from its initial position, and hence the system gets closer and closer to the pull-in instability. Since the term of the applied AC voltage is small there is no presence for the nonlinearity. So, we would like to investigate the nonlinearity effect for the applied DC voltage at a high AC voltage. As it can be shown from Figure 5.9, by increasing the value of the applied AC voltage to 5 Volt, the hardening-type nonlinearity appears at high values of the DC voltage. This indicates that the mid-plane stretching term is significant, since it is responsible for this nonlinearity.

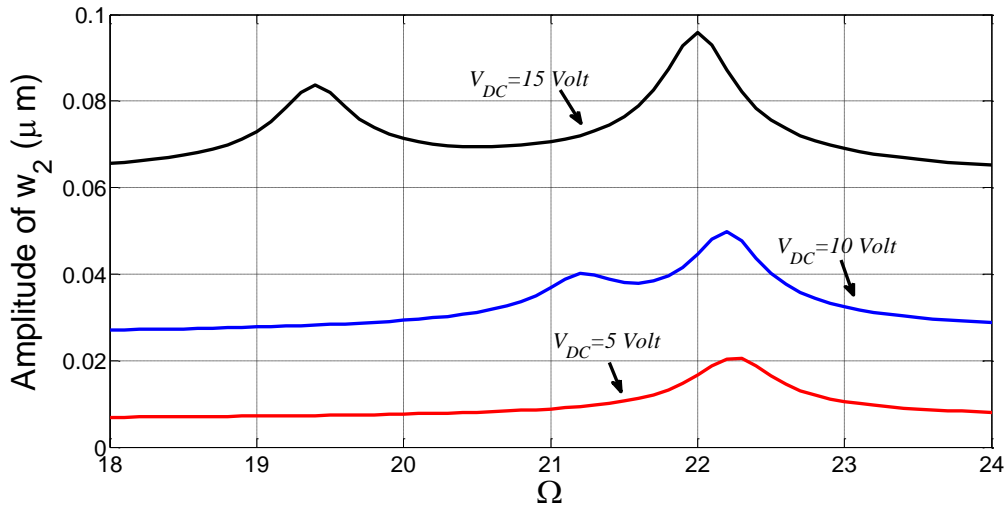


(a)

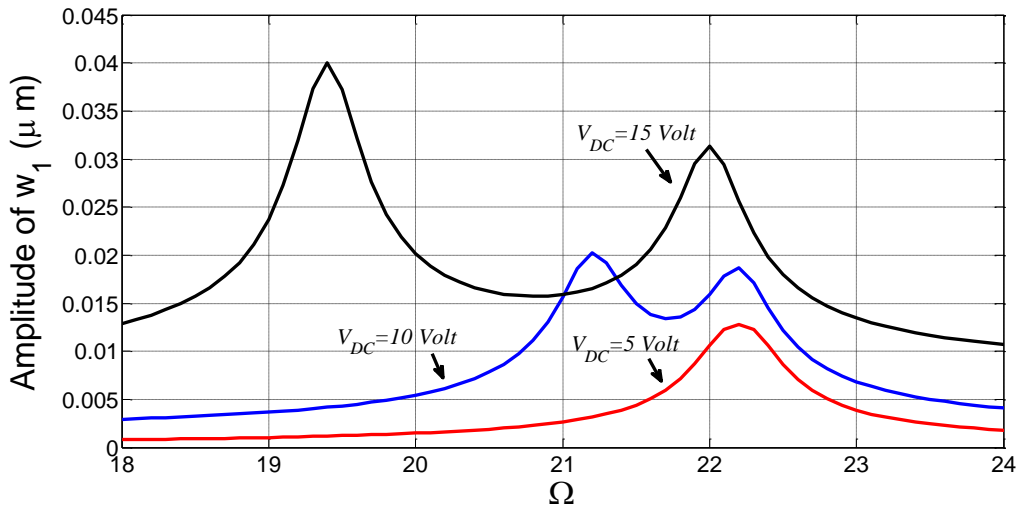


(b)

Figure 5.7: Effect of the quality factor (Q) on the frequency response curve of the (a) lower microbeam and (b) upper microbeam for $V_{DC}= 10$ Volt and $V_{AC}=0.5$ Volt

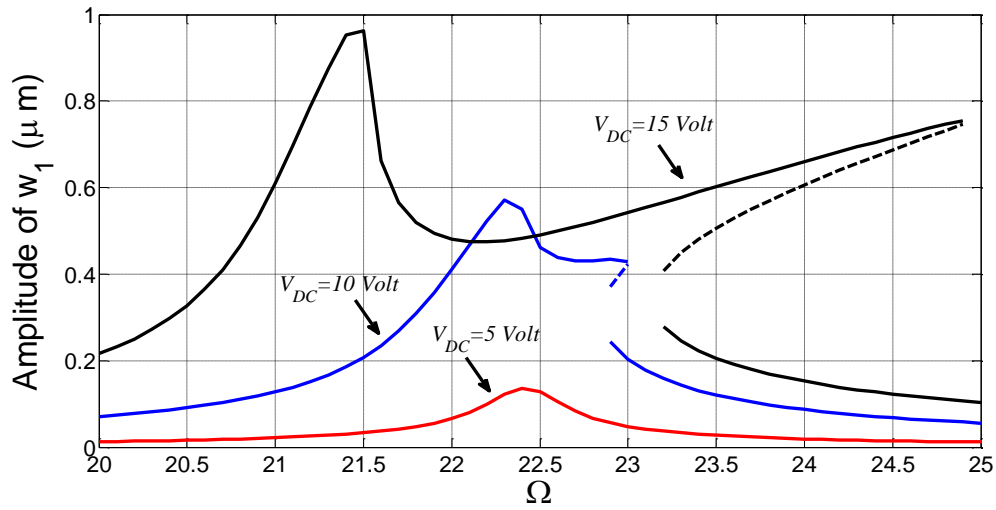


(a)

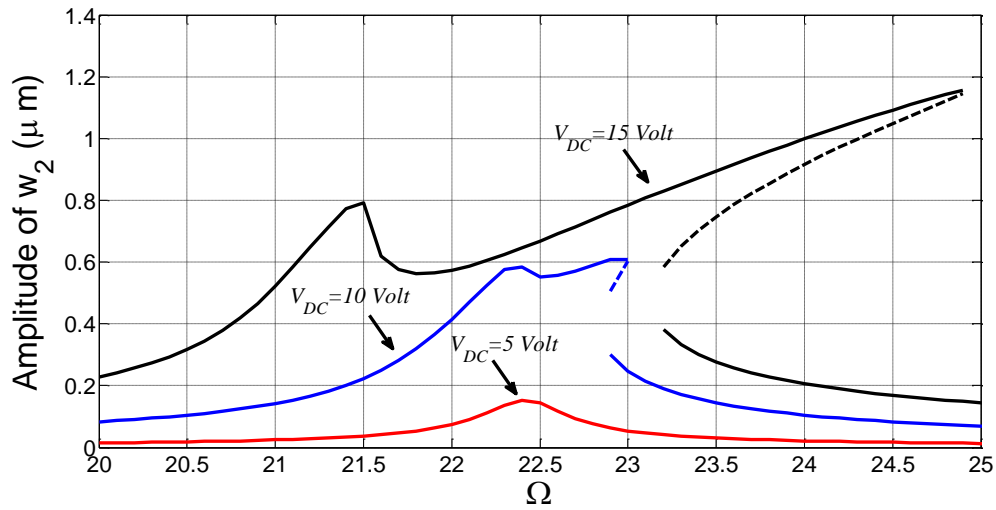


(b)

Figure 5.8: Effect of the applied DC voltage (V_{DC}) on the frequency response curve of the (a) lower microbeam and (b) upper microbeam for $V_{AC} = 0.1$ Volt



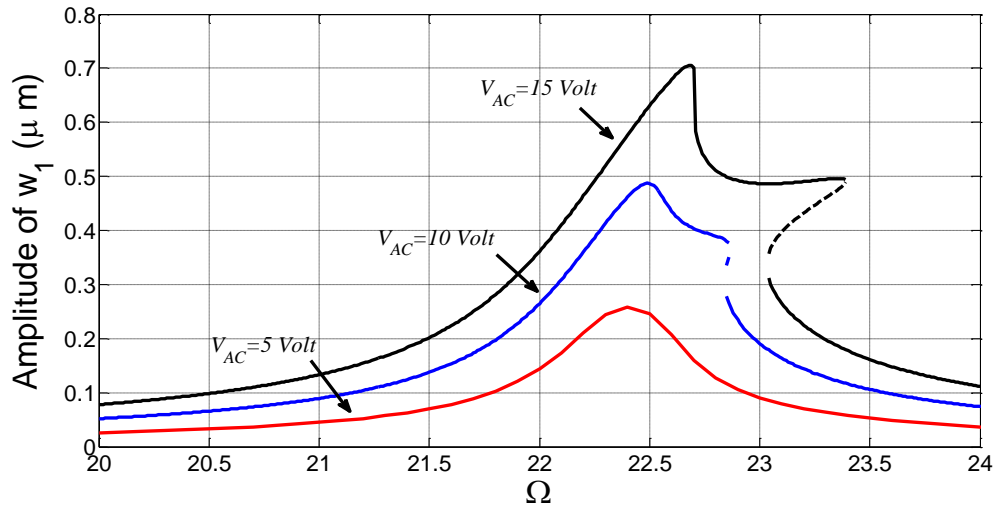
(a)



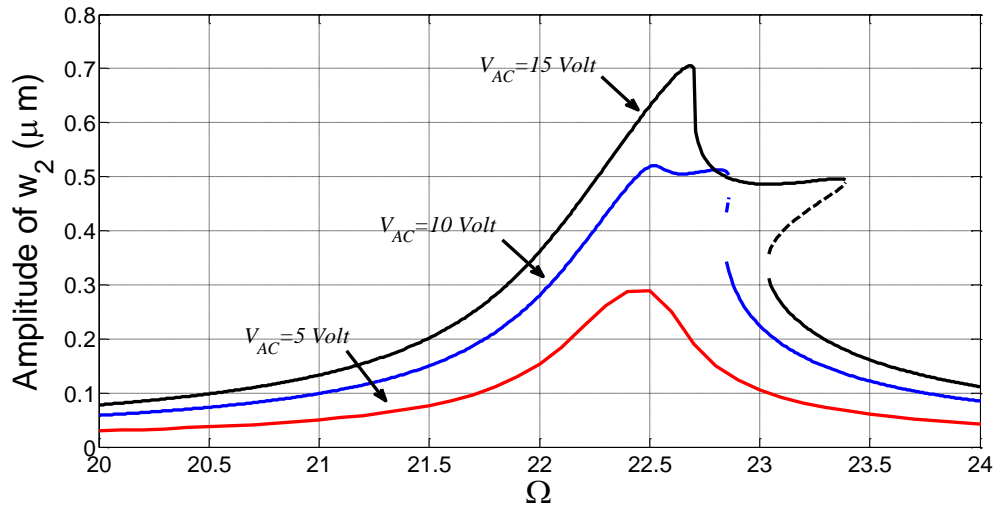
(b)

Figure 5.9: Effect of the applied DC voltage (V_{DC}) on the frequency response curve of the (a) lower microbeam and (b) upper microbeam for $V_{AC} = 5$ Volt

d) Effect of the AC Load (V_{AC})



(a)



(b)

Figure 5.10: Effect of the applied AC voltage (V_{AC}) on the frequency response curve of the (a) lower microbeam and (b) upper microbeam for $V_{DC} = 2$ Volt

Figure 5.10 shows the effect of the applied AC voltage on the amplitude. For this investigation, three different AC voltages were selected which are 5, 10 and 15 *Volt*. Unlike the DC voltage, the applied AC voltage has no effect on the natural frequencies, which is predictable since the dynamic loading has no effect on the natural frequencies. As shown in the figures, increasing the AC voltage increases the amplitude as well as produces a hardening type of nonlinearity.

CHAPTER 6: SUMMARY, CONCLUSIONS AND FUTURE WORK

6.1 Summary

This work concentrates on an investigation of the features of static and dynamic double clamped-clamped microbeams. At the beginning of the work, the results of the related problems in single microbeam were produced. In a single microbeam, the obtained deflection at low voltage was low, so hitting the pull-in instability requires the consumption of much power and time.

Then, the results of the static double-microbeams were obtained using ROM. In comparing the results with the single microbeam, it was shown that the double-microbeams configuration may provide high deflection in low voltages and reach the pull-in instability much faster in comparison with the single microbeam case. As a result, it requires a low actuation voltage, which will both save power, and reduce the switching time.

The analysis of the eigenvalue problem was conducted for both single and double-microbeams. The results showed that for a single microbeam the natural frequencies are far from each other and only the fundamental frequency is affected by the load, which decreases with the applied load until reaching zero at the pull-in. For double-microbeams, when a similar geometry is used for both microbeams, each two natural frequencies are close to each other. However, only the fundamental frequency is affected by the applied DC load.

For the analysis of the dynamics of double-microbeams, two methods were used which are ROM and the perturbation method. The comparison between the two methods showed that they are in good agreement. While the ROM is more accurate, it cannot capture all of the branches which

the perturbation is capable of, and so the perturbation method was used in generating the parametric study.

6.2 Conclusions

In conclusion, the use of double-microbeams configuration was shown to be useful for applications that require low actuation voltage and pull-in voltage, and large deflections. Two numerical methods were used to perform the dynamic analysis, which are perturbation analysis and ROM. The results showed that the outcomes of the two methods are in good agreement. Although, the ROM is more accurate in obtaining the behavior, it cannot capture all of the solution's branches, which the perturbation can perform, so the perturbation method is better in the nonlinearity zone.

The effects of changing the air gap depths on the double-microbeams configuration revealed about interesting profiles. For example, both microbeams could be directed down to the fixed electrode or the upper microbeam could be directed down while the lower is up. Also, the pull-in voltage will differ between the cases, and it can be reached whether from the lower microbeam as it hits the fixed electrode, the lower microbeam as it sticks with the upper microbeam or the upper microbeam as it pulls toward the lower microbeam.

Based on the dynamical parametric study, the effects of the parameters selection are significant on the resonance profiles. For example, increasing the length (L) is significant and will produce a softening nonlinearity; the quality factor (Q) will maximize the resonance profile; increasing the DC voltage (V_{DC}) will shift the two resonance peaks away from each other, while producing a hardening-type nonlinearity at high AC voltage, and the AC voltage (V_{AC}) will produce the

hardening nonlinearity. So, interesting features can be obtained by manipulating these parameters, which may have useful applications.

6.3 Future Work

The following are recommended as an extension for this work:

- Use the concept of localization to explore the potential of using the double-microbeams configuration with an electrostatic force in designing a very sensitive mass sensor.
- Solve for a multi-microbeams configuration and investigate its features and feasibility.
- Use the arch-microbeams instead of the straight-microbeams and perform its static and dynamic analysis.

References

1. Marek, J., B. Hoefflinger, and U.-M. Gomez, *MEMS—Micro-Electromechanical Sensors for the Internet of Everything*, in *CHIPS 2020 VOL. 2*. 2016, Springer. p. 221-229.
2. Abeysinghe, D.C., et al., *A novel MEMS pressure sensor fabricated on an optical fiber*. *Photonics Technology Letters, IEEE*, 2001. **13**(9): p. 993-995.
3. Lee, J.-S., et al. *Development of a piezoresistive MEMS pressure sensor for a precision air data module*. in *Control, Automation and Systems (ICCAS), 2014 14th International Conference on*. 2014. IEEE.
4. Luczak, S., W. Oleksiuk, and M. Bodnicki, *Sensing tilt with MEMS accelerometers*. *Sensors Journal, IEEE*, 2006. **6**(6): p. 1669-1675.
5. Gonseth, S., et al., *Miniaturized high-performance MEMS accelerometer detector*. *CEAS Space Journal*, 2015: p. 1-8.
6. Loeppert, P.V. and S.B. Lee. *SiSonic™—The first commercialized MEMS microphone*. in *Proceedings of the Solid-State Sensors, Actuators, and Microsystems Workshop*. 2006.
7. Hopper, D.G. *Creation and transition of digital light processing technology to defense applications*. in *Defense and Security*. 2005. International Society for Optics and Photonics.
8. Brown, A.K., *Gps/ins uses low-cost mems imu*. *Aerospace and Electronic Systems Magazine, IEEE*, 2005. **20**(9): p. 3-10.
9. Lee, S., S. Park, and D.-i.D. Cho, *The surface/bulk micromachining (SBM) process: a new method for fabricating released MEMS in single crystal silicon*. *Microelectromechanical Systems, Journal of*, 1999. **8**(4): p. 409-416.

10. Kurhekar, A.S., P. Apte, and S. Dutttagupta, *Design and Fabrication of Bulk Micro-machined, High Resilience, High-Q, High Tilt Angle, Low Driving Voltage, Flexure Beam Micro-mirrors on Mono-crystalline Silicon*. Silicon, 2015: p. 1-14.
11. Umesh, G., B. Nayak, and A. Deshpande. *Design and Analysis of a Capacitively-Coupled Clamped-Clamped MEMS Resonator*. in *Computational Intelligence and Communication Networks (CICN), 2014 International Conference on*. 2014. IEEE.
12. Mulloni, V., et al., *RF-MEMS switch design optimization for long-term reliability*. Analog Integrated Circuits and Signal Processing, 2014. **78**(2): p. 323-332.
13. Younis, M.I., F. Alsaleem, and D. Jordy, *The response of clamped-clamped microbeams under mechanical shock*. International Journal of Non-Linear Mechanics, 2007. **42**(4): p. 643-657.
14. Yu, Y.-T., W.-Z. Yuan, and D.-Y. Qiao, *Electromechanical characterization of a new micro programmable blazed grating by laser Doppler vibrometry*. Microsystem technologies, 2009. **15**(6): p. 853-858.
15. Zook, J.D., et al., *Optically excited self-resonant microbeams*. Sensors and Actuators A: Physical, 1996. **52**(1): p. 92-98.
16. Shamshirsaz, M. and M. Asgari, *Polysilicon micro beams buckling with temperature-dependent properties*. Microsystem Technologies, 2008. **14**(7): p. 957-961.
17. Alsaleem, F.M., M.I. Younis, and H.M. Ouakad, *On the nonlinear resonances and dynamic pull-in of electrostatically actuated resonators*. Journal of Micromechanics and Microengineering, 2009. **19**(4): p. 045013.

18. Zavracky, P.M., S. Majumder, and N.E. McGruer, *Micromechanical switches fabricated using nickel surface micromachining*. *Microelectromechanical Systems, Journal of*, 1997. **6**(1): p. 3-9.
19. Choi, B. and E. Lovell, *Improved analysis of microbeams under mechanical and electrostatic loads*. *Journal of Micromechanics and Microengineering*, 1997. **7**(1): p. 24.
20. Bouchaala, A.M. and M.I. Younis, *A Model of Electrostatically Actuated MEMS and Carbon Nanotubes Resonators for Biological Mass Detection*, in *Design and Modeling of Mechanical Systems-II*. 2015, Springer. p. 501-512.
21. Caruntu, D.I. and I. Martinez, *Reduced order model of parametric resonance of electrostatically actuated MEMS cantilever resonators*. *International Journal of Non-Linear Mechanics*, 2014. **66**: p. 28-32.
22. Younis, M., E.M. Abdel-Rahman, and A. Nayfeh, *A reduced-order model for electrically actuated microbeam-based MEMS*. *Microelectromechanical Systems, Journal of*, 2003. **12**(5): p. 672-680.
23. Nayfeh, A.H., M.I. Younis, and E.M. Abdel-Rahman, *Reduced-order models for MEMS applications*. *Nonlinear dynamics*, 2005. **41**(1-3): p. 211-236.
24. Nayfeh, A.H., M.I. Younis, and E.M. Abdel-Rahman, *Dynamic pull-in phenomenon in MEMS resonators*. *Nonlinear dynamics*, 2007. **48**(1-2): p. 153-163.
25. Ouakad, H.M. and M.I. Younis, *On using the dynamic snap-through motion of MEMS initially curved microbeams for filtering applications*. *Journal of Sound and Vibration*, 2014. **333**(2): p. 555-568.

26. Sahai, T., R.B. Bhiladvala, and A.T. Zehnder, *Thermomechanical transitions in doubly-clamped micro-oscillators*. International Journal of Non-Linear Mechanics, 2007. **42**(4): p. 596-607.
27. Zook, J., et al., *Characteristics of polysilicon resonant microbeams*. Sensors and Actuators A: Physical, 1992. **35**(1): p. 51-59.
28. Tilmans, H.A. and R. Legtenberg, *Electrostatically driven vacuum-encapsulated polysilicon resonators: Part II. Theory and performance*. Sensors and Actuators A: Physical, 1994. **45**(1): p. 67-84.
29. Gui, C., et al., *Nonlinearity and hysteresis of resonant strain gauges*. Microelectromechanical Systems, Journal of, 1998. **7**(1): p. 122-127.
30. Nayfeh, A.H., *Perturbation methods*. 2008: John Wiley & Sons.
31. Ouakad, H.M. and M.I. Younis, *Dynamic response of slacked single-walled carbon nanotube resonators*. Nonlinear Dynamics, 2012. **67**(2): p. 1419-1436.
32. Warminski, J., *Frequency locking in a nonlinear MEMS oscillator driven by harmonic force and time delay*. International Journal of Dynamics and Control, 2015. **3**(2): p. 122-136.
33. Turner, G. and M. Andrews. *Frequency stabilisation of electrostatic oscillators*. in *Solid-State Sensors and Actuators, 1995 and Eurosensors IX.. Transducers' 95. The 8th International Conference on*. 1995. IEEE.
34. Younis, M. and A. Nayfeh, *A study of the nonlinear response of a resonant microbeam to an electric actuation*. Nonlinear Dynamics, 2003. **31**(1): p. 91-117.
35. Afrang, S. and E. Abbaspour-Sani, *A low voltage MEMS structure for RF capacitive switches*. Progress In Electromagnetics Research, 2006. **65**: p. 157-167.

36. Chaffey, J.P. and M. Austin. *Analytical modeling of the electromechanical coupling of cantilever beams*. in *SPIE's International Symposium on Smart Materials, Nano-, and Micro-Smart Systems*. 2002. International Society for Optics and Photonics.
37. Samaali, H., et al., *A double microbeam MEMS ohmic switch for RF-applications with low actuation voltage*. *Nonlinear Dynamics*, 2011. **63**(4): p. 719-734.
38. Ouakad, H.M., M.A. Hawwa, and H.M. Al-Qahtani, *Modeling the Electrostatic Deflection of a MEMS Multilayers Based Actuator*. *Mathematical Problems in Engineering*, 2013. **2013**.
39. Ouakad, H.M., *Static response and natural frequencies of microbeams actuated by out-of-plane electrostatic fringing-fields*. *International Journal of Non-Linear Mechanics*, 2014. **63**: p. 39-48.
40. Wijesiri, A. and Y. Amarasinghe, *MEMS Based Microneedle Actuator with Piezoresistive Force Feedback System for Biomedical Applications*. *International Journal of Scientific Engineering and Technology*, 2014. **3**(12): p. 1449-1454.
41. Krylov, S., et al., *The pull-in behavior of electrostatically actuated bistable microstructures*. *Journal of Micromechanics and Microengineering*, 2008. **18**(5): p. 055026.
42. Rebeiz, G.M., *RF MEMS: theory, design, and technology*. 2004: John Wiley & Sons.
43. Ouakad, H.M., *Nonlinear Structural Mechanics of Micro and Nano Systems*, 2010, State University of New York.
44. Hayt Jr, W. and J. Buck, *Engineering Electromagnetics. 7th edn McGraw-Hill*. New York, 2006.

45. Abdel-Rahman, E.M., M.I. Younis, and A.H. Nayfeh, *Characterization of the mechanical behavior of an electrically actuated microbeam*. Journal of Micromechanics and Microengineering, 2002. **12**(6): p. 759.
46. Younis, M.I., *MEMS linear and nonlinear statics and dynamics*. Vol. 20. 2011: Springer Science & Business Media.
47. Nayfeh, A.H., *Introduction to perturbation techniques*. 2011: John Wiley & Sons.
48. Gander, M.J. and G. Wanner, *From Euler, Ritz, and Galerkin to Modern Computing*. SIAM Review, 2012. **54**(4): p. 627-666.
49. Noack, B.R., et al., *Galerkin method for nonlinear dynamics*. 2011: Springer.
50. Truesdell, C., *The rational mechanics of flexible or elastic bodies, 1638-1788, 1960*. Sert d'introduction à O. II. **10**.
51. Gere, J. and B. Goodno, *Mechanics of materials*. 2012: Nelson Education.

Vitae

Name : Abdulrahman Mohammed Alofi
Nationality : Saudi Arabian
Date of Birth : 25/11/1989
Email : amaloufi@kfupm.edu.sa
Address : Hamza Street – KFUPM – Dhahran – Saudi Arabia

Academic Background :

- M.Sc. Mechanical Engineering: King Fahd University of Petroleum and Minerals (KFUPM), Dhahran, Saudi Arabia (GPA: 3.719 out of 4) November 2015.
- B.Sc. Mechanical Engineering: King Fahd University of Petroleum and Minerals (KFUPM), Dhahran, Saudi Arabia (GPA: 3.579 out of 4) January 2013.

Publications :

- **Abdulrahman M. Alofi** and Hassen M. Ouakad “*Nonlinear structural behavior of multi-layer based microbeam actuator*” [Under Preparation].
- **Abdulrahman M. Alofi**, Hassen M. Ouakad and Ali H. Nayfeh “*Dynamic analysis of multi-layer based resonators*” [Under Preparation].